UNIVERSITY OF ASTON IN BIRMINGHAM

THE TRANSFER FUNCTION FOR A SUBCRITICAL SYSTEM MEASURED BY PROMPT GAMMA RADIATION

Thesis submitted for Degree

of

Doctor of Philosophy

by

Mohamad Reza Eskandari M.Sc.

Department of
Physics

October
1978

SUMMARY

THE TRANSFER FUNCTION FOR A SUB-CRITICAL SYSTEM MEASURED BY PROMPT GAMMA RADIATION

Mohamad Reza Eskandari
Doctor of Philosophy
1978

The source transfer function has been measured in a natural uranium-light water moderated sub-critical assembly as a function of source frequency and position. A square wave input of fast neutrons from the D-T reaction was supplied by a SAMES type J accelerator suitably modified for the purpose. Prompt gamma radiation from fission, energy above 2.5 Mev was detected with a sodium iodide scintillation counter and the time variation of the detector output was recorded on a multi-channel analyser used in the time sequence storage mode and synchronised with the source pulsing frequency. By Fourier analysing the recorded waveform the source transfer function was found.

Two group diffusion theory was used to determine the spatially dependent source transfer function for a system similar to the experimental one. The computer programs ATEST and GAMMARESFU, were written to calculate the neutron flux in the core and also prompt fission gamma rays response function outside the subcritical assembly at chosen frequency and detector position. The method gave good agreement with the experiment.

Transfer/Function/Subcritical/Prompt/Gamma

ACKNOWLEDGEMENTS

I would like to express my gratitude to Dr.P.N. Cooper, my supervisor, for his continued help and invaluable guidance throughout the research project. I wish to convey my thanks to Professor S.E. Hunt, in whose department this project was carried out, and to thank the Atomic Energy Organization and Ministry of Science and Higher Education of Iran for providing the research grant.

Finally, I would like to thank my wife Nahid for her understanding and assistance throughout the period of this project.

To my Wife and Parents

TABLE OF CONTENTS

LIST OF FIGURES

CHAPTER 1

INTRODUCTION

1.1 Historically, subcritical assemblies have been used as a very important and useful tool for the experimental study of thermal reactor systems. A subcritical assembly is smaller than a critical assembly but having similar lattice and fuel with effective multiplication factor less than one. Therefore, a self-sustaining chain reaction is not possible in such a nuclear system. The steady state condition is achieved by providing an external neutron source. So the external neutron source makes up the deficit between neutron leakage and absorption on the one hand and high fission produced neutrons on the other.

The subcritical assemblies have been used to study different reactor parameters such as the infinite multiplication constant and diffusion parameters.

1.2 PROVIDING EXTERNAL NEUTRON SOURCE:

The variation of external neutron source strength has also been used extensively in determining neutron diffusion parameters since its early application in 1942. Manely and Haworth and Luebke in 1941, directly observed the time variation of slow neutron density in a large volume of water during and after irradiation by neutrons

from D-D reaction, and they obtained the mean lifetime of neutrons in water (205±10) microsecond [1]. Moderators, in particular, have been studied repeatedly with pulsed neutron technique [2,3]. Beckurts in 1961 and Lopez in 1962 studied the kinetic behaviour of neutrons in matter and neutron diffusion parameters in water at 26.7°C respectively. The theory of pulsed neutron source measurements has been discussed by Garelis and Russel [4,5,6].

1.3 NEUTRON WAVE TECHNIQUE:

A supplement to the pulsed neutron experiments has been the neutron wave technique in which the neutron source strength varies in a regular periodic manner. Raievski and Horowitz used the neutron wave method to measure the transport mean free path of thermal neutrons in heavy water [7]. They made a similar measurement in graphite, that was subsequently repeated by Drouler, Lacour, and Raievski [8]. A more accurate value for the transport mean free path was obtained. Propagation of neutron waves in moderating media were used by Perez and Uhrig in 1963 to obtain variation of the phase angle as a function of position which were dependent upon the frequency of modulation and the neutron diffusion and thermalization parameters of the media in which the waves were being propagated [9]. The Perez and Uhrig investigations were continued by Mortensen and Smith to extend the neutron-wave theory [10].

Experiments have been made to measure the propagation properties (such as variation of the attenuation and phase lag with frequency) of thermal neutrons wave in heavy water natural uranium subcritical assembly by Wanger [11]. Sobhana, Singh and Ghatak used the propagation of a sinusoidal disturbance introduced into the neutron distribution in the moderating media [12].

The essential contribution to the field of reactor physics from those investigations is that the relative attenuation and phase shift of neutron wave excited by an external modulated neutron source are strongly dependent upon the physical and nuclear properties of the medium through which the wave propagates. Such neutron wave experiments have been used to obtain information regarding the diffusion, absorption and thermalization properties of the media. Also, many theoretical studies have been carried out for understanding the neutron-wave problem. Particular mention in this respect should be made of the work of Jacob, [13], Mortensen [10], Moore [14], Williams [15], Wood [16], Brehm [17], and Kunaish [18]. The general opinion is that there is no fundamental difference between neutron-wave propagation and neutron-pulse propagation from the point of view of the time-dependent diffusion and thermalization phenomena [19]. However, the neutron wave technique provides the advantages, compared with the pulsed-neutron experiments, that the method allows for two independent quantities to be measured, attenuation and

phase shift. From the standpoint of reactor control, the dynamic behaviour of a reactor (or indeed of any system) is customarily described by its response to small disturbances. This response as a function of the frequency of disturbance is called the transfer function of the reactor. The term "Transfer function" is used here in its classical electrical-engineering sense as a relation between input and output. No connection is implied with the familiar "reactivity transfer function" of space-independent kinetics. Since reactivity is an integral or whole-reacter parameter, specification of the reactivity effect of an input does not uniquely specify the input in a space dependent situation. (That is, a large number of different configuration changes could give the same reactivity change, and yet induce completely different dynamic effects [20]. Therefore there is no such things as a space-dependent reactivity transfer function.

1.4 THE AIM OF PRESENT WORK

is to study the space dependent transfer function of a given multiplying system by prompt fission γ-rays induced by neutron waves. A reactor or multiplying assembly, however is not a lumped parameter system. The distance between the input and output devices, as well as their relative locations in the system, can have a large effect on the measured attenuation and phase shift of a disturbance as it propagates through the system.

The dispersive nature of the neutron wave propagation phenomena in both multiplying and non-multiplying media was observed in the late fifties by Uhrig and later, Kylstra and Cohn [20] provided further evidence, both theoretically and experimentally, of the space dependent nature of the reactor transfer function.

Most studies of fluctuations and correlations in neutron distribution are based upon the direct detection of neutrons. An exception is an experiment performed at Pennsylvania State University in which an attempt was made to observe neutron fluctuations by monitoring the Cerenkov radiation [21]. Gelians and Osborn [22] suggested that, in principle, it is possible and perhaps even advantageous, in some cases, to perform reactor noise experiments by detecting the high energy prompt-gamma radiation (E>5Mev) generated by neutron interaction with the core.

The investigations suggested by Gelians and Osborn were carried out by L ehto and Carpenter [23-24] and Bars and Markkanen [25].

The results obtained by these workers clearly verify the applicability of gamma observation techniques in reactor noise measurements as a substitute and complement to noise measurements via neutron detection. Due to the small mean free path of thermal neutrons in a nuclear system, especially a water moderated one, a neutron detector "sees" neutrons essentially only in that volume which the detector itself occupies physically in

the system plus approximately one mean free path around. Previous work at Aston University has shown the strong spatial effect on transfer function when using neutron detection [26]. In the case of higher energy gamma ray quanta which may have a greater mean free path than thermal neutrons, the gamma detector is capable of receiving gamma rays that have travelled a considerable distance through the core and reflector. This of course, implies that the capability to observe spatially dependent effect is reduced.

Therefore, it follows that a gamma detector does not necessarily have to be placed into the core, thereby, the perturbations commonly induced by neutron-detecting devices can be avoided. Furthermore, neutron detectors are not feasible when used to measure shut-down reactivities of power reactors due both to possible radiation damage and to the mechanical difficulties involved in the insertion of detectors inside the core.

1.5 THE PRINCIPAL OBJECTIVE OF THIS WORK

was to select suitable experimental conditions to determine experimentally the subcritical assembly transfer function by detecting the high energy prompt-gamma radiation generated by neutron interaction within the core. It was also of interest to compare theoretical calculations of space dependent transfer functions with the experimental results.

The prompt gamma-ray spectrum contains a significant number of quanta with energies above ~5Mev, while the fission-product spectrum contains very few [27]. Meinschein et al [28] reported that there is a negligible delayed gamma-ray emission due to fission product decay in the time interval between 10^{-4} and 1 sec. after fission. Delayed gamma emission in shorter time intervals (less than 10^{-4} secs. after fission) behaves as prompt [22] and it is also a negligible fraction of the total gamma-energy emitted per fission event [28]. Long lived fission products can be troublesome in the sense that they are the source of considerable background due to low energy pile-up. Also, Chapman et al [29] show that fission-product gamma radiation for energies greater than 5 Mev is considerably less than that arising promptly from fission. The same conclusions apply down to about 2.5 Mev giving greater sensitivity but still avoiding the prompt gamma-radiation from neutron capture in hydrogen.

Considerable improvements have been made to the external pulsing method of the S.A.M.E.S. accelerator to produce a square beam current waveform with an operating frequency range from 1HZ to higher than 2KHZ. This was used to produce a constant amplitude square-waveform source of fast neutrons from the D-D and D-T reactions. Since the square wave can be Fourier analysed into an infinite number of harmonics of the fundamental it can be considered as the superposition of harmonically related

sinusoidal inputs and therefore the methods of analysis can be based on a sinusoidal input.

A natural uranium light water moderated subcritical assembly was supplied with the thermalized square wave of fast neutrons produced by the S.A.M.E.S accelerator. By varying the input frequency and Fourier analysing the system response at different locations, the transfer function of the subcritical assembly was measured as a function of frequency and space.

1.6 EXPERIMENTAL ARRANGEMENT FOR DATA ACQUISITION

Gamma signals were detected by NaI(Tℓ) scintillator counter. These signals were fed sequentially into a RIDL pulse height analyser used in the time sequence storage mode. Thus, by suitable photon-energy discriminations, and adequate shielding (to reduce low energy pile up), it was possible to obtain space dependent response function of multiplying system by detecting high energy prompt photons emitted by fission. The experimental results, after analysis, have been compared with those obtained theoretically. An NE213 (xylene based liquid scintillator) scintillation counter was used to look at the square wave fast neutrons produced from the S.A.M.E.S instead of target current measurement.

This work has been organised as follows. In Chapter 2 a detailed description of the experimental equipment used is presented. Chapter 3 contains the method developed for

the analysis of the experimental results, also including some experimental results. Chapter 4 deals with theoretical method used to evaluate the spatially dependent transfer functions, neutron flux distribution in subcritical assembly and prompt gamma induced. Chapter 5 deals with the efficiency of Na I (Tℓ) detector. In Chapter 6 the theoretical results are summarized and compared with those obtained experimentally. Finally, in Chapter 7, the principle conclusions drawn from this work are given.

CHAPTER 2

EXPERIMENTAL EQUIPMENT

In this chapter the nuclear system and the equipment used to generate the square waveform neutron population and experimental equipment used are presented in detail.

2.1 NUCLEAR SYSTEM

The nuclear system consisting of a light-water moderated, natural uranium subcritical assembly was used as a test medium.

The assembly construction was arranged to have near maximum infinite multipication factor and also to provide a moderating material between the fast neutron source and the assembly.

Fig. 2.1 shows the main components of the subcritical facility. It consists of a stainless steel tank, base 1120mm X 876mm and 914mm high, placed on top of a graphite pedestal 533mm high. This provides both slowing down material for the source neutrons and a bottom reflector for the subcritical assembly.

The natural uranium was in the form of 196 cylindrical bars of outside diameter 29.2mm, 813mm long and weight 10 Kg. These were inserted in aluminium cans with wall thickness of 0.91mm. The fuel was protected from water

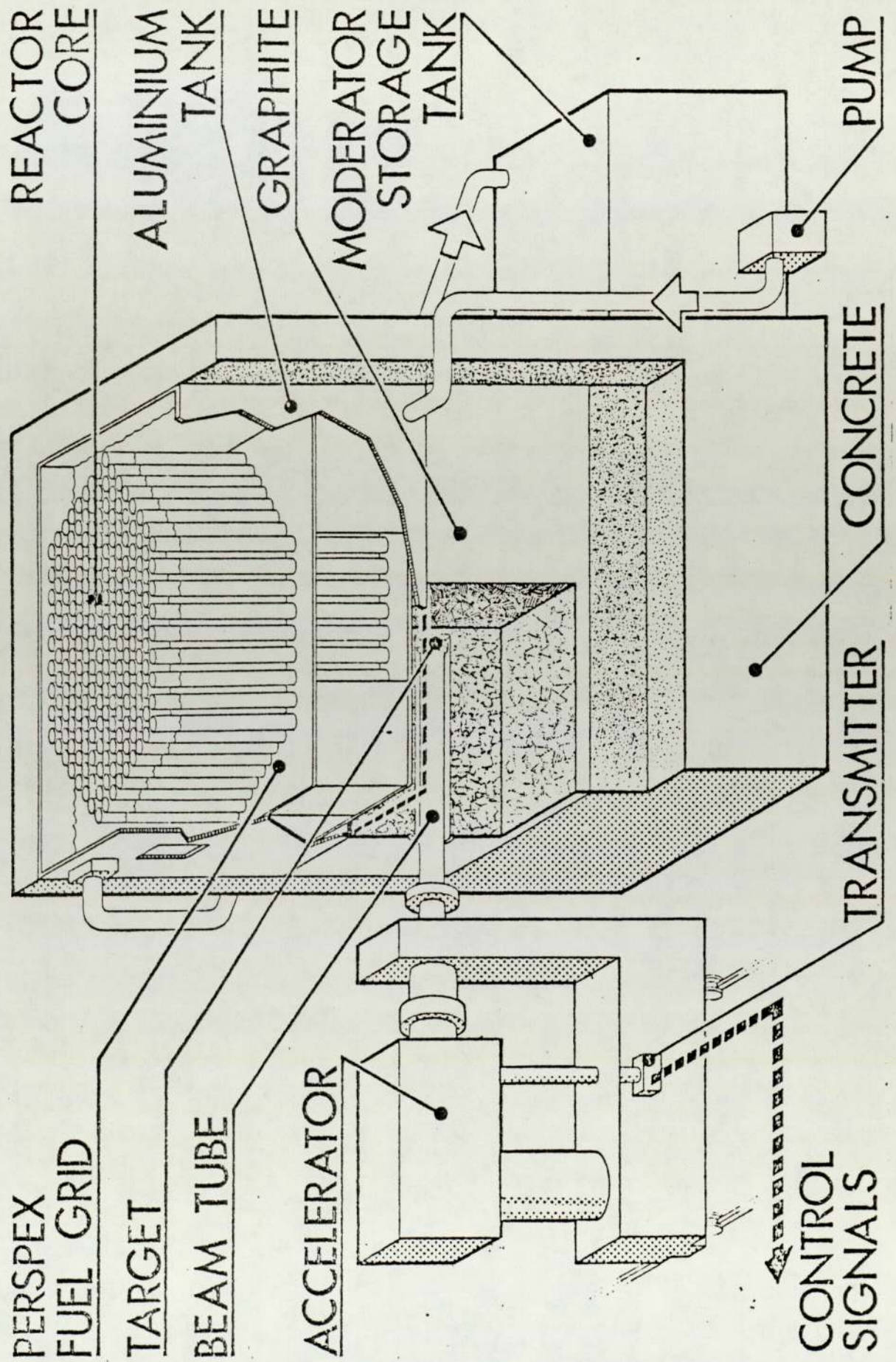

FIG.2.1 Main components of subcritical assembly

by having both ends of the cans properly sealed.

Two perspex fuel grids, 12.7mm thick, one at the bottom and the other 400mm above were fixed centrally inside the tank. These held the natural uranium bars vertically. The core shape was almost hexagonal with a triangular pitch of 45.2mm, as shown in Figs. 2.2 and 2.3 respectively.

This arrangement had an effective core radius of 333mm and infinite multiplication factor of 0.996, calculated for a water to uranium volume ratio of 1.5:1. The volume fractions were :

$$U_{nat} = 0.379 \quad ; \quad Al = 0.048 \quad ; \quad H_2O = 0.573$$

An ion-exchange column supplied the water at a resistivity of about 2MΩCm. The whole of the water was periodically changed to maintain a high purity. In use the water was pumped from a storage tank up into the core tank and allowed to run out through an overflow to maintain a constant level. The maximum water level was of the same height as the fuel rods, thus the core was unreflected on the top horizontal face. The vertical faces of the system were reflected by water with thickness varying between 100mm and 270mm. A flight tube from the S.A.M.E.S accelerator which projected into the graphite pedestal was coupled to the target assembly. The target assembly contained a tritium target type TRT51 which consisted of titanium evaporated on a copper disc 0.25mm thickness. The

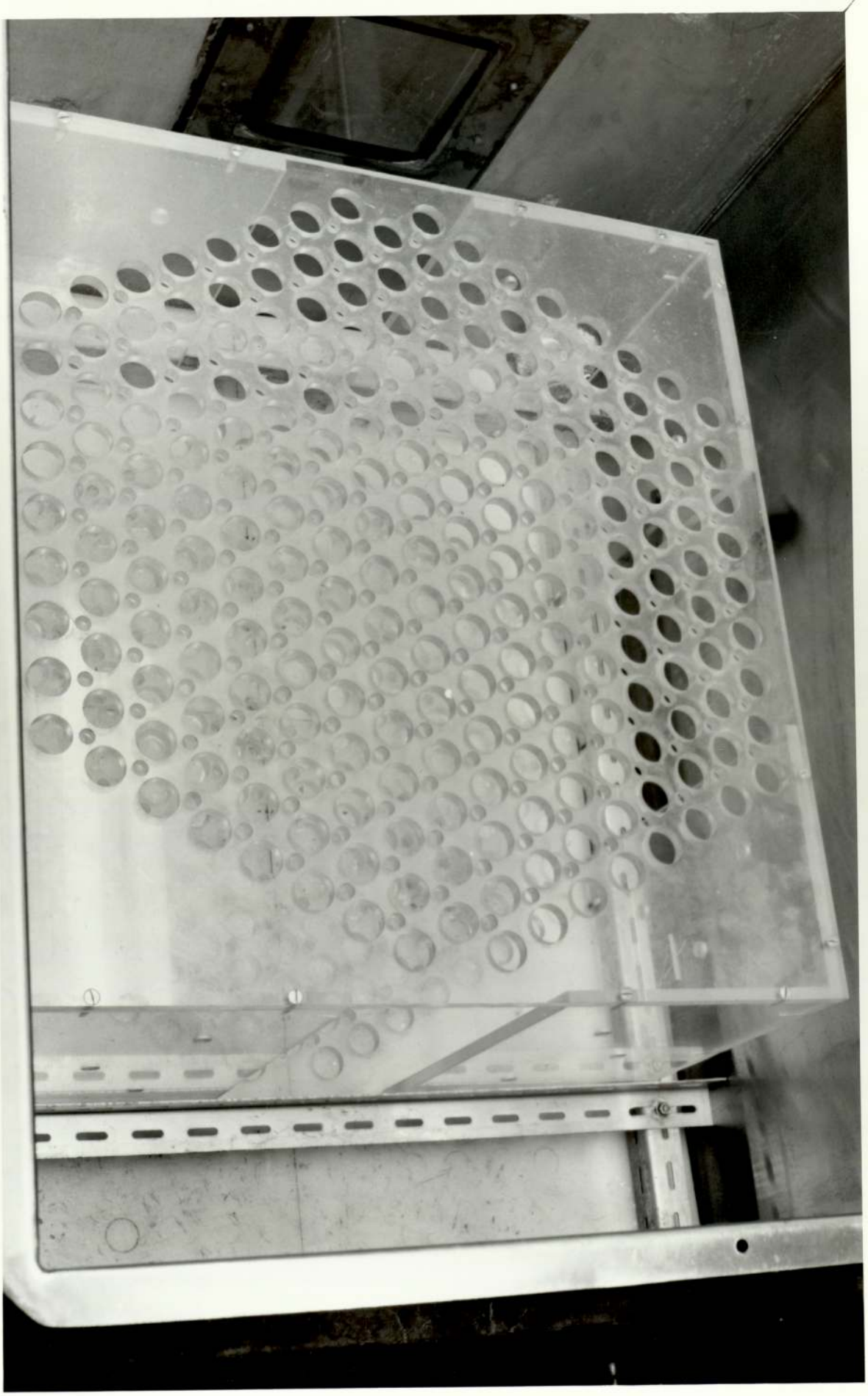

FIG.2.2 Core shape and sub-critical assembly lattice plate.

A. Fuel rod hole

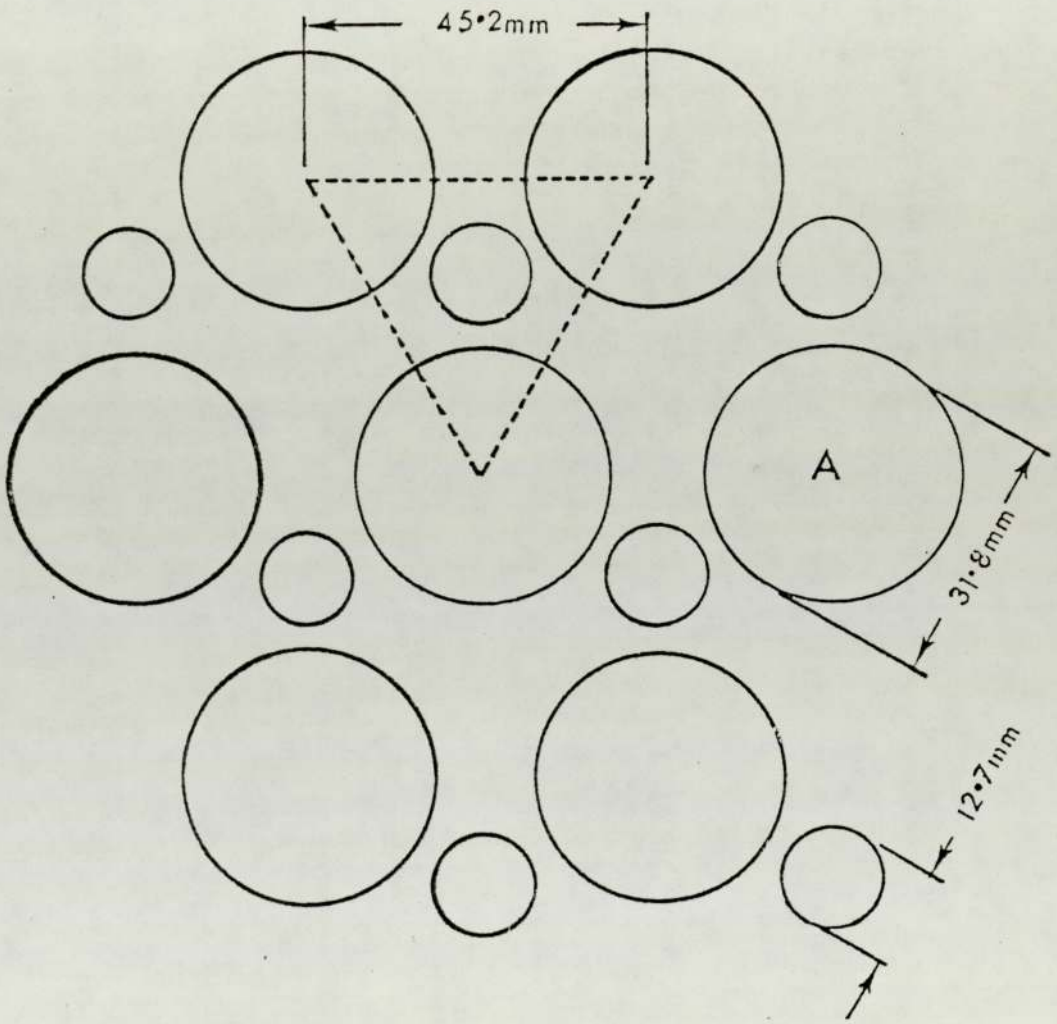

FIG.2.3 Detail of subcritical assembly lattice arrangement & triangular pitch.

titanium minimum thickness 1.09mg cm^{-2}. A more detailed description of the target assembly is given elsewhere[30, 31]. A summary of the most relevant nuclear parameters of the subcritical assembly is presented in Appendix A. A more comprehensive description of the subcritical assembly can be found in references 26 and 19.

2.2 NEUTRON GENERATING SYSTEM:

2.2.1 Neutron generation reaction:

Neutrons, at energy of 14 Mev were produced from a S.A.M.E.S. type J accelerator by using the $T(d,n)^4He$ reaction with an accelerated deutron beam of energy up to 150 Kev incident on the titanium-tritide target type TRT51. The fast neutrons were moderated by graphite pedestal and entered inside the assembly as a plane source from the bottom surface.

2.2.2 S.A.M.E.S. accelerator:

The J type accelerator is composed of three parts:

THE HIGH VOLTAGE ELECTROSTATIC GENERATOR, type K 150.2, positive polarity. The accelerating voltage can be varied from 0-160 KV. THE ACCELERATOR ITSELF, consisting of a chassis and castors to enable it to be moved into position, and containing:

- High voltage electrode: polished casing enclosing the ion source, and focusing voltage generator.
- Horizontal, two-stage, accelerator tube, which can be completely dismantled. It is equipped with a system for

centering the ion source.

- Pumping unit: high speed oil diffusion pump, liquid nitrogen trapped, backing pump and Penning gauge for reading high vacuum.

- Target and accessories: water cooled target supports, secondary electron suppressor polarised at -200 volts, gate valve for rapid target changing.

THE CONTROL DESK containing:

- Controls for vacuum pumps and high voltage generator.

- Controls for top terminal, gas admission into source, oscillator RF power, extraction voltage and focusing voltage. These controls are carried out by the intermediary of isolating transformers.

- Meters for high voltage and current output from generator, high vacuum, target current, and ion current arriving on the diaphragm.

The deutron beam was furnished by the S.A.M.E.S type J accelerator shown in Fig. 2.4. Deuterium gas, from a reservoir, is admitted to the ion source through a thermally activated palladium leak. The ion source is excited by a 100 MHZ oscillator and can produce currents on a target up to about 200μA under favourable conditions of steady running. Excitation into the acceleration system is effected by applying a 0-6 KV repelling voltage to the extraction electrode. The ions are concentrated at the entrance of the extraction canal by the magnetic

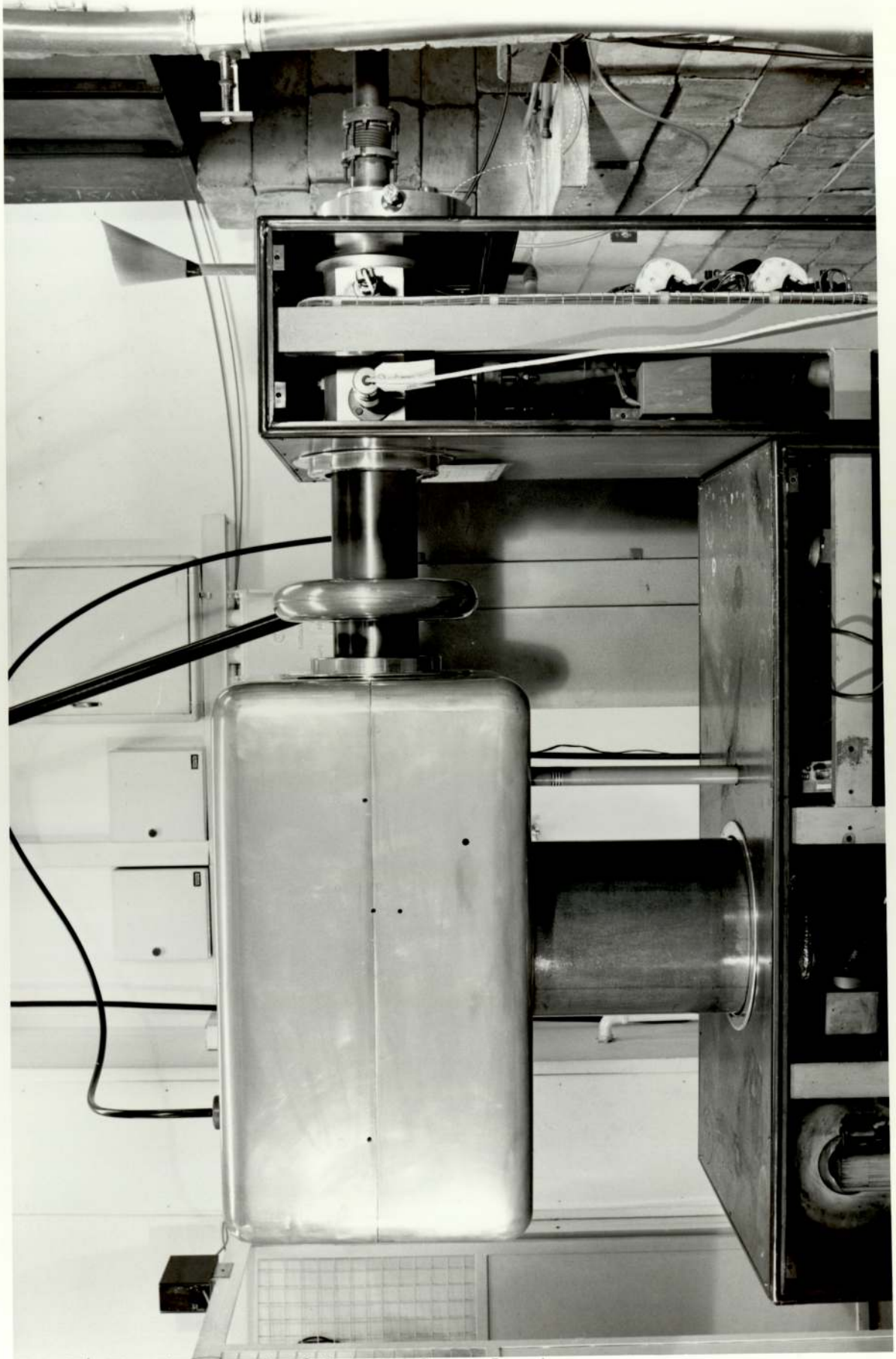

FIG.2.4 The photograph of S.A.M.E.S accelerator

field of the coil located at the base of the ion source bottle. An oil immersed cockcroft-walton multiplier circuit supplies the 0-50 KV required for beam focusing.

2.3 PULSING METHOD:

The S.A.M.E.S accelerator was modified to produce a square waveform ion beam for a wide range of input frequencies because studies of frequency response functions for subcritical systems necessitate a periodic neutron source with a period from less than a millisecond to about 1 second. A sinusoidal variation would be best for analysis but for neutrons produced at an accelerator target, the nearest easily obtained waveform is a square wave.

One important aspect of the present measurement is that the output from the radiation detectors had to be sampled by a multiscaler at regular intervals during each cycle of the neutron pulse. Therefore the pulsing frequency had to be a submultiple of that controlling the channel-advance command of the analyser. Therefore it was necessary to pulse the accelerator with an externally supplied signal in order to maintain synchronism.

A simplified diagram of the S.A.M.E.S (Fig. 2.5) accelerator shows that a pulsed beam could be produced by post acceleration beam deflection or by ion source pulsing. Post acceleration deflection could not be used due to lack of space in the graphite moderating pedestal under the sub-critical assembly.

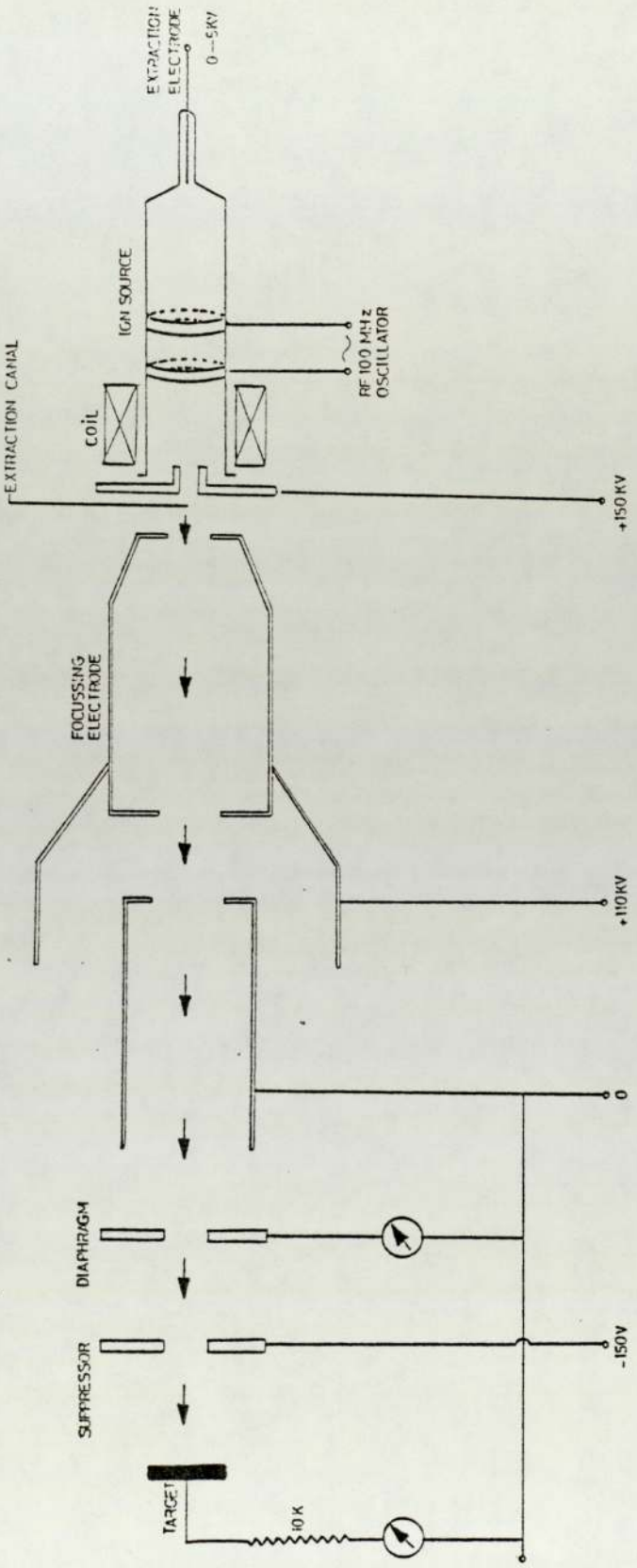

DIAGRAM OF THE SAMES ACCELERATOR (NOT TO SCALE)

However, there are three possible methods available to obtain pulsed neutron beam by modulating the ion source:

(A) Pulsing the R.F. oscillator which causes the ionisation.

(B) Extraction voltage pulsation.

(C) Combination of methods A and B.

Method B, pulsing the extraction voltage, seems at first sight more satisfactory, as the ion source remains operative throughout the whole process. This makes the rise and fall rates of the pulse independent of the time of ionisation and de-ionisation (the minimum rise time is limited to about 2-3 μsec. by the plasma ionisation time[32]). In order to obtain a sharply rising or falling beam current pulse this method calls for very rapid pulses of the order of 5-10 KV at a few milliamps to be applied to the extraction electrode. In view of the difficulties of developing this method for the S.A.M.E.S accelerator and also since a low beam current exists at zero extraction voltage, ion source modulation was chosen.

Both ion source modulation and extractor pulsing involve transmitting a signal to the high voltage terminal containing the ion source through a potential difference of 150 KV.

The radiofrequency signal transmission has been successfully used by Hanna in which he used the high voltage terminal as the receiving antenna [33]. But the

risk of creating stray R.F. fields affecting the upper floors of the building, made it necessary to use a different method.

One of the earliest applications of light beam modulation was to control and telemeter the high voltage terminal of a 4 Mev Van de Graaf accelerator [34]. More recently light pulses have been used to transmit trigger pulses [35]. Particular mention in this respect should be made to works done in Aston University [36],[37] in which the trigger pulses were conveyed to the high voltage terminal by an optical link using semiconductor devices (because of their compactness and cheapness) in the near infra-red region to produce a square beam current waveform.

2.4 RE-ADJUSTMENTS AND MODIFICATIONS OF ELECTRONIC SYSTEM

Fig. 2.6 shows the block diagram of the complete pulsing arrangement. The control signal was obtained at the high voltage terminal by optically linking a light transmitter and photodetector.

A more powerful light emitting diode type FPE104 was selected. This has an output of 10 mw at 100 mA. The narrow beam characteristic of this diode eliminates the need for lenses arranged in the P.V.C. tube. The diode is coupled into the collector circuit of an 2N3053 (npn) transistor with maximum power of 800 mw, this is fed with square wave output derived from a frequency dividing circuit consisting of two integrated circuit semiconductor

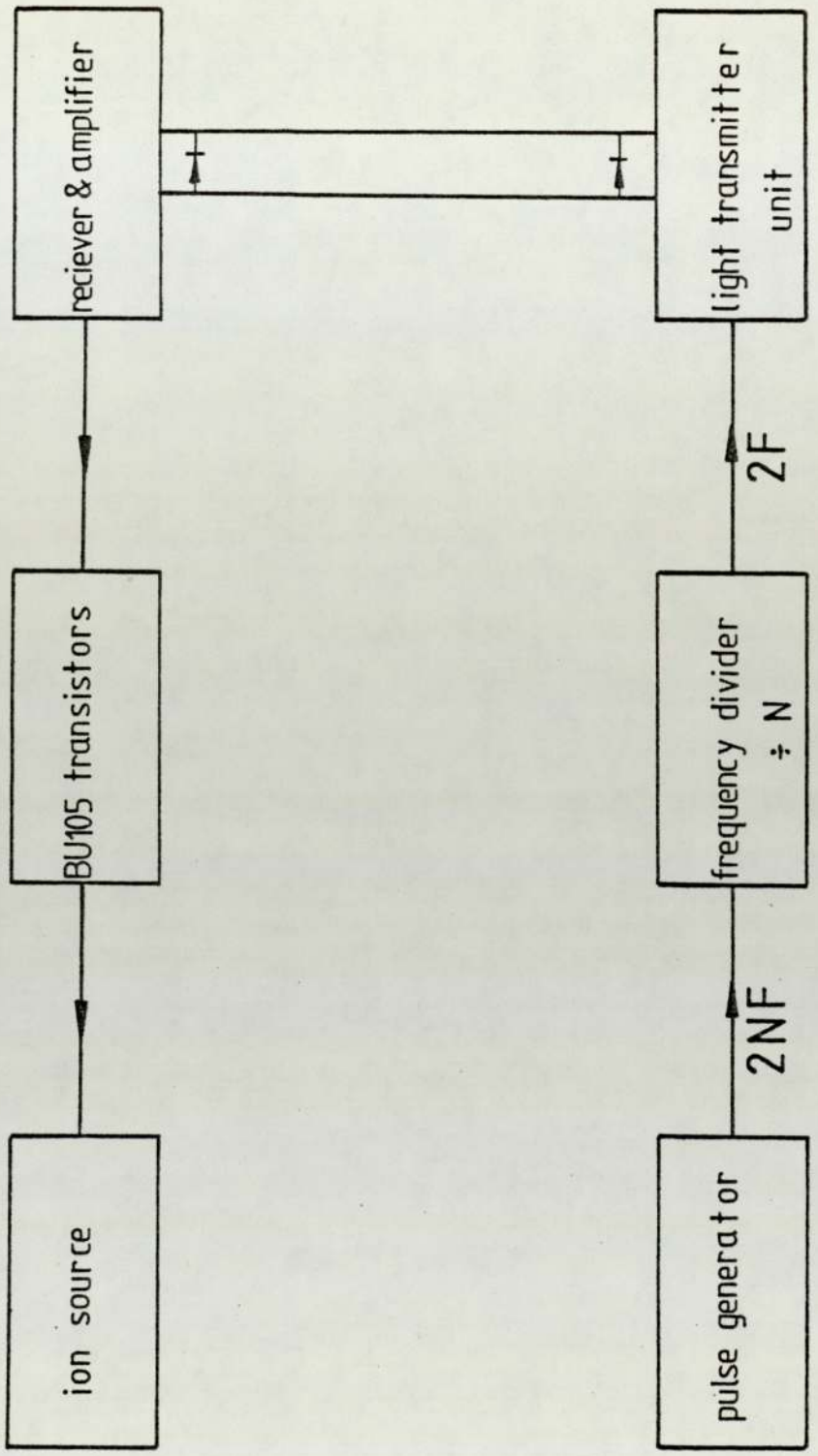

FIG.2.6. Block diagram of complete pulsing arrangement.

network type SN7490AN. Figs. 2.7 and 2.8 give circuit details of the light transmitter unit and frequency divider respectively.

The frequency divider was improved by adding ÷100, so that when using two detectors the detector order for the analyser (RIDL, used as a 100 channel) is fixed. Also, for resetting the integrated circuits a reset circuit was added on the frequency divider circuit.

The choice of light receiver was a compromise between speed of response and sensitivity. The photo detector used was an LS400 (npn) planar silicon photodevice with a sensitivity of 300 $\mu A mW^{-1} cm^2$, a rise time of 1.5μsec. and fall time of 15 μsec. This was followed by an amplifier and emitter follower giving a waveform closely following the transmitted light signal with an amplitude of about 3 volts. Improvements were also introduced on the light receiver unit Fig. 2.9 by adding a Darlington pair, based on the two BU105 transistors, to switch the oscillator high tension more effectively as a single transistor used in [37] was not found to give good cut-off to high tension under certain operating conditions. This improvement made beam pulsing mush more reliable.

The FPE104 emitting diode and LS-400 receiver were mounted on a heat sink at the lower end and top end of a light tight P.V.C. tube respectively, which ran parallel to the main vertical insulating column, as shown by the

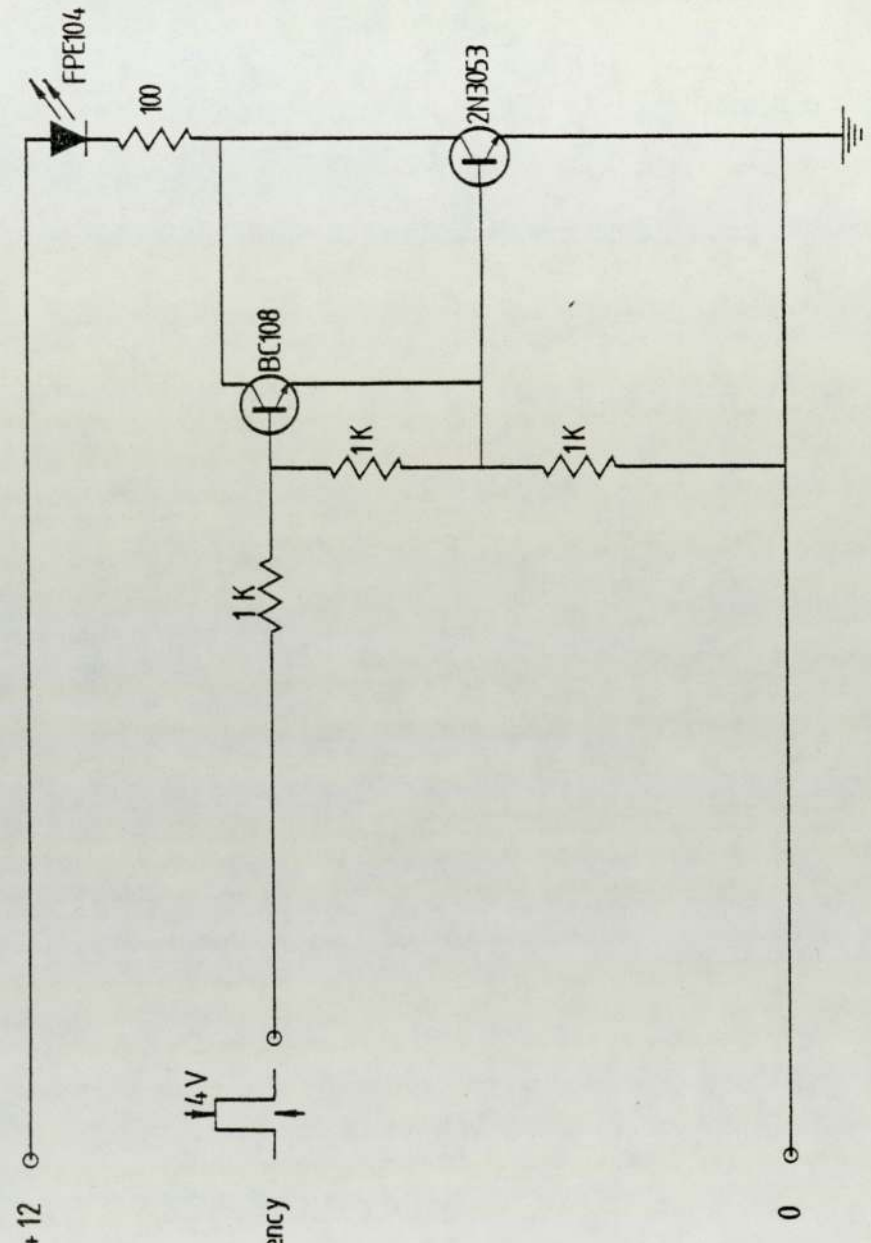

FIG. 2.7. Driver and transmitter circuit diagram.

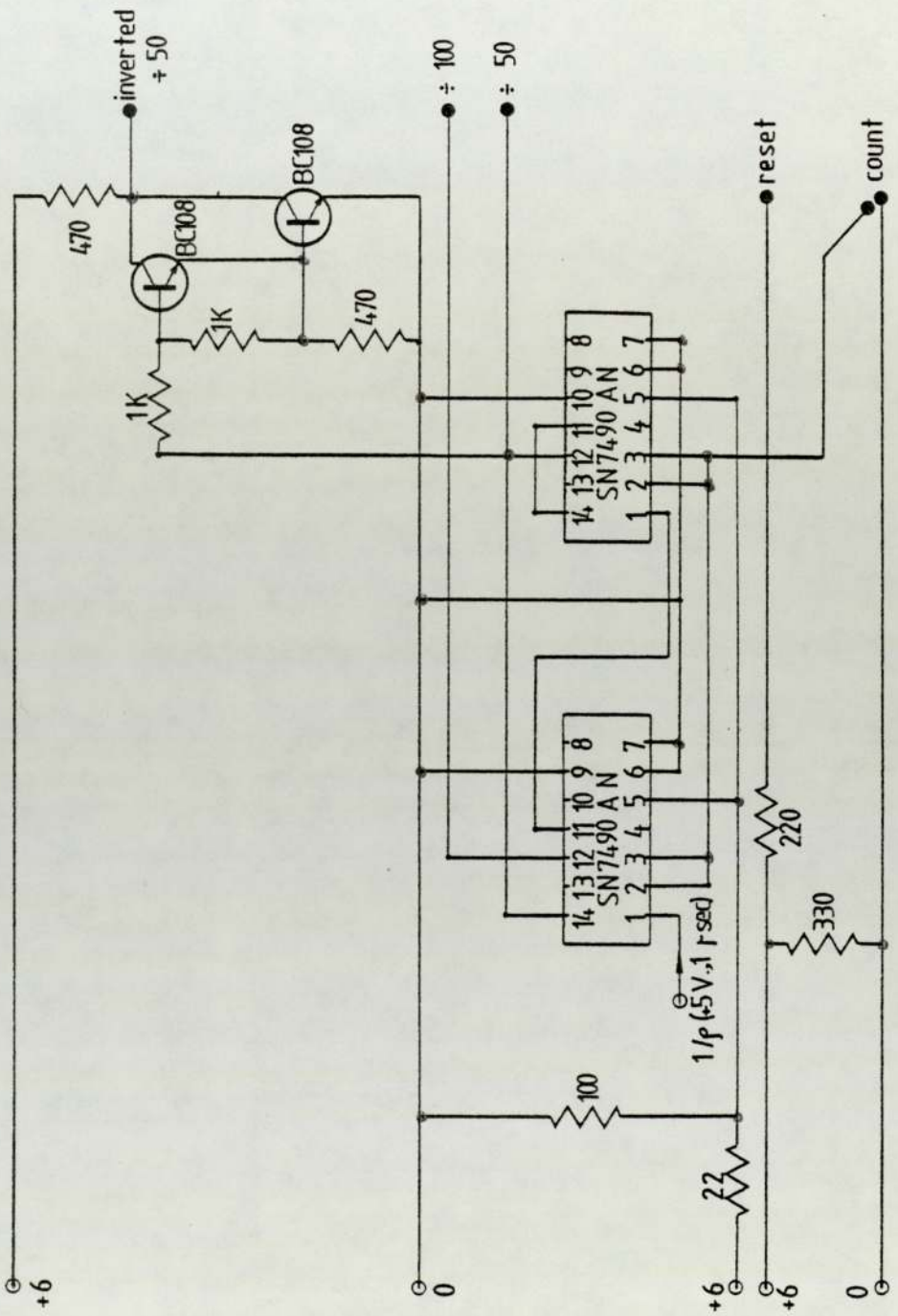

FIG.2.8 Frequency divider circuit diagram .

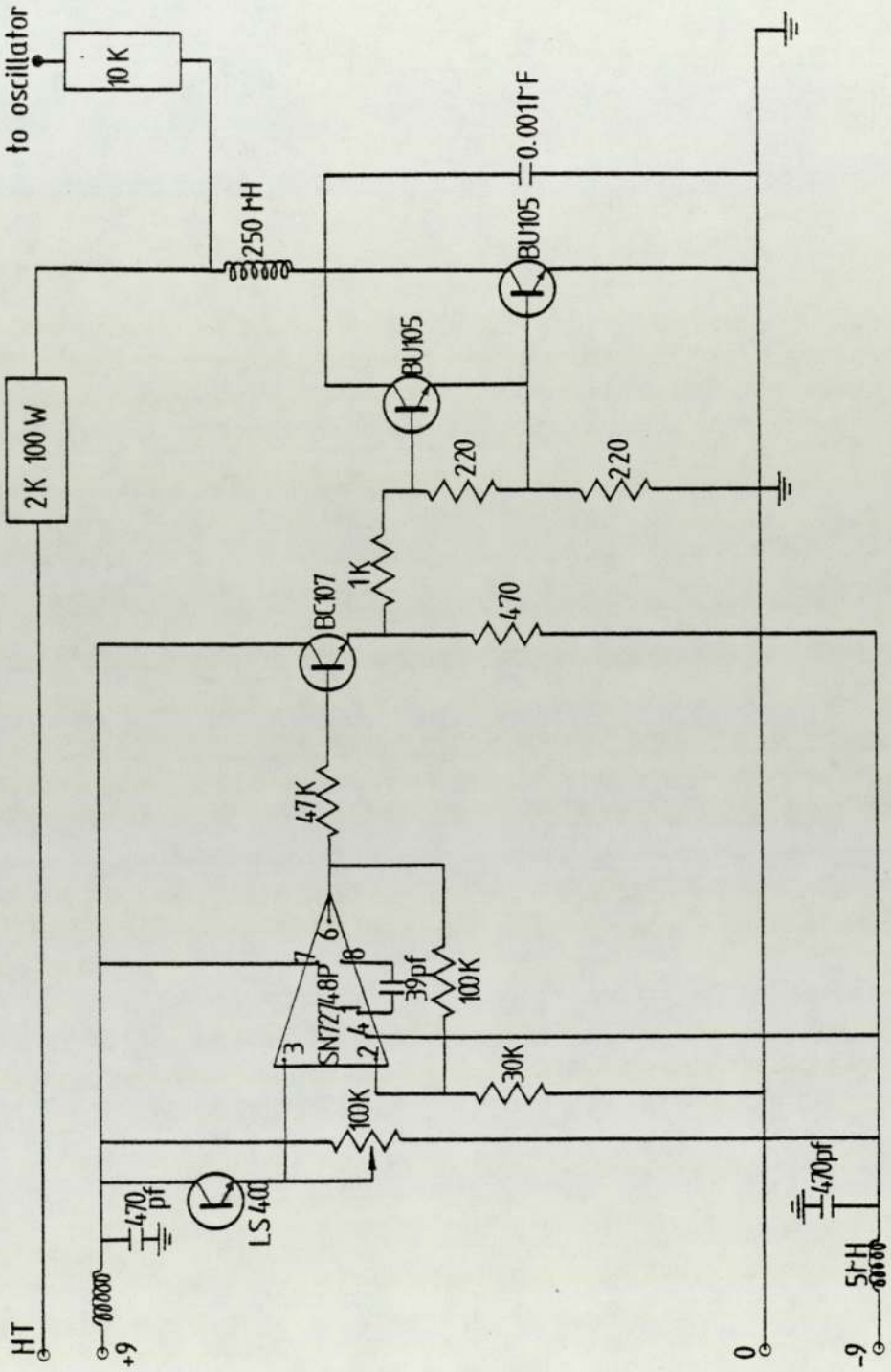

FIG.2.9. Light receiver circuit diagram.

photograph (Fig. 2.10). The receiver was enclosed inside a 60mm deep cavity and placed on the base plate of the high voltage terminal and was coupled to the heat sink of receiver diode. This arrangement, provided adequate screening from the R.F. produced by the ion source oscillator.

2.5 ION SOURCE PULSING:

The voltage variation to the anode of QQV06-40A double tetrode, was made by using two high voltage (npn) transistors type BU105 in Darlington pair (Fig. 2.11) to switch the H.T. to earth. A 2K 100W wirewound resistor was inserted into the high tension lead between the power pack and the BU105 to act as a current limiter . In addition, a stabilised power supply giving 400 volts at up to 200mA was used instead of the simple LC smoothed supply original to the S.A.M.E.S. This led to much more uniform beam currents during the on half of the cycle, particularly at lower frequencies.

2.6 MEASURING SYSTEM:

The variation of high energy gamma ray population emerging from the subcritical assembly was monitored as follows: In all measurements two detectors were used simultaneously. One of them, a fast neutron scintillation detector with a type NE213 liquid scintillator was used to monitor fast neutron production from the target. This detector should ideally have been placed inside the

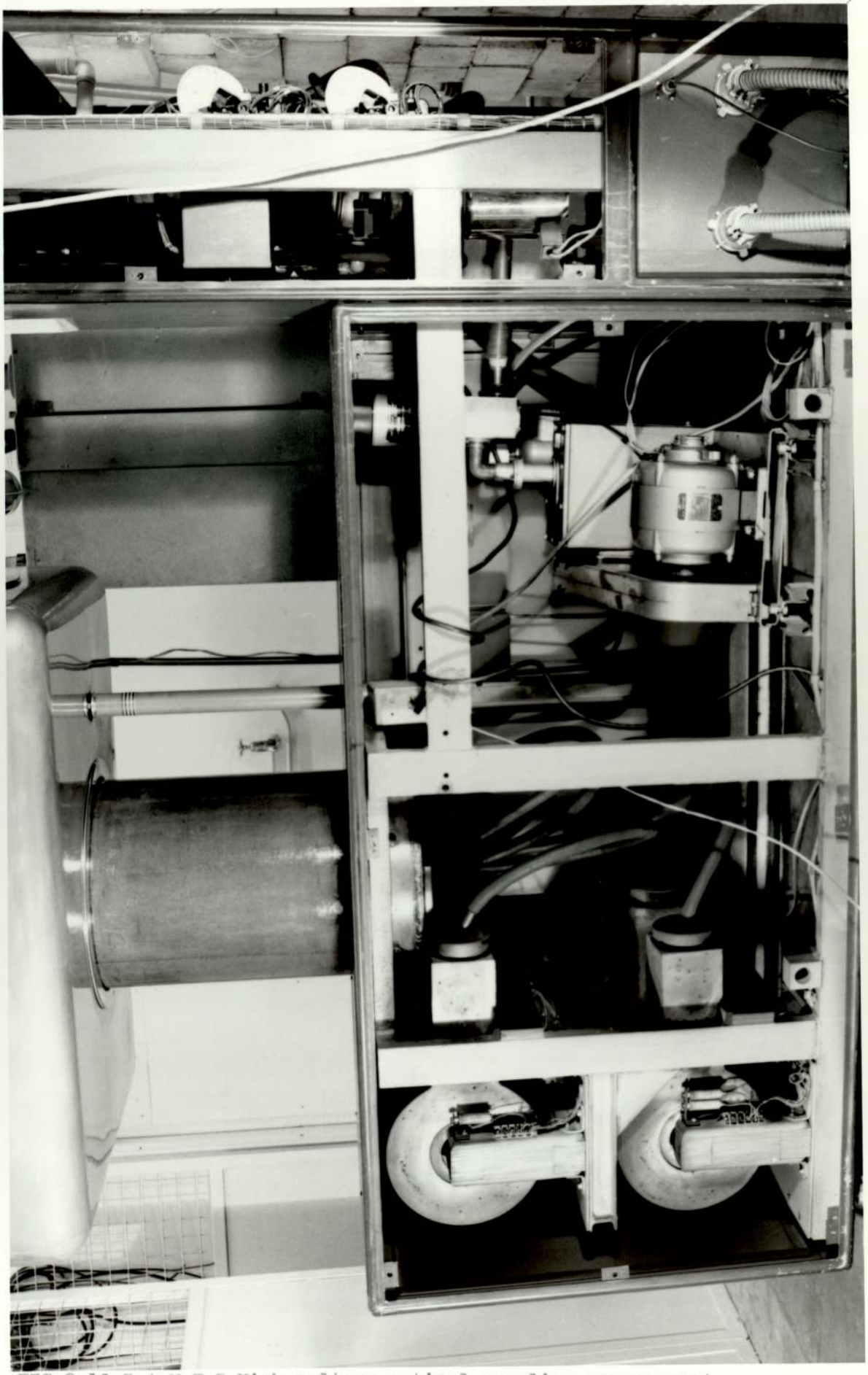

FIG.2.10 S.A.M.E.S High voltage optical coupling arrangement

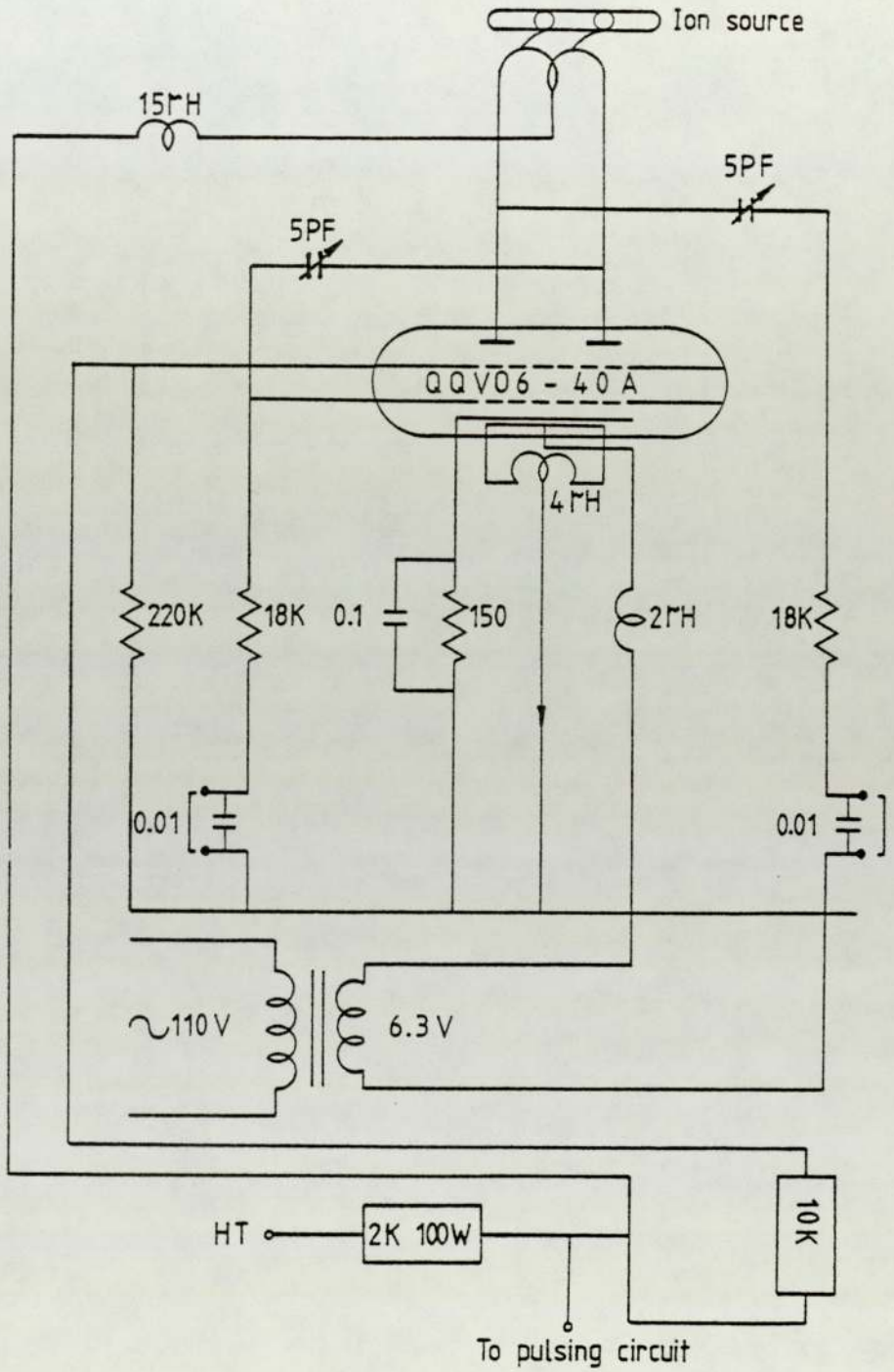

FIG.2.11. SAMES 100 MHZ oscillator showing link with pulsing system.

graphite near the target, but due to lack of space the detector was always placed at the front end of the graphite pedestal very near to the beam tube entrance to the graphite. This was used to find the best running condition for the machine (gas, R.F ,HT) to get a good square wave of fast neutrons and also permitted the direct comparison between phase and amplitude of square fast neutrons and produced prompt high energy gamma rays. The gamma ray detector was placed in the front side of the subcritical tank in the same plane but at different height (Fig. 2.12).

2.6.1 Gamma detectors:

All nuclear radiation detection is based on the interaction of the radiation with matter. Electromagnetic radiation gives rise to energetic electrons by one of the three processes, namely photoelectric effect, Compton scattering and pair production. It is easily understood that for gamma-ray spectrometry, only interactions are important in which the photon loses all its energy. This eliminates the Compton effect which results in a partial absorption of the electromagnetic radiation. Gamma ray-spectroscopy is almost entirely based on scintillation detectors and semiconductor detectors. The gas type detectors were not considered because of having very low stopping power for high energy gamma rays. Two important properties considered in the choice of detector were the detector efficiency and the neutron response. The high

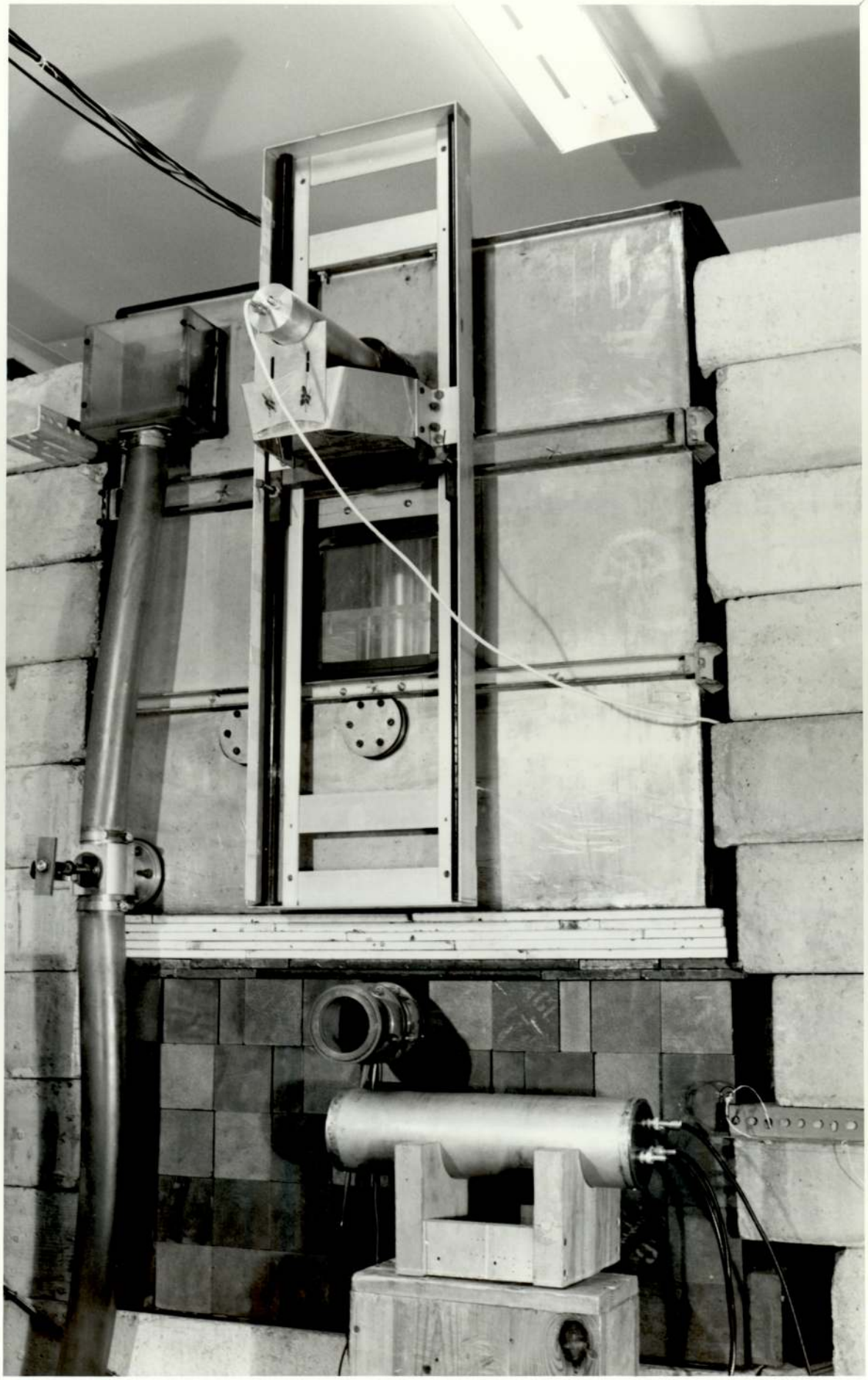

FIG.2.12 Fast neutron and gamma detectors locations.

Z detection material is to be preferred to enhance interaction by the photoelectric effect ($\delta_{pE} \simeq \lambda Z^5$) and a lesser extent by the pair production process ($\delta_{pp} \alpha Z^2$) [38]. The two more useful detectors from each class of gamma-ray detectors were considered to find out which is best for our purpose:

a. Semi-conductor detectors:

Lithium drifted germanium, |(Ge(Li)| detectors are more suitable than Silicon detectors for the detection of electromagnetic radiation. It may be recalled that the photoelectric and pair production cross sections are proportional to Z^5 and Z^2 and therefore germanium (Z=32) is more efficient than silicon (Z=14) for detection of gamma rays [39]. The much better resolution of the solid state detectors, compared with scintillation detectors, is offset by two means. One is the lower atomic number of germanium. Consequently, this detector has a poor efficiency for gamma ray detection [40] compared to the alkali-halide scintillation detectors (Iodine has an atomic number of 53). The other is that its excellent energy resolution would be unimportant in the present measurements because we are concerned with a very broad spectrum. The main disadvantage with the detector is its sensitivity to neutrons, particularly fast neutrons. Radioactive capture processes are the main detection mechanism for slow neutrons i.e. energies below about 0.5 Mev. The (n,γ) cross section for germanium is 2.4 barns for thermal

neutrons [41]. The main fast neutron processes are the $(n,n'\gamma)$, (n,P) and (n,α) reactions. Both the (n,p) and (n,α) reactions, besides causing prompt neutron detection, generally produce unstable reaction products [42]. It has a very high susceptibility to be damaged by continuous exposure of fast neutrons. Fast neutrons produce crystal defects, mainly radiation damage, and affects the energy resolution of the detector. Ortec, one of the manufacturers of Ge(Li) detectors, state that a rapid deterioration is produced by a fast neutron exposure of more than 10^8 neutrons Cm^{-2}.

b. Scintillation detectors:

Gamma rays passing through matter (i.e. the detector) transfer part or all of their energy to electrons. These secondary electrons dissipate their energy in turn by ionisation or excitation of the molecules. The detector consists of a luminescent material, i.e. the de-ionisation and de-excitation of the molecule results in the emission of a fluorescent radiation. In other words, the scintillator converts a fraction of the obtained energy into photons. As the direction of these photons are random, the Scintillator is generally surrounded by a reflector which maximises the number of photons collected on a photosensitive cathode. This cathode is part of a photomultiplier. Most of the collected photons cause the ejection of photoelectrons from the cathode. The photoelectrons are accelerated by the applied potential field towards the

first dynode. Striking the latter, they release secondary electrons which in turn eject ternary electrons from the second dynode and so on until a large charge pulse is finally collected at the anode.

Typical multipication factors range from 10^5 to 10^8. The voltage pulse produced is determined by the capacity of the anode and output cable and can be further amplified by an external electronic amplifier.

Scintillators particularly suited for gamma ray detection are sodium or caesium iodides activated with thallium as they have high photoelectric detection efficiency. The caesium iodide-thallium activated is probably the most used scintillator for gamma ray detection. Owing to the built-in advantages of higher atomic number for the caesium (Z=55), this scintillator has especially high photoelectric efficiency. The linear attenuation coefficient δ, τ, χ are about 1.47, 1.56 and 1.42 times those of sodium iodide [43,44] where δ, τ, χ are the Compton and photoelectric and pair production attenuation coefficients respectively. Large crystals have become available. It appears that with a 5X3.5in.caesium iodide crystal the photofraction obtained equals that of a 8X8in. sodium iodide crystal. The resolution is comparable to that obtained with sodium iodide crystals of equal dimensions. For scintillation spectrometry of highly energetic gamma rays, the use of caesium iodide has some other advantages: [44]

- The shape of the spectrum is very similar to the shape of the spectrum obtained with sodium iodide.
- The caesium iodide is almost non-hygroscopic, the crystal can easily be machined and packed.
- Caesium iodide being softer and more plastic, can withstand severe shocks, acceleration, and vibration, as well as large temperature gradients. This scintillator can be considered as an important alternative to sodium iodide. However, in the present work, the use of the caesium iodide detector was not thought to be justified due to the much greater cost.
- Sodium iodide-thallium activated is a water-clear, quite hygroscopic [45], cubic crystal. It is a very dense material, 3.67 gr.cm^{-3}, and Iodine atomic number is 53; these make it very good gamma ray absorbing material with a very good gamma-ray detection efficiency. On the other hand, the NaI(Tℓ)detector is sensitive to neutrons.

Because of the variation of neutron reaction cross-section with energy, the neutron response is very energy-dependent. For slow neutrons, the main process is radiative capture in iodine. This reaction cross-section is 7.0 barns [46] for thermal neutrons. Neutron capture in iodine will increase the background due to 25min. decay of ^{128}I to ^{128}Xe. The predominant neutron detection mechanism in the fast neutron energy range (0.5 Mev-14.5 Mev) is by inelastic scattering [48]. In the lower energy end, the induced activity is mainly due to the (n,γ) reaction, and at the high energy end of the range, (n,2n)

and (n,p) reactions with the iodine. These reactions, which again lead to an increase in the background, have cross-section of 1.3b. and 230mb. respectively for a neutron energy of 14.5 Mev [46].

As a result of compromise between neutron response and detection efficiency, the NaI(Tℓ) scintillator detector was used for present measurements. Adequate detector-shielding was arranged to protect the crystal from exposure of neutrons.

Detector specifications:

The NaI(Tℓ) crystal (size 43.94mm. dia. X 25.4mm. thickness) was optically coupled to an EMI 6097B photo-multiplier. The detector was used in connection with charge sensitive amplifier-discriminator unit type NM 115. The high tension for the detector was provided by an NM 120 unit. The discriminator threshold voltage was set to eliminate pulses below 2.5 Mev. This would cut off detecting γ-rays less than these energies which were not considered as prompt fission gamma-rays, such as the capture gamma ray from hydrogen.

2.6.2 Gamma detector shielding:

The detector shield should provide:

1) absorption of slow neutrons. (Fast neutrons are to a large extent, moderated by water and graphite reflectors).
2) absorption of secondary penetrating radiation such as low energy gamma-rays.

There are three widely used materials for slow neutron absorption:

a) Cadmium ; b) Boron ^{10}B ; c) Lithium ^{6}Li

a) Cadmium is a very efficient thermal neutron absorber. The absorption is radioactive capture process with a cross-section of 2.445 Kb.[48] at thermal energy. The many hard gamma-rays emitted in a single capture process make it unacceptable for use in a neutron shield requiring a low gamma-ray background.

b) Boron ^{10}B: has an isotopic abundance of 19.8±0.1%[49,50]. It was not chosen as a shield because of domination of $^{10}B(n,\alpha)^{7}Li^{*}$ reaction. Its cross-section is 3840 barns for 0.0253 ev neutrons. In 94 per cent of the reactions, the nucleus is formed in an excited state giving rise to a 0.424 Mev gamma-ray.

c) Lithium ^{6}Li: The dominant neutron reaction on lithium in thermal neutron range is the $^{6}Li(n,\alpha)^{3}H$ reaction. Its cross-section is 945 barns at 0.0253eV and more important, there are no gamma-rays produced. Lithium has radiative capture cross-section of 70.4m barn. Also, the lithium neutron scattering cross-section is negligible, compared with the capture cross-section. $^{6}_{3}Li$ abundance is 7.42 per cent.

For these advantages ^{6}Li was chosen as a shield in the form of Lithium metal for compactness and it was cast inside a stainless steel cap as shown in Fig.(2.13). The detector was protected from thermal neutrons as follows:

40mm. from the front and 40mm. from the side for shielding the NaI (Tℓ) crystal, and 20mm. in the front end

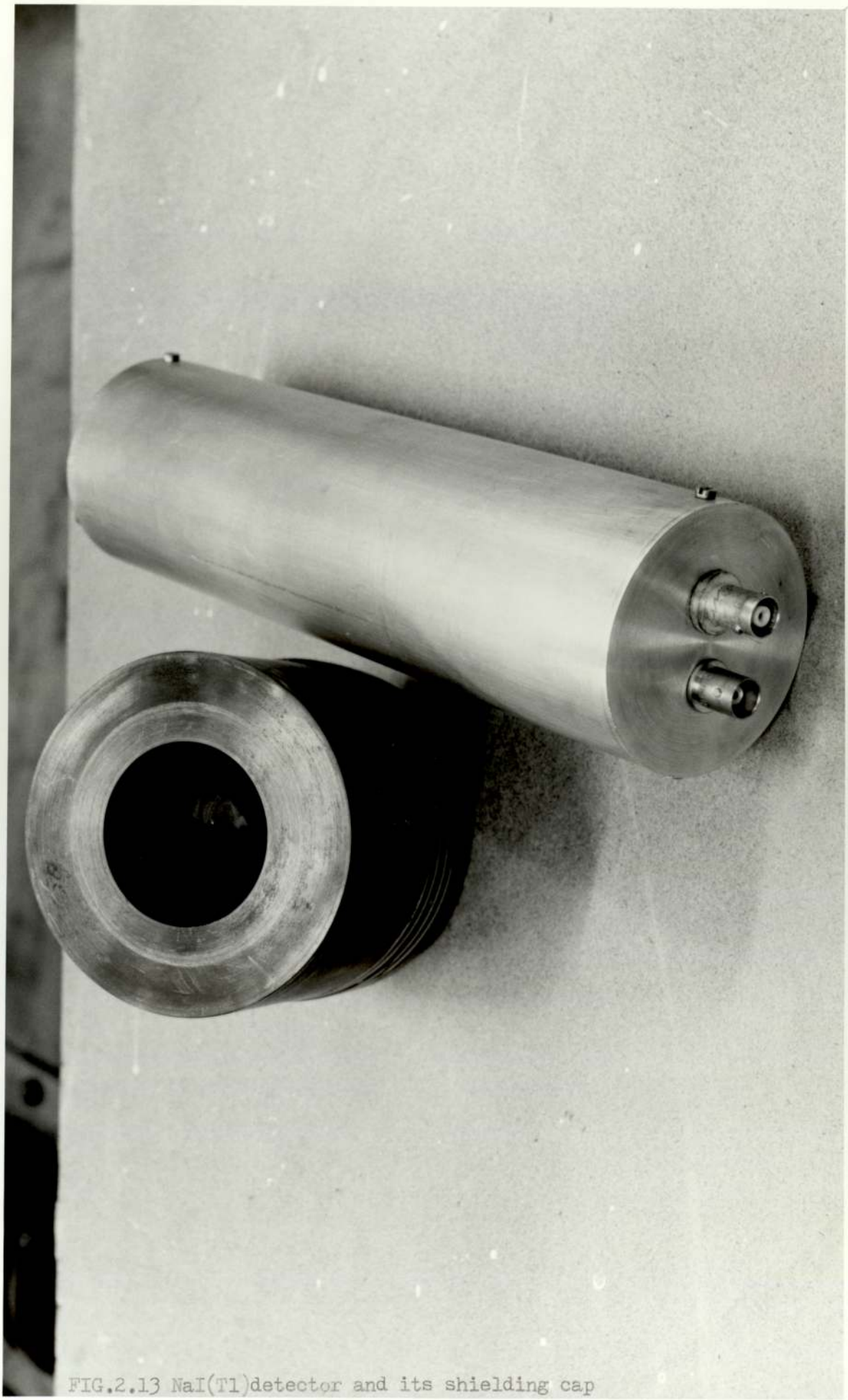

FIG.2.13 NaI(Tl)detector and its shielding cap

end of the photomultiplier tube. The shield was 84mm. in diameter.

A lead foil of thickness 3mm. was placed between the detector and ^{6}Li shield to strongly attenuate the low energy γ-rays produced by radioactive decay of the uranium.

The detector was placed outside the subcritical assembly, (Fig. 2.12), horizontally in a central position in the front side. Different axial positions were achieved by sliding the detector upwards and downwards.

2.6.3 Fast neutron detection:

There has been in use for some years, a fast neutron based on detection of recoil protons in a scintillation spectrometer using NE-213 liquid organic scintillation and gamma ray background was rejected by pulse shape discrimination using the Zero Crossing Technique to reject the gamma rays.

A capsule of NE-213 liquid scintillator 25.4mm. high by 38 mm. dia. was chosen for the present work. The scintillator is glass encapsulated and was purged with pure nitrogen to remove the undesirable oxygen which selectively quenches the slow component of light emission [51,52,53].

The Zero Crossing makes use of information contained in the time dependence of the current pulse of the photo-

multiplier. The current pulse is formed by two components one of short decay time and the other with a longer decay time. The energy contained in the longer term decay component is different for electron and proton, assuming equal recoil energies. When the pulses are integrated and differentiated by two successive differentiating networks, a bipolar pulse is produced whose cross-over point is different for neutrons and gamma rays.

The NE-213 Liquid scintillator was mounted on a fast 14 stage photomultiplier type 56AVP[52]. A block diagram of the spectrometer and the dynode chain used is shown in Fig. (2.14). This type of photomultiplier has a high degree of time definition and a high time resolution which are required for fast measurements. The cathode is operated at - 1900 volts and the anode near earth potential. A high voltage supply capable of supplying ∿2mA to the dynode chain is necessary. The pulse at dynode 10 is developed across a resistor between the dynode and the voltage chain and is applied to a charge sensitive preamplifier which has a 50μs decay time. Further amplification and double differentiation are accomplished in the main amplifier to give an output of bipolar voltage pulses which pass through the base line at different times depending on the shape of the input pulses, but independent of their amplitude. Measuring of the width of these pulses is difficult to perform in practice owing to the necessity of triggering the measuring instrument. To overcome this

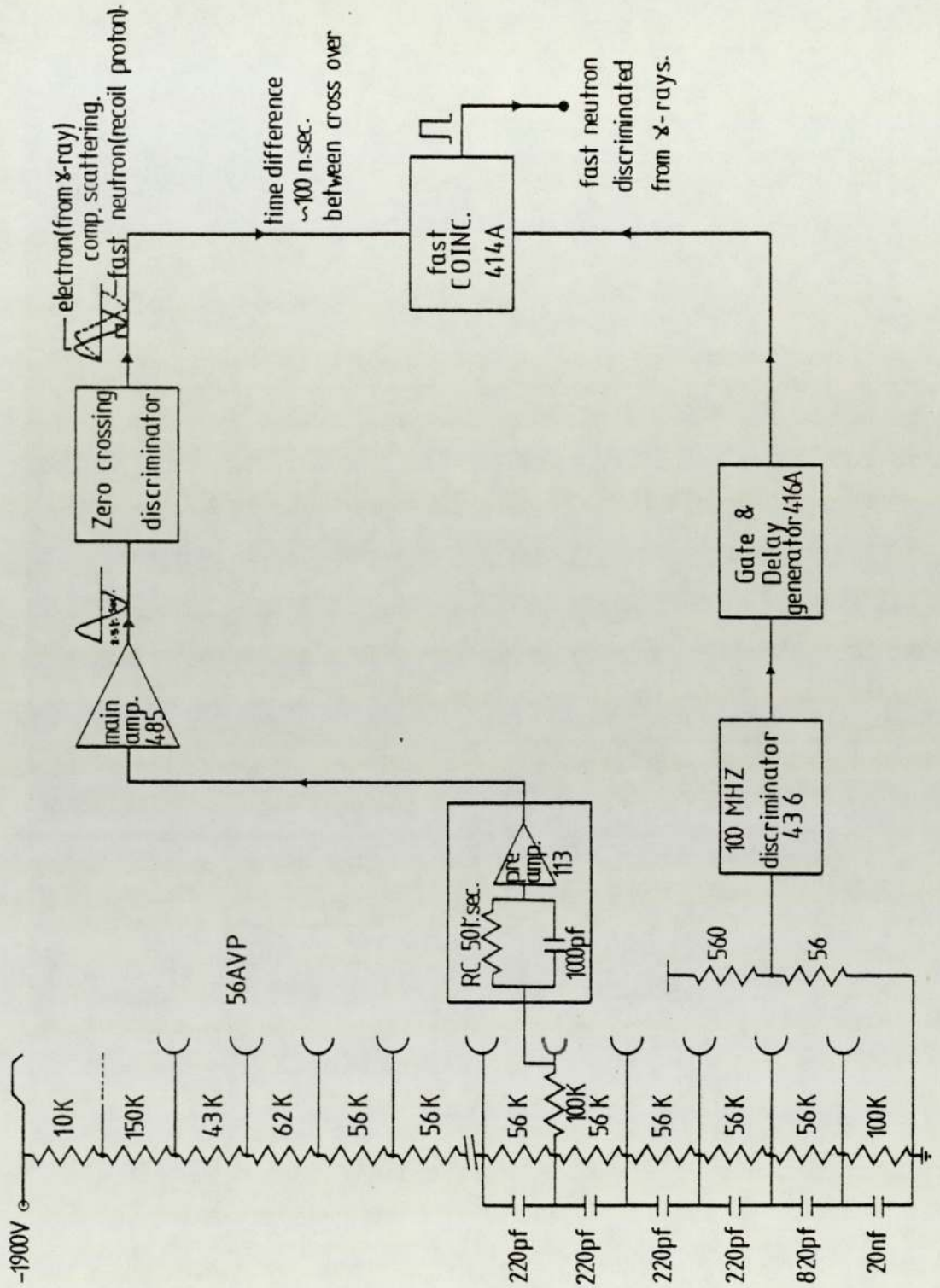

FIG.2.14 The block diagram of fast neutron spectrometry.

problem the anode current pulse was used as a zero time reference and the time difference between this signal and the zero crossing of the dynode voltage pulses was measured.

The zero crossing discriminator was used to measure the zero crossing times of these doubly differentiated pulse. Small time differences are commonly measured by time to pulse amplitude converters which produce output signals of amplitude proportional to the time difference between the input signals. In the system the time to amplitude converter is substituted by a coincidence system. The pulse shape discrinination is set up by measuring the count rate at the output of the coincidence as a function of the delay in the delay and gate generator.

This detector was simultaneously used with gamma detector to monitor the square wave fast neutrons produced from the accelerator. The detector was located always in the front side of the graphite very near to the ion beam tube. Fig. (2.12) shows the fast neutron detector location.

2.7 DATA ACQUISITION SYSTEM:

The block diagram of the experimental set-up, including the pulsing network and detection, together with the data acquisition system is shown in Fig. (2.15). Data acquisition was with a RIDL (Nuclear Chicago), model 24.2, 400 channel analyser. This was used in Time Sequence

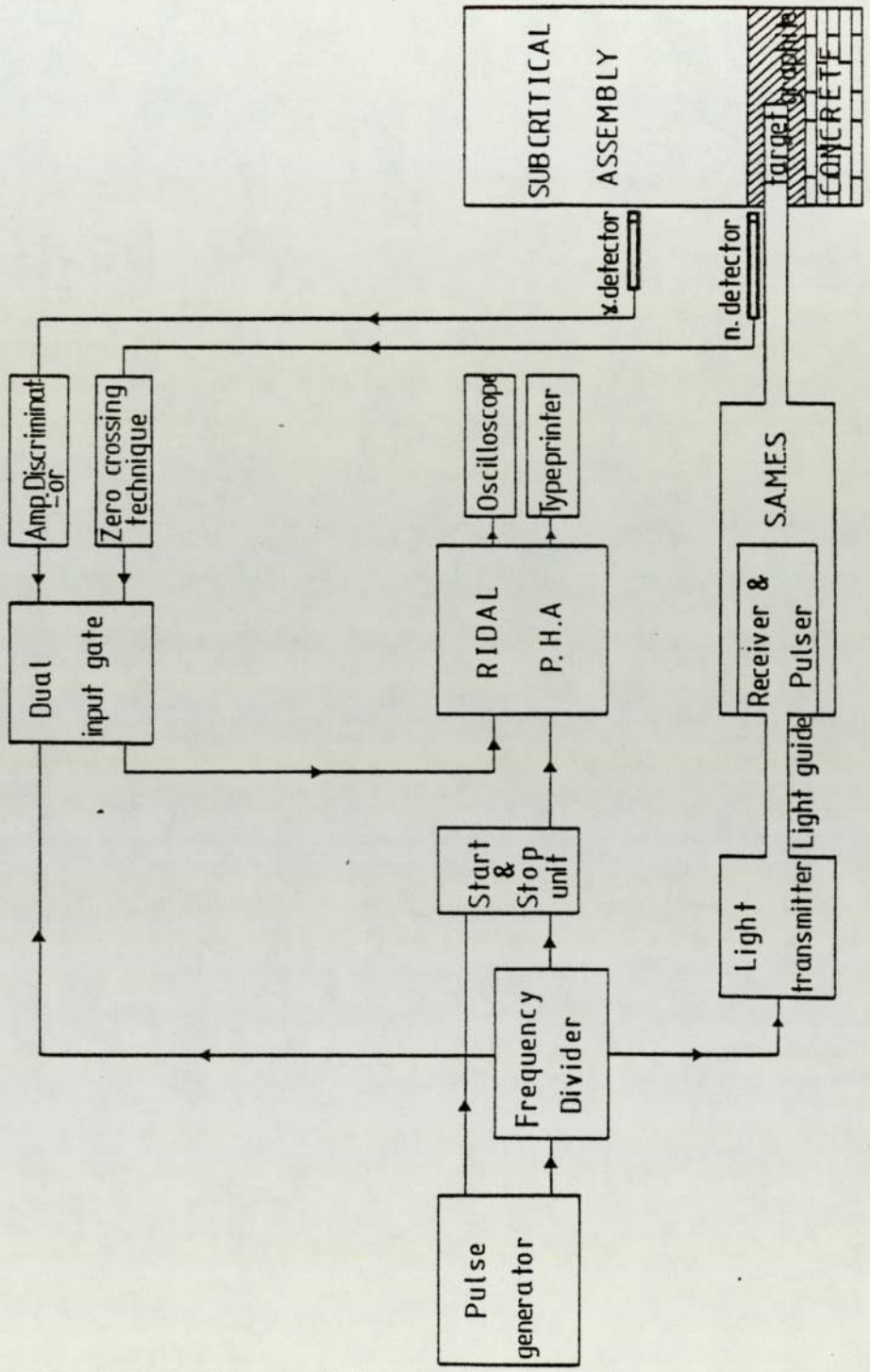

FIG 2.15 Block diagram of the experimental set-up.

Storage (T.S.S.) mode and as a 100 channel analyser. In (T.S.S.) mode, each channel accepts the number of pulses delivered to the analyser during a fixed time interval. i.e. each channel records the number of count between time t and t+dt, where dt is the channel width.

Two input signals were fed into the analyser;

(i) signals input from the detectors.
(ii) the channel-advance address signal.

The total time required for a 100 channel sweep is 100 dt. As both detectors were used simultaneously, the signal from each detector was fed into the analyser for an alternate period of 50dt. By this procedure, each half of the analyser memory was allocated to the same detector.

The required signals to control the whole experiment arrangement were supplied by a Farnell modular pulse generator giving signals identical in frequency but with different heights and polarities. The channel-advance address command of the P.H.A. was triggered by one of the signals of the pulse generator, negative, of 10 volt amplitude and 1 μ. sec. duration.

The other signal from the pulse generator, positive, of 6 volt amplitude, 1 μ . sec. duration and frequency F(HZ) (same frequency for negative pulse) was fed into the frequency divider network as described in Section 2.4. The divider unit produces square pulses of +4 volt amplitude of frequency $F/_{50}$, $F/_{100}$, which were used to control

the following networks:

(i) The driver and transmitter for the external pulsing with frequency $F/_{50}$.

(ii) A dual input gate unit, with frequency $F/_{50}$.

(iii) A start-stop unit, with frequency $F/_{100}$.

The Dual input gate diagram is shown in Fig. (2.16). Basically, it is a bistable circuit based on BC107 (npn) transistors. This unit is used to gate the input pulses coming from one detector while the pulses from the other detector were allowed to pass through. When a positive voltage is applied to the base of one of the transistors, it conducts and the signal is earthed through the diode OA200. At the same time, the other transistor is not conducting and a positive voltage is being applied to the anode of the diode, thus allowing the pulses to be transmitted.

The P.H.A. memory requires signals of +12 volt in amplitude and 1 μ . sec. duration, so the pulses had to be amplified and shaped to be compatible to the analyser requirements. To eliminate the random-starting of the P.H.A. and to provide the first 50 channels for one detector and the other 50 channels for the second detector in the whole experiment, a start-stop unit was used. This unit synchronizes the first channel address advance signal reaching the P.H.A. with the detector gate triggering pulse.

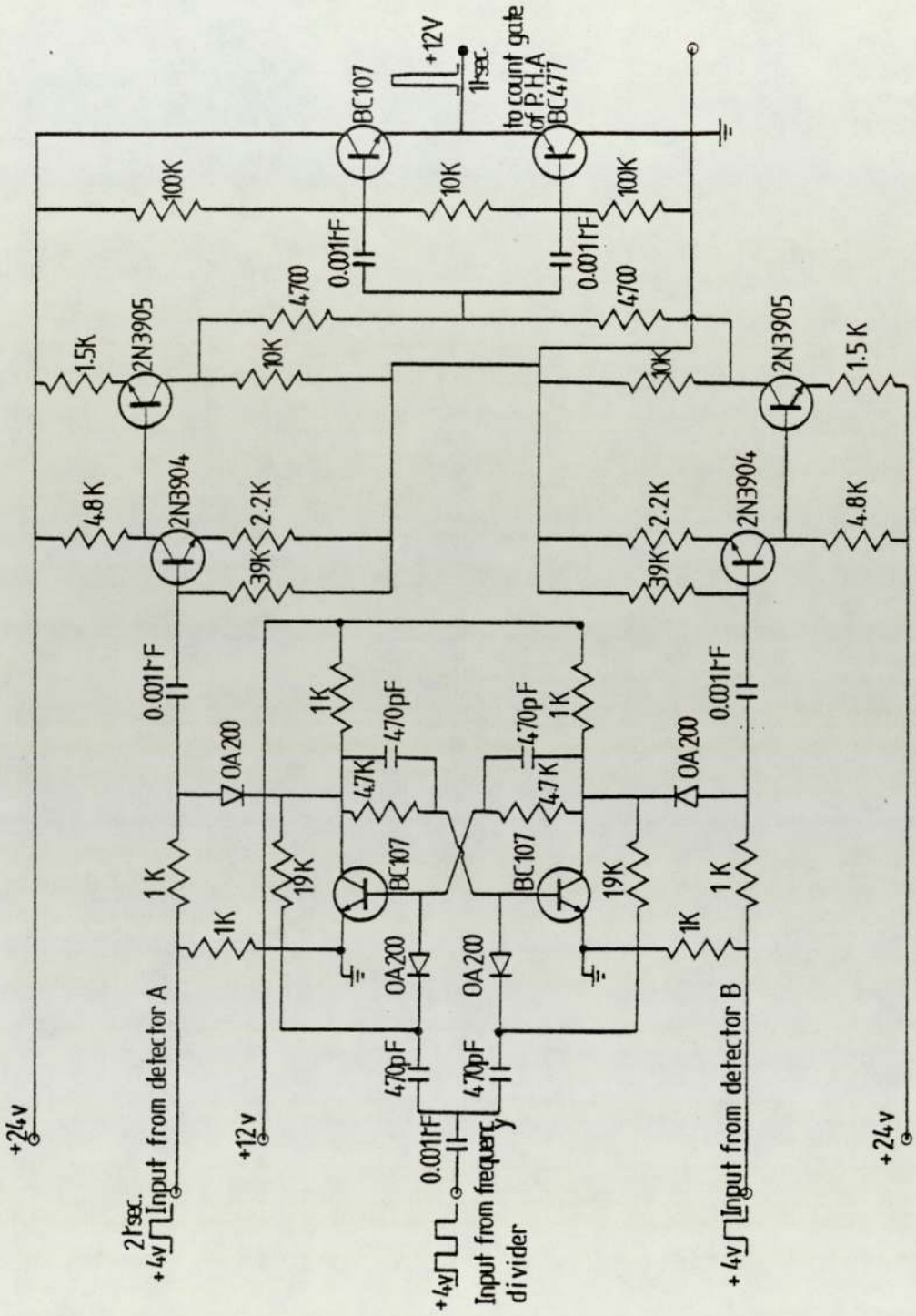

FIG 2 16 Dual input gate circuit.

This synchronization was achieved by using a set-reset bistable circuit gating unit based on BC477 (PnP) transistors. $F/_{100}$ signal from the frequency divider was used as a triggering pulse to allow the -10 volt signals to path through. The network of start and stop unit is represented in Fig. (2.17).

2.7.1. Measurement procedure:

The following procedure had to be followed in every measurement:

(i) The start-stop unit was stopped by pushing stop button. Therefore no pulses reached the channel advance command of the P.H.A.

(ii) The P.H.A. was started by pushing the start push button. As the channel advance signal did not reach the P.H.A.,all pulses reaching the P.H.A. from the detectors were stored in the first channel.

(iii) The start button of the start-stop unit was pressed to allow channel advance pulses to reach the channel advance command of the analyser.

(iv) The recording of pulses was stopped at any required time either by stopping the P.H.A. or the start-stop unit.

(v) Finally, the output of the measurement was displayed on an oscilloscope and also recorded on a typewriter.

Figs.(2.18) to (2.23) show the photographs of the output for different frequencies (F) and gamma detector height (H) on the oscilloscope. First fifty channels correspond to fast neutrons and the second fifty to gammas.

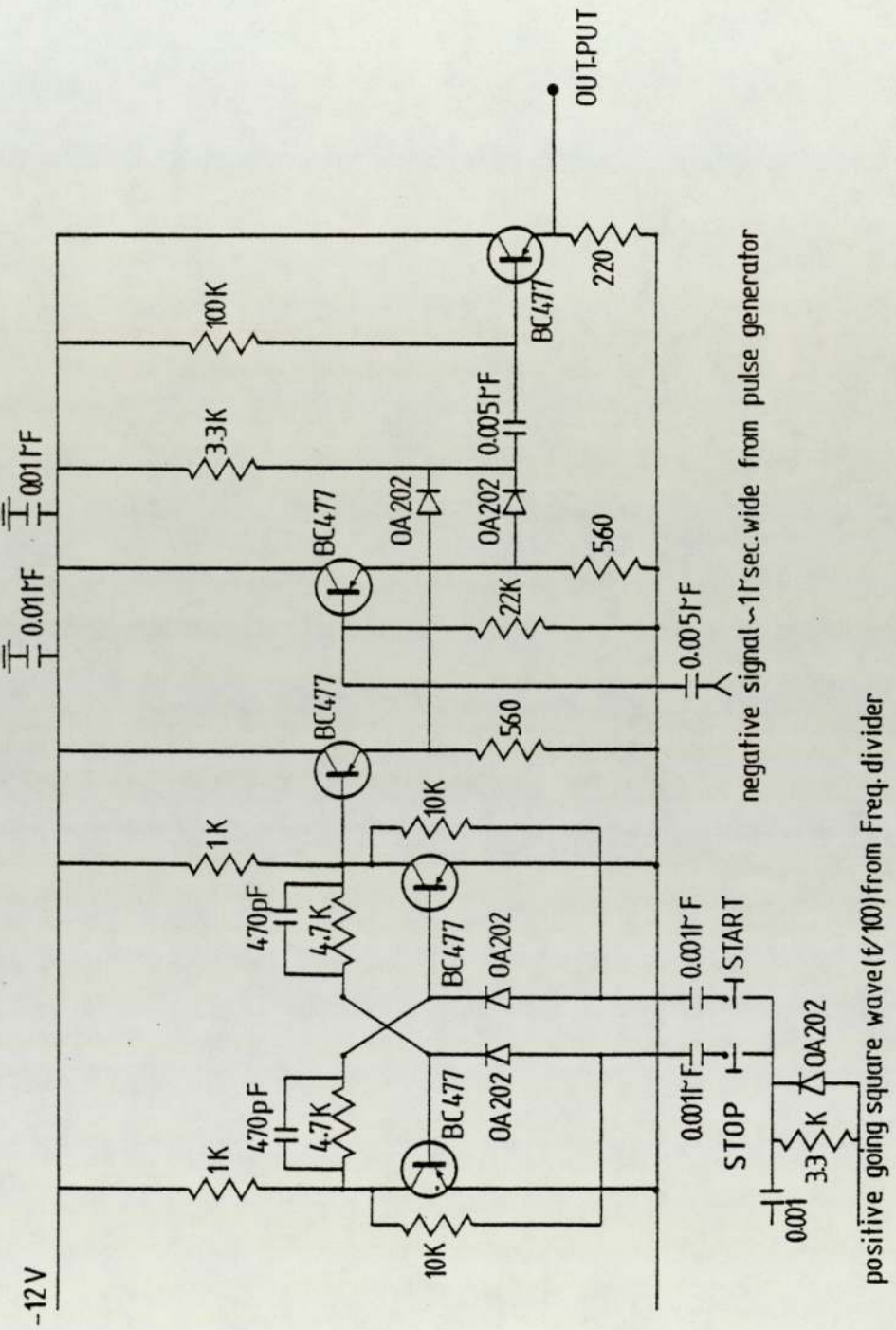

FIG 2.17 Start and stop unit circuit

FAST NEUTRON AND GAMMA DETECTORS

F=frequency RESPONSE H=gamma detector height

F=10 HZ

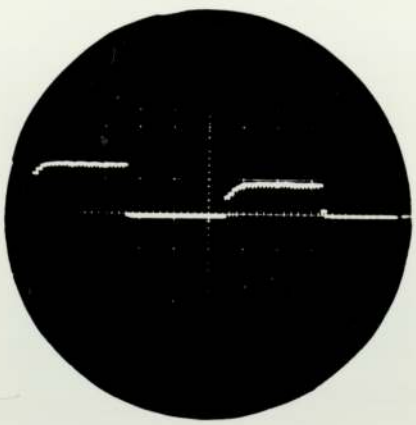

H =20CMS.

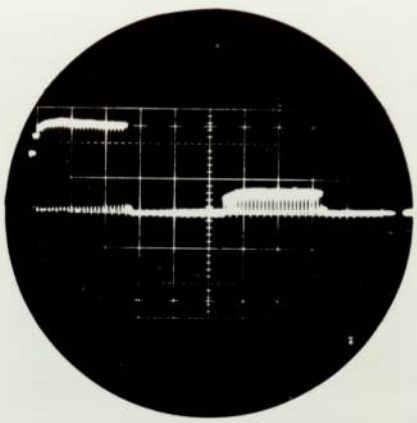

H =40CMS.

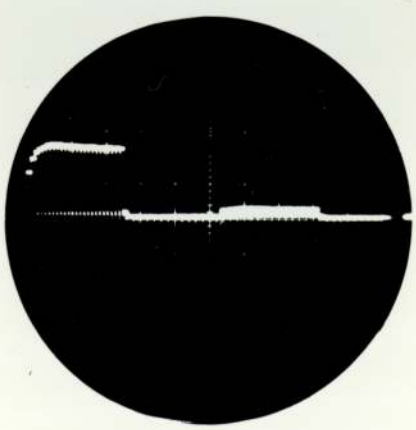

H =60CMS.

FIG.2.18

F=50 HZ

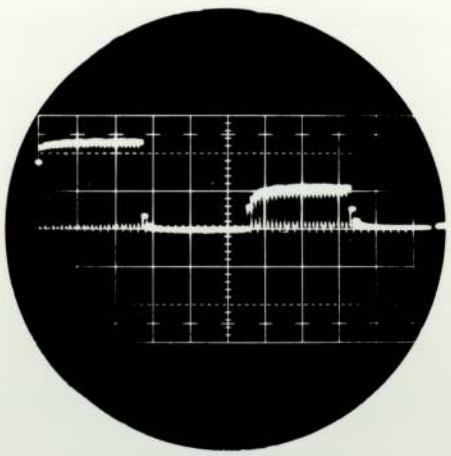

H=20CMS.

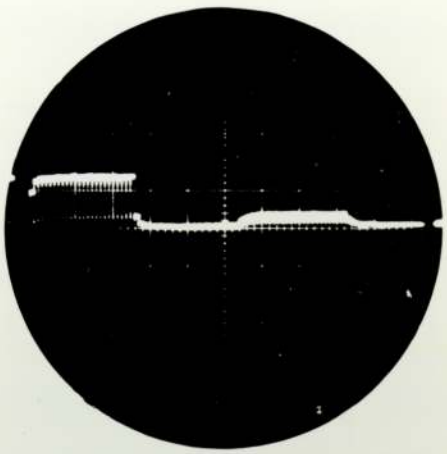

H =40CMS.

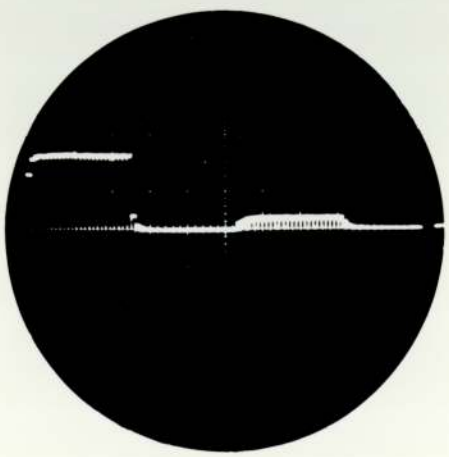

H =60CMS.

FIG.2.19

F =100HZ

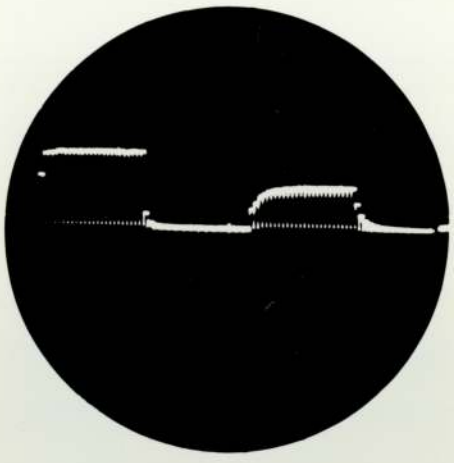

H =20 CMS.

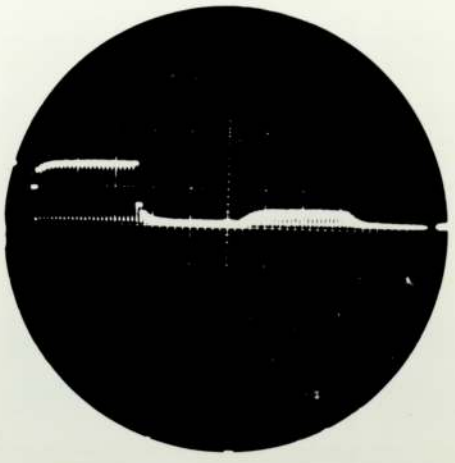

H =40CMS.

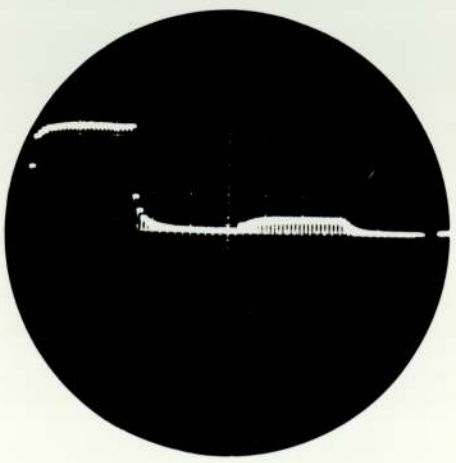

H =60CMS.

FIG.2.20

F =200HZ

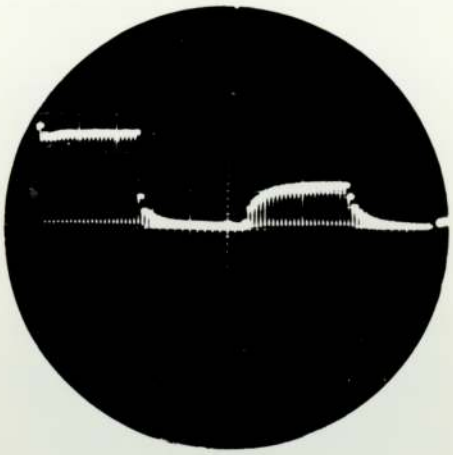

H =20CMS.

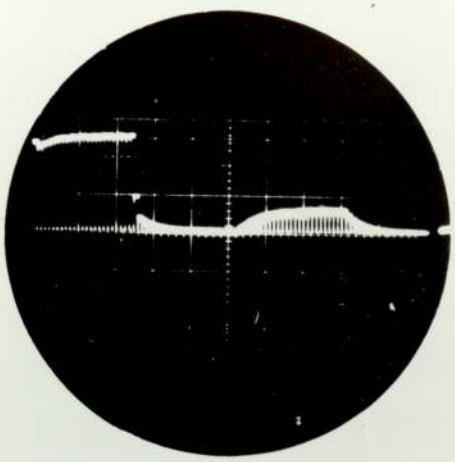

H=40CMS.

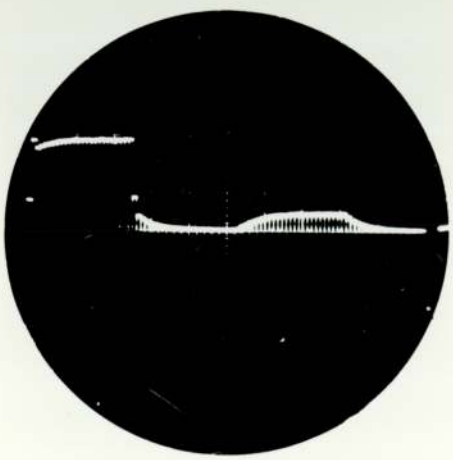

H =60CMS.

FIG.2.21

F = 400HZ

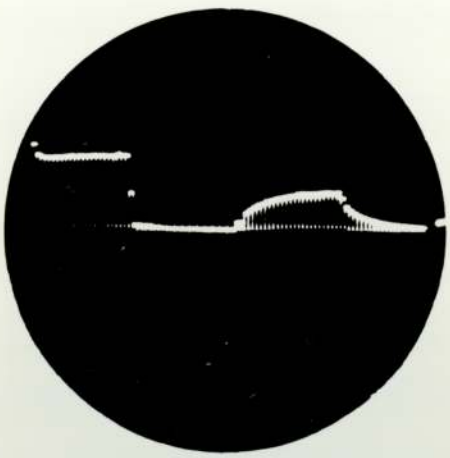

H = 20CMS.

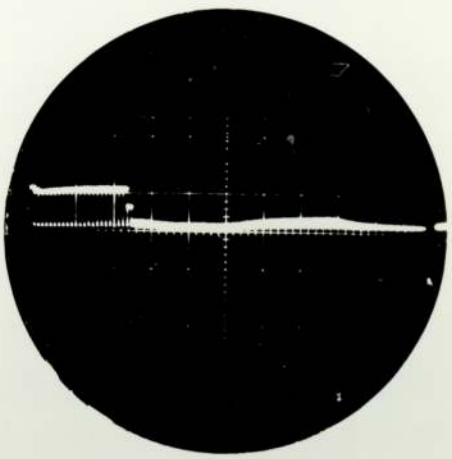

H = 40CMS.

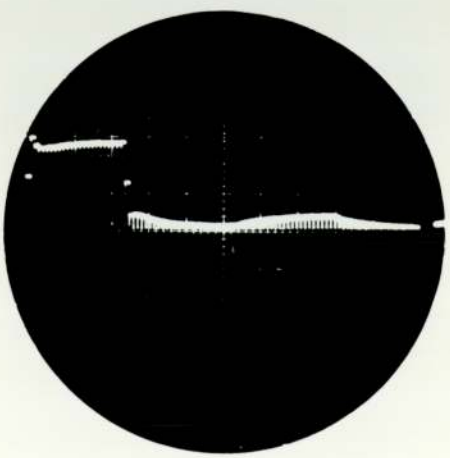

H = 60CMS.

FIG. 2.22

F =1000HZ

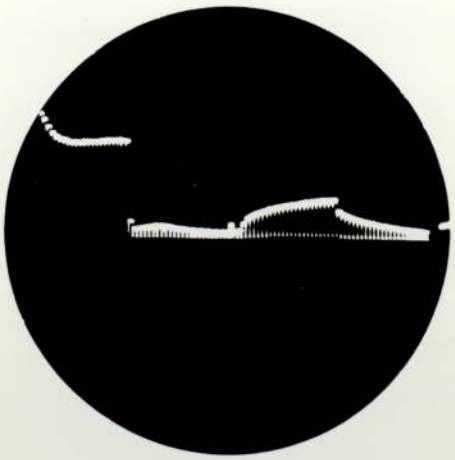

H =20CMS.

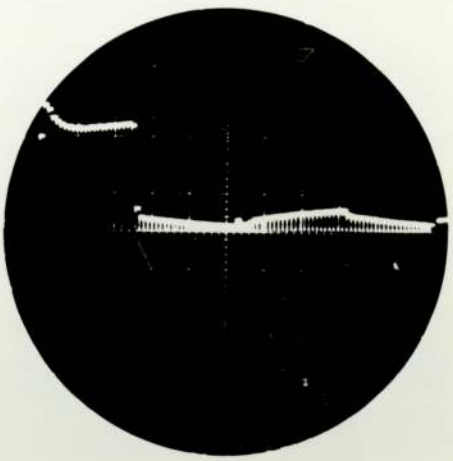

H =40CMS.

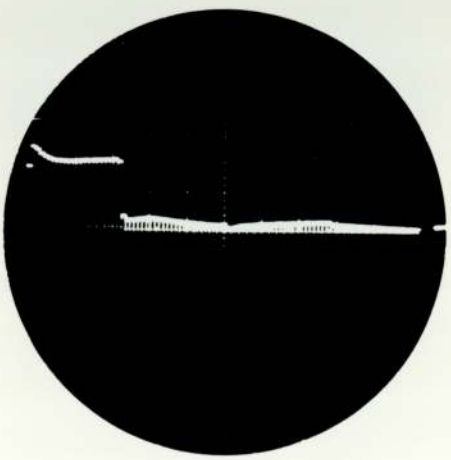

H =60CMS.

FIG. 2.23

It is clear from the photographs that the counts stored in the half memory of the analyser for gamma rays decreases with the height of the detector location. Also Fig. (2.24) shows the comparison of the output for the different frequencies.

A complete photograph of the data acquisition system and associated equipment is represented in Fig. (2.25).

$F_1 = 200HZ$

$F_2 = 400HZ$

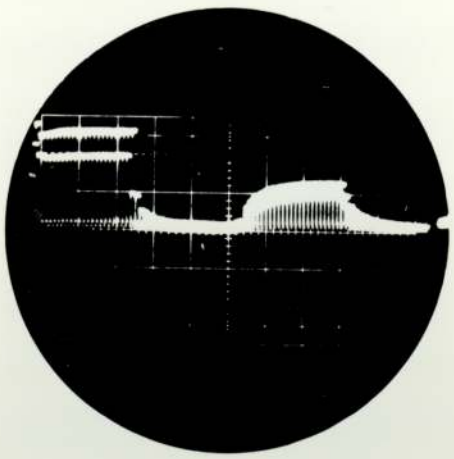

H = 20CMS.

$F_1 = 50$ HZ

$F_2 = 100$ HZ

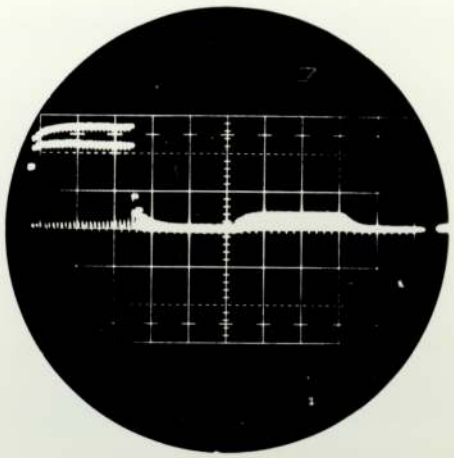

H = 60CMS.

$F_1 = 200$ HZ

$F_2 = 400$ HZ

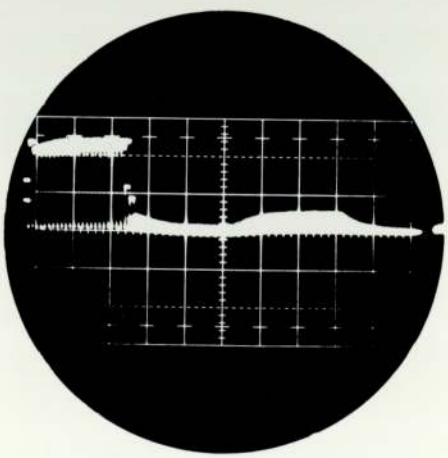

H = 60CMS.

FIG. 2.24

FIG.2.25 Data acquisition system and associated components.

CHAPTER 3

ANALYSIS OF EXPERIMENTAL DATA AND EXPERIMENTAL RESULTS

In this chapter, the method used to obtain the frequency response characteristics of the subcritical assembly from the experimental data is presented. The method used the following procedures:

(i) Raw data correction for the effect of losses due to the analyser.

(ii) Background correction.

(iii) Fourier analysing the corrected data, the output response of the system is resolved into components harmonically related to the fundamental period.

(vi) Finally, the amplitude and phase angle both for the fundamental period and its related harmonics are determined from the Fourier analysis.

3.1 LOSS OF DATA DUE TO ANALYSER

The channel content should be corrected for dead-time losses due to analyser operating in Time Sequence Storage mode. As described in Chapter 2, each channel of the analyser records the number of pulses delivered into it during an assigned period of time. Thus, each channel records the number of counts between time t and $t+dt$, where dt is the channel width. These losses occur because

of the multiple incidences into the same channel and the time needed to transfer the data to the analyser memory core.

Now, if C is the average true count rate per cycle and N represents the number of neutron cycles, after a recording period of time, the true counts Q that should be in a given channel is given by:

$$Q = N.C.\ dt \qquad \ldots\ldots\ldots \quad (3.1)$$

But in practice, the recorded counts per channel, Q^1 are somewhat smaller than the true counts that should be in that channel. In this section, a relationship between Q and Q^1 is found by taking into account the analyser memory transfer time (τ) and dead time (δ).

The probability that n counts will be recorded into the same channel in time t is given by the Poisson distribution as

$$P(n,t) = \frac{(ct)^n \quad e^{-ct}}{n!} \qquad \ldots\ldots\ldots \quad (3.2)$$

where ct is the average count rate in time t and is given by the expression

$$Ct = 0 \times P(0,t) + 1XP(1,t) + 2XP(2,t) + \cdots \qquad \ldots\ldots\ldots \quad (3.3)$$

For the RIDL analyser (model 24.2) the memory transfer time, τ, is 12.5 μ sec. There is a temporary store which records <u>one</u> count occurring in this time. Thus the

stored counts in time τ averaged over many cycles are given by the expression,

$$r(\tau) = 1Xp(1,\tau) + 1\,Xp(2,\tau) + 1Xp(3,\tau) + \ldots\ldots$$

$$\text{or} \quad r(\tau) = c\tau\, e^{-c\tau} + \frac{(c\tau)^2\, e^{-c\tau}}{2!} + \frac{(c\tau)^3\, e^{-c\tau}}{3!} + \ldots\ldots$$

$$= e^{-c\tau}\left[-1+1+c\tau+\frac{(c\tau)^2}{2!}+\frac{(c\tau)^3}{3!}+\ldots\ldots\right]$$

regarding Taylor series

$$e^{c\tau} = 1+c\tau+\frac{(c\tau)^2}{2!}+\frac{(c\tau)^3}{3!}+\ldots\ldots$$

Therefore $\quad r(\tau) = \left[\,1-e^{-c\tau}\,\right] \qquad \ldots\ldots \qquad (3.4)$

Since $c\tau$ is the average counts occurring in time τ then the fraction of counts, F, recorded in the temporary store is

$$r(\tau)/_{c\tau} \quad \text{or}$$

$$F = \frac{1 - e^{-c\tau}}{c\tau}$$

Therefore, the recorded counts per channel are given by the expression,

$$Q' = Nc\left[(dt-\tau) + \tau\left(\frac{1-e^{-c\tau}}{c\tau}\right)\right] =$$

$$= Ncdt\left[\left(1-\frac{\tau}{dt}\right) + \frac{\tau}{dt}\left(\frac{1-e^{-c\tau}}{c\tau}\right)\right] \qquad \ldots\ldots (3.5)$$

If each incidence (or count) processed has an associated dead time δ, then, neglecting memory transfer time τ the TRUE count rate c is related to the measured count rate c′ by the expression, [23, 16],

$$c = \frac{c'}{1-c'\delta}$$

or $$c' = \frac{c}{1+c\delta} \qquad \ldots\ldots\ldots \quad (3.6)$$

This applies to the counts received in the interval $dt-\tau$ but not in the memory transfer time. Therefore when this correction factor is applied to the equation (3.5),

$$Q' = \left[\frac{(1-\frac{\tau}{dt})}{1+c\delta} + \frac{\tau}{dt} \left(\frac{1-e^{-c\tau}}{c\tau} \right) \right] \overset{\cdot\cdot}{N}c\,dt \qquad (3.7)$$

the Correction factor (C.F.) is $Q'/_Q$ or

$$C.F. = \left[\frac{1-\frac{\tau}{dt}}{1+c\delta} + \frac{\tau}{dt} \left(\frac{1-e^{-c\tau}}{c\tau} \right) \right]$$

This correction factor was used to correct each channel content recorded by the analyser. This was done by means of subroutine CORRECT (computer program FOURIDL, given in Appendix B) in which an interative technique was used [26,19] to evaluate an approximate value of the true count rate c. This value became nearly constant (<±0.1%) after two or three interations. The initial value taken for c was the uncorrected count rate.

3.2 HARMONIC ANALYSIS OF CORRECTED DATA

The frequency response of nuclear system was measured by means of the amplitude and relative phase of

the output. The process was repeated for all frequencies of interest. Since the square wave is the superposition of sinusoidal waves it can be Fourier analysed[54] into an infinite number of odd harmonics of the fundamental frequency. Conventionally, the amplitude and relative phase of output are measured by Fourier coefficients. By definition [55,56], any arbitrary periodic function f(x) in the interval $-\pi \leq x \leq \pi$ can be represented by the infinite trigonometric series of the type,

$$f(x) = \frac{1}{2} a_o + \sum_{n=1}^{\infty} (a_n . \cos nx + b_n \sin nx) \quad \ldots \quad (3.8)$$

where a_o, a_n, b_n, for n=1,2, ... are constants and defined as,

$$a_o = \frac{1}{\pi} \int_{-\pi}^{+\pi} f(x)dx ,$$

$$a_n = \frac{1}{\pi} \int_{-\pi}^{+\pi} f(x) \cos nx \, dx, \quad \ldots\ldots \quad (3.9)$$

$$b_n = \frac{1}{\pi} \int_{-\pi}^{+\pi} f(x) \sin nx \, dx$$

The constants a_o, a_n, b_n defined by (3.9) are called Fourier coefficients of f(x). When a_o, a_n, b_n for n=1,2,... are defined by the (3.9) the series (3.8) is called the Fourier series representation of f(x).

The terms of Fourier series are sine and cosines series as it was observed above. Therefore it will be

useful to state those properties of sin nx and cos nx, where n and m are integers.

$$\int_{-\pi}^{+\pi} \sin mx \cos nx \, dx = \int_{-\pi}^{+\pi} \sin mx \, dx = \int_{-\pi}^{+\pi} \cos mx dx = 0$$

$$\int_{-\pi}^{+\pi} \text{Cos}mx \, \text{cos}nx dx = \int_{-\pi}^{+\pi} \text{Sin } mx \text{ Sin } nx \, dx = \begin{cases} 0 \text{ when } m \neq n \\ \pi \text{ when } m = n \end{cases}$$

..... (3.10)

In the present work, the channel content for each of the 2N channels contained in a cycle was expanded in a series of sine and cosine terms as in equation (3.8).

The calculated Fourier coefficients of a_r and b_r were used to determine the amplitude A_r and phase angle ε_r for the different r harmonics by using the relationship,

$$a_r \text{Cos}rx + b_r \text{ Sin}rx = A_r \text{ Sin } (rx + \varepsilon_r) \quad ..... \quad (3.11)$$

By equating equivalent terms,

$$A_r = (a_r^2 + b_r^2)^{\frac{1}{2}} \quad ..... \quad (3.12)$$

and

$$\varepsilon_r = \arctan (a_r/b_r) \quad ..... \quad (3.13)$$

3.2.1 Numerical Determination of Fourier Coefficients

Corresponding to the usual theory which is based on

knowing the function in an entire interval of length 2π, there is a theory based on knowing the function at a discrete set of equally spaced points[57]. We shall adopt as a basis of discussion 2N equally spaced points. In this Section, the method used to determine the Fourier coefficients is presented. It is remarkable factthat if we use summation in place of integration, the set of functions $\cos \frac{\pi n}{N}$ and $\text{Sin } \frac{\pi n}{N}$, $(n=0,1,\ldots,2N-1)$ would appear in Fourier expansion of the values f_n taken by a function $f(x)$ at the points $x_n = \frac{\pi n}{N}$, $(n=0,1,\ldots,2N-1)$ in such a way that equation (3.14) are satisfied.

$$F_n = \frac{a_o}{2} + \sum_{r=1}^{N-1} \left(a_r \text{Cos } \frac{\pi nr}{N} + b_r \text{ Sin } \frac{\pi nr}{N}\right) + \frac{a_N}{2} \text{Cos}\pi n \qquad \ldots(3.14)$$

The solution of the system (3.14) is well known[57,58].

The orthogonality relations are $(K \leq N,\ m \leq N)$

$$\sum_{x=0}^{2N-1} \sin \frac{\pi}{N} Kx \ \text{Sin } \frac{\pi}{N} mx = \begin{cases} 0 & \text{if } K \neq m \\ N & \text{if } K=m \neq 0 \end{cases}$$

$$\sum_{x=0}^{2N-1} \sin \frac{\pi}{N} Kx \ \text{Cos } \frac{\pi}{N} mx = 0$$

$$0 \quad \text{if } K \neq m$$

$$\sum_{x=0}^{2N-1} \cos \frac{\pi}{N} Kx \ \text{Cos } \frac{\pi}{N} mx = \begin{cases} N & \text{if } K=m \neq 0,N \\ 2N & \text{if } K=m=0,N \end{cases}$$

By using the orthogonality relations the Fourier coefficients could be determined. To obtain a_r (r=1,2,.., N-1), multiply both sides of equation (3.14) by Cos $(\frac{\pi nr}{N})$ and sum over all r. we get

$$\sum_{n=0}^{2N-1} F_n . \text{Cos} \frac{\pi n . r}{N} = Na_r$$

and similarly for b_r and a_o.

Finally, Fourier coefficients are,

$$a_r = \frac{1}{N} \sum_{n=0}^{2N-1} F_n \text{ Cos } \frac{\pi nr}{N}$$

$$b_r = \frac{1}{N} \sum_{n=0}^{2N-1} F_n \text{ Sin } \frac{\pi nr}{N} \qquad \ldots\ldots\ldots \qquad (3.15)$$

$$a_o = \frac{1}{N} \sum_{n=0}^{2N-1} F_n$$

Thus, by making F_n correspond to the content of the 2N channels contained in a cycle, the Fourier coefficients a_r and b_r could be used to determine the amplitude and phase angle for up to r(r=0,1,.....,N-1) different harmonics. For simplification and speeding the programming to calculate the Sine and Cosines the following method was used:

$$\text{Cos}(r\,\theta) = \text{Cos}[(r-1)\,\theta + \theta] =$$

$$= \text{Cos}\,(r-1)\,\theta \,\text{Cos}\theta - \text{Sin}(r-1)\theta\ \text{Sin}\,\theta$$

$$= 2\text{Cos}(r-1)\,\theta\text{Cos}\theta - [\text{Cos}(r-1)\,\theta\text{Cos}\theta + \text{Sin}(r-1)\,\theta\text{Sin}\theta]$$

$$= 2\cos(r-1)\,\theta\cos\theta - \cos\left[(r-1)\,\theta - \theta\right]$$

$$= 2\cos(r-1)\,\theta\cos\theta - \cos(r-2)\,\theta$$

$\therefore$ For r=1 $\quad \cos\theta = \cos\theta$

r=2 $\quad \cos 2\theta = 2\cos^2\theta - 1$

r=3 $\quad \cos 3\theta = 2\cos 2\theta \cos\theta - \cos\theta$

r=4 $\quad \cos 4\theta = 2\cos 3\theta \cos\theta - \cos 2\theta$

....

and similarly for sines:

$\therefore$ For r=1 $\quad \sin\theta = \sin\theta$

r=2 $\quad \sin 2\theta = \sin\theta\,(2\cos\theta)$

r=3 $\quad \sin 3\theta = \sin\theta\,(2\cos 2\theta + 1)$

r=4 $\quad \sin 4\theta = \sin\theta\,(2\cos 3\theta + 2\cos\theta)$

... .

Therefore the actual Fourier coefficients were determined by adding these sines and cosines in the orders of equations (3.15).

This method was applied to develop the computer program subroutine Fourier which evaluates the constants a_r and b_r and computes the values of the amplitude and phase angle for every one of the N-1 harmonics.

In practice, it was found that reliable information could be found up to and including the fifth harmonic. The subroutine Fourier is listed in Appendix B as part of the computer program FOURIDL.

This method of calculation was also successfully used by other workers with both an odd and an even number of data points. Particular mention should be made to references [19,26,59].

3.3 COMPUTER PROGRAM FOURIDL

The experimental frequency response characteristics of the subcritical assembly were analysed by means of computer program FOURIDL. This program, given in Appendix B, with input and output examples, is written in ALGOL for the ICL-1905 Computer. The output from the analyser was fed into the program which performs the following operations:

Reduces the data to one neutron cycle by adding up the time equivalent contents from each cycle. (This is already done by using the analyser as 100 channels). Therefore it just calculates the average content per channel. This is performed by subroutine ARRANGE.

Corrects the experimental and background content per channel for dead-time and memory transfer time losses by subroutine CORRECT. This subroutine is based on the scheme discussed in Section 3.1.

Once the data has been corrected for losses due to the analyser and the background content per channel subtracted, a Fourier analysis (as discussed in the previous sections) is carried out by subroutine FOURIER.

...SITY ...LIBRARY

Subroutine FOUREXIT provides numerical output for subroutine FOURIER. The numerical output includes both amplitude and phase shift and was limited to the first seven harmonics.

The heading for the lineprinter output of subroutine FOURIER was provided by means of subroutine FOURHEAD.

The program can be used with data corresponding to either one or two detectors.

Finally, a schematic block diagram of the code is also shown in Appendix B.

3.4 EXPERIMENTAL RESULTS

All the experimentally obtained figures presented in this work correspond to measurements carried out with source neutrons produced from D-T reactions. The reasons for using the D-T instead of the D-D reaction can be summarized as follows:

(i) Much higher neutron yield (approximately 100 times). This was of vital importance in the present experiments where the oscillator R.F. and ion source extraction voltage had to be kept as low as possible in order to provide a reliable and steady operation of the pulsing system.

(ii) Experimental measurements have shown how the system response characteristics (transfer functions) do not depend either on the neutron source intensity or strength.

The space-dependent transfer function of the system for different source-frequency configuration was measured by varying the frequency of the square wave modulated neutron source and obtaining the amplitude and phase shift of the resultant fluctuating component of the detector response as a function of source frequency. The neutron source frequency was varied and the previous section's techniques were used to analyse the detector response.

Figure (3.1) shows the amplitude of the frequency response function of the subcritical assembly for a particular detector location. The results obtained over a wide range of frequencies show that, up to and including the fifth harmonic, the data obtained from higher harmonics is seen to be in good agreement with that computed from the fundamental component of the detector response. Furthermore, data corresponding to the seventh harmonic proved to be reliable for source frequencies included in the range of 10HZ. to 500HZ, but was unrealistic and showed significant variations for source frequencies outside this range.

Measurements were taken for different axial detector positions. Figs. (3.2) and (3.3) show typical examples of the gamma ray detector responses over a number of different axial locations. It can be clearly seen from graphs (3.2) and (3.3) how for frequencies of up to 100 HZ the amplitude decreases very slowly. For higher

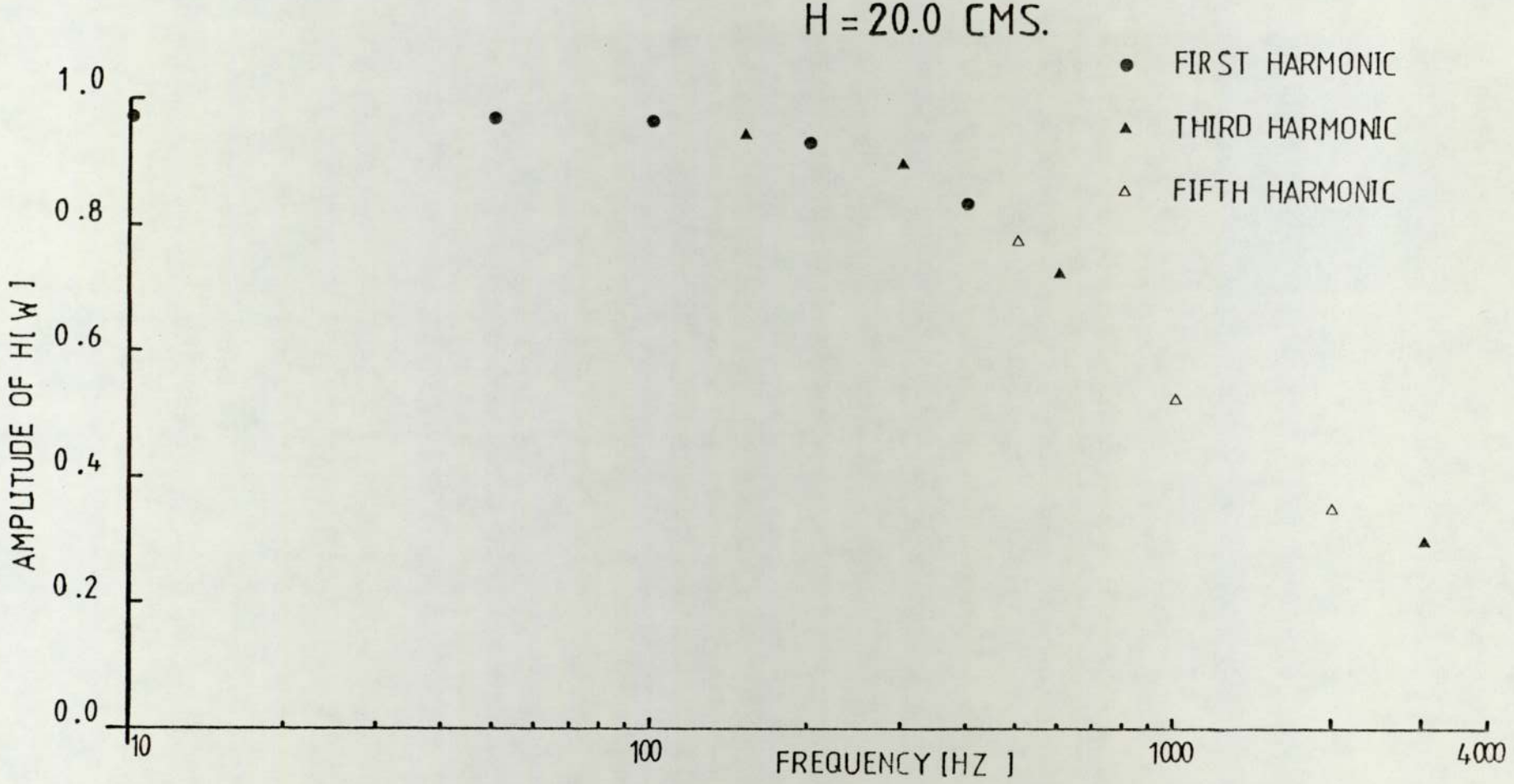

FIG.(3.1) Experimental amplitude response

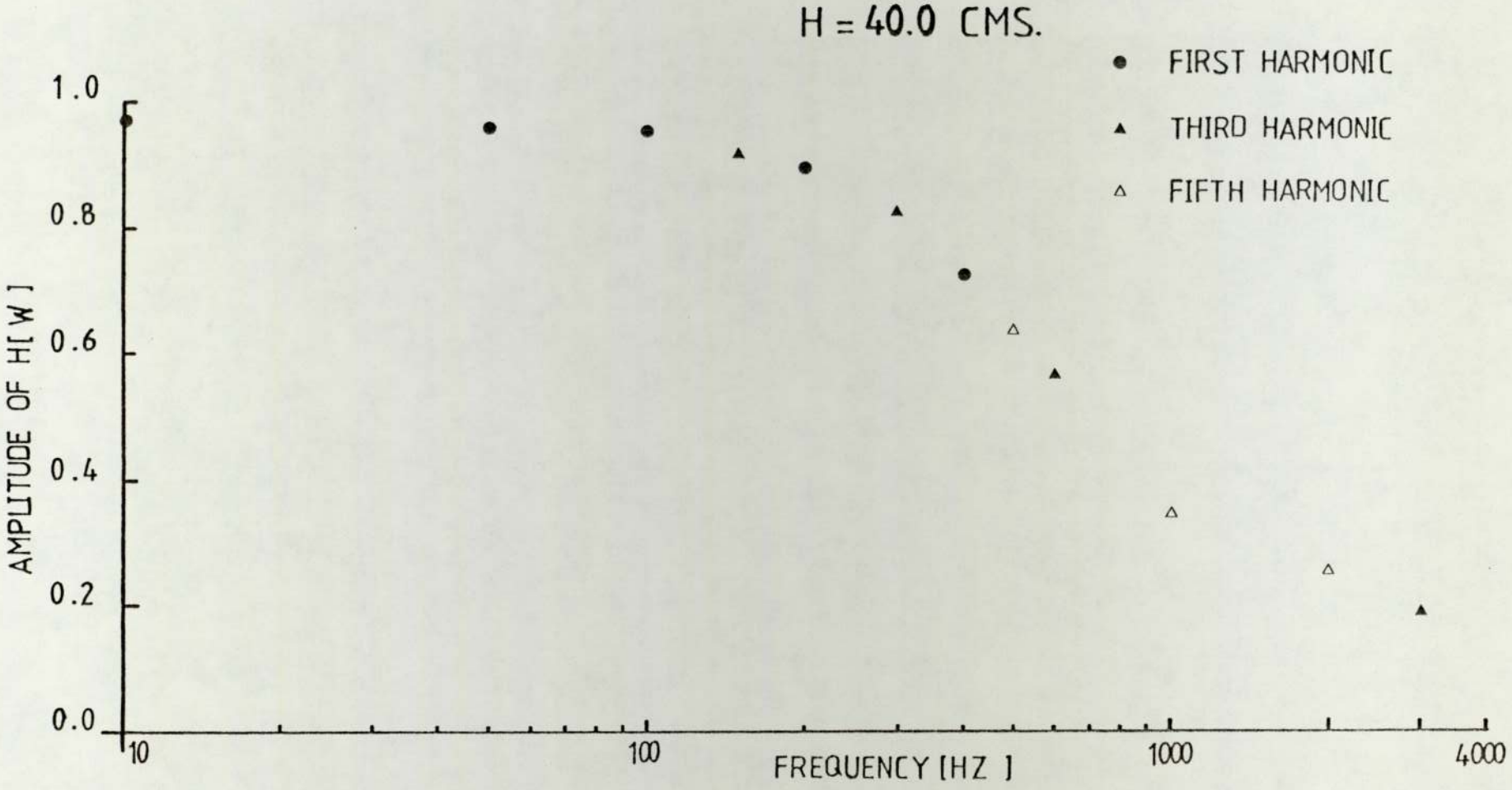

FIG.(3.2) EXPERIMENTAL AMPLITUDE RESPONSE

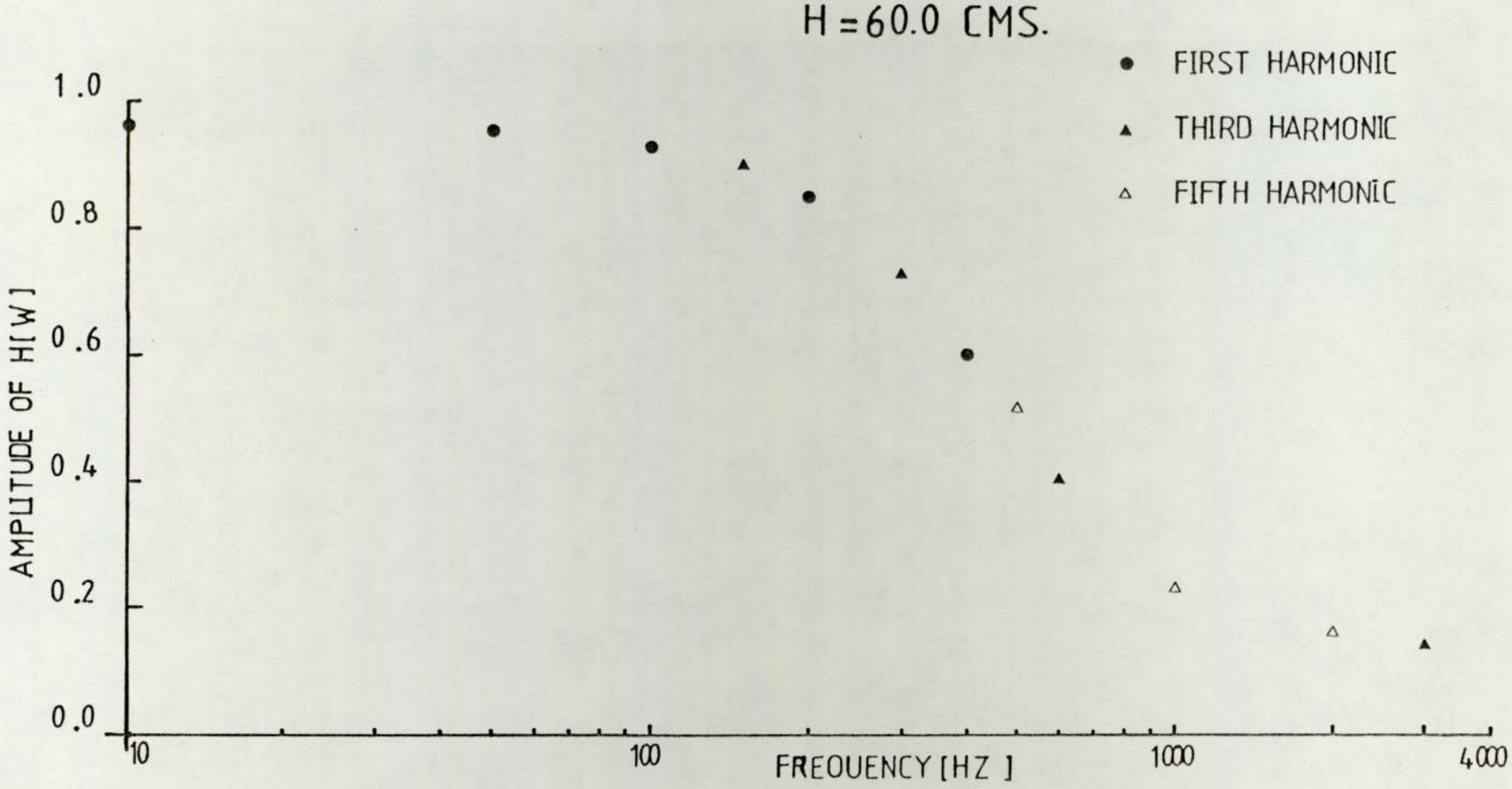

FIG.(3.3) EXPERIMENTAL AMPLITUDE RESPONSE

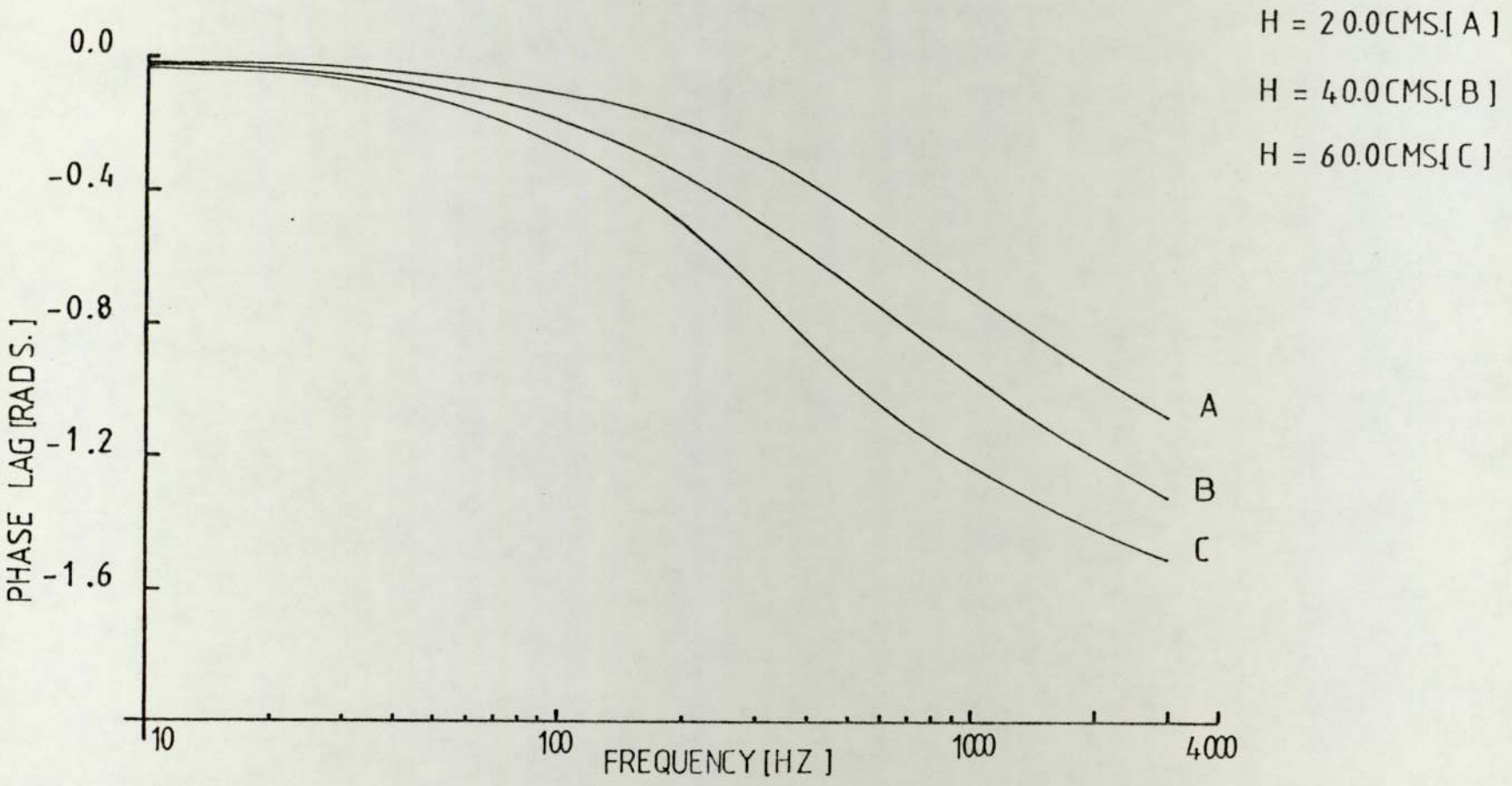

FIG.(3.4) EXPERIMENTAL PHASE RESPONSE FOR DIFFERENT AXIAL POSITION

frequencies, the amplitude decreases much more rapidly and the spatial differences become more noticeable.

In general, the comparison between the results obtained from the gamma-ray detections are in very good agreement with those obtained by using the neutron detection ([26], previous work done in Aston University.) But in the earliest detection method there was a much bigger spatial difference which was found in the reflector where the response is more attenuated due to the much longer neutron life-time in the water reflector. This was overcome by using the gamma ray detection, with a very small attenuation of it by water reflector. With regard to the phase resonse characteristics of the subcritical assembly, a very similar pattern is observed (Fig. 3.4)

CHAPTER 4

THEORY

In order to obtain the prompt fission gamma response outside the subcritical assembly where the detector was located it was necessary to calculate the neutron flux variation along the z axis of the core. This was performed by using the multigroup model of flux calculations.

4.1 NEUTRON FLUX CALCULATIONS

Two group diffusion theory was chosen to calculate the neutron fluxes of

$$\phi_{th} = (\phi_4 + j\phi_2)\, e^{jwt} \qquad \text{(thermal)}$$

$$\phi_f = (\phi_3 + j\phi_1)\, e^{jwt} \qquad \text{(fast)}$$

Writing down the two group diffusion equations,

$$D_1\nabla^2\phi_f - \Sigma_1\phi_f + \nu\Sigma_f\phi_{th} = \frac{1}{V_f} \cdot \frac{\partial\phi_f}{\partial t} \qquad \text{(fast)}$$

and

$$D_3\nabla^2\phi_{th} - \Sigma_3\phi_{th} + \Sigma_{s1}\,\phi_f = \frac{1}{V_{th}} \cdot \frac{\partial\phi_{th}}{\partial t} \qquad \text{(thermal)}$$

substitute in ϕ_{th} and ϕ_f. This involved real and imaginary fluxes, so calculations were effectively four groups. The four group diffusion equations can be written in general terms as

$$D_1\nabla^2\phi_1 - \Sigma_1\phi_1 + \Sigma_{21}\phi_2 + \Sigma_{31}\phi_3 + \Sigma_{41}\phi_4 = 0 \qquad \text{(fast imaginary)}$$

$$D_2\nabla^2\phi_2 - \Sigma_2\phi_2 + \Sigma_{12}\phi_1 + \Sigma_{32}\phi_3 + \Sigma_{42}\phi_4 = 0 \qquad \text{(thermal imaginary)}$$

$$D_3\nabla^2\phi_3 - \Sigma_3\phi_3 + \Sigma_{13}\phi_1 + \Sigma_{23}\phi_2 + \Sigma_{43}\phi_4 + 0 \qquad \text{(fast real)}$$

$$D_4\nabla^2\phi_4 - \Sigma_4\phi_4 + \Sigma_{14}\phi_1 + \Sigma_{24}\phi_2 + \Sigma_{34}\phi_3 = 0 \qquad \text{(thermal real)}$$

..... (4.1)

where,

D_i = i th group diffusion coefficient

Σ_i = i th group removal or absorption cross section

$\Sigma_{12}\phi_1$ = production of neutrons in group 2 by down scattering etc. from Group 1.

$\Sigma_{21}\phi_2$ = production of neutrons in Group 1 from Group 2. i.e. from fission or from artificial upscattering as required in the time dependent (2 real, 2 imaginary groups) model.

$\Sigma_{13}\phi_1$ = etc. have similar meanings to $\Sigma_{12}\phi_1$

$\Sigma_{31}\phi_3$ = etc. have similar meanings to $\Sigma_{21}\phi_2$

Let $\nabla^2\phi_i = -B^2\phi_i$ ..... (4.2a)

where B^2 is defined as Buckling and a constant to be found. [60,61,62,63,64]. It is assumed to be common to both fluxes. Replace the $\nabla^2\phi_i$ with its equivalent in the general four group diffusion equations.

Therefore, $-(D_1B^2 + \Sigma_1)\Phi_1+\Sigma_{21}\Phi_2+\Sigma_{31}\Phi_3+\Sigma_{41}\Phi_4 = 0$

$+\Sigma_{12}\Phi_1 -(D_2B^2+\Sigma_2)\Phi_2+ \Sigma_{32}\Phi_3+\Sigma_{42}\Phi_4 = 0$

$+\Sigma_{13}\phi_1 +\Sigma_{23}\phi_2 -(D_3B^2+\Sigma_3)\phi_3 + \Sigma_{43}\phi_4= 0$

$+\Sigma_{14}\phi_1 +\Sigma_{24}\phi_2 +\Sigma_{34}\phi_3 -(D_4B^2+\Sigma_4)\phi_4 = 0$

..... (4.1a)

which can be written in matrix form as

$$\begin{vmatrix} -(D_1B^2+\Sigma_1) & \Sigma_{21} & \Sigma_{31} & \Sigma_{41} \\ \Sigma_{12} & -(D_2B^2+\Sigma_2) & \Sigma_{32} & \Sigma_{42} \\ \Sigma_{13} & \Sigma_{23} & -(D_3B^2+\Sigma_3) & \Sigma_{43} \\ \Sigma_{14} & \Sigma_{24} & \Sigma_{34} & -(D_4B^2+\Sigma_4) \end{vmatrix} \begin{vmatrix} \phi_1 \\ \phi_2 \\ \phi_3 \\ \phi_4 \end{vmatrix} = 0$$

There are four values for B^2 and these make the following determinant equal to zero.

$$\begin{vmatrix} -(D_1B^2+\Sigma_1) & \Sigma_{21} & \Sigma_{31} & \Sigma_{41} \\ \Sigma_{12} & -(D_2B^2+\Sigma_2) & \Sigma_{32} & \Sigma_{42} \\ \Sigma_{13} & \Sigma_{23} & -(D_3B^2+\Sigma_3) & \Sigma_{43} \\ \Sigma_{14} & \Sigma_{24} & \Sigma_{34} & -(D_4B^2+\Sigma_4) \end{vmatrix} = 0$$

.....(4.2)

This determinant can be expanded into the form

$$a_1(B^2)^4+b_1(B^2)^3+c_1(B^2)^2+d_1(B^2)+e_1 = 0 \qquad \ldots\ldots\ldots (4.3)$$

where

$$a_1 = D_1D_2D_3D_4 \qquad \ldots\ldots\ldots (4.4)$$

$$b_1 = \sum_1 D_2D_3D_4 + D_1\sum_2 D_3D_4 + D_1D_2\sum_3 D_4 + D_1D_2D_3\sum_4 \qquad \ldots\ldots (4.5)$$

and

$$c_1 = -D_1D_2\sum_{34}\sum_{43} - D_1\sum_{23}\sum_{32}D_4$$

$$-D_1\sum_{24}D_3\sum_{42} - \sum_{12}\sum_{21}D_3D_4$$

$$-\sum_{13}D_2\sum_{31}D_4 - \sum_{14}D_2D_3\sum_{41}$$

$$+\sum_1\sum_2 D_3D_4 + \sum_1 D_2\sum_3 D_4$$

$$+D_1\sum_2\sum_3 D_4 + \sum_1 D_2D_3\sum_4$$

$$+D_1\sum_2 D_3\sum_4 + D_1D_2\sum_{34}\sum \qquad \ldots\ldots\ldots (4.6)$$

$$d_1 = -D_1\sum_{24}\sum_{32}\sum_{43} - D_1\sum_{23}\sum_{34}\sum_{42} - \sum_{13}\sum_{21}\sum_{32}D_4$$

$$-\sum_{14}\sum_{21}D_3\sum_{42} - \sum_{12}\sum_{23}\sum_{31}D_4 - \sum_{14}D_2\sum_{31}\sum_{43}$$

$$- \sum_{12}\sum_{24} D_3 \sum_{41} - \sum_{13} D_2 \sum_{34}\sum_{41} - \sum_{1} D_2 \sum_{34}\sum_{43}$$

$$- D_1 \sum_{2}\sum_{34}\sum_{43} - \sum_{1}\sum_{23}\sum_{32} D_4 - D_1 \sum_{24}\sum_{3}\sum_{42}$$

$$- \sum_{1}\sum_{24} D_3 \sum_{42} - \sum_{12}\sum_{21}\sum_{3} D_4 - \sum_{12}\sum_{21} D_3 \sum_{4}$$

$$- \sum_{13}\sum_{2}\sum_{31} D_4 - \sum_{13} D_2 \sum_{31}\sum_{4} - \sum_{14}\sum_{2} D_3 \sum_{41}$$

$$- \sum_{14} D_2 \sum_{3}\sum_{41} + \sum_{1}\sum_{2}\sum_{3} D_4 + \sum_{1}\sum_{2} D_3 \sum_{4}$$

$$+ \sum_{1} D_2 \sum_{3}\sum_{4} + D_1 \sum_{2}\sum_{3}\sum_{4} - D_1 \sum_{23}\sum_{32}\sum_{4}$$

..... (4.7)

$$e_1 = - \sum_{14}\sum_{21}\sum_{32}\sum_{43} - \sum_{13}\sum_{21}\sum_{34}\sum_{42}$$

$$+ \sum_{12}\sum_{21}\sum_{34}\sum_{43} + \sum_{13}\sum_{24}\sum_{31}\sum_{42}$$

$$- \sum_{14}\sum_{23}\sum_{31}\sum_{42} - \sum_{12}\sum_{24}\sum_{31}\sum_{43}$$

$$- \sum_{12}\sum_{23}\sum_{34}\sum_{41} + \sum_{14}\sum_{23}\sum_{32}\sum_{41}$$

$$- \sum_{13}\sum_{24}\sum_{32}\sum_{41} - \sum_{1}\sum_{2}\sum_{34}\sum_{43}$$

$$- \sum_{1}\sum_{23}\sum_{32}\sum_{4} - \sum_{1}\sum_{24}\sum_{3}\sum_{42}$$

$$- \sum_{14}\sum_{2}\sum_{3}\sum_{41} - \sum_{13}\sum_{2}\sum_{31}\sum_{4}$$

$$- \Sigma_{12}\Sigma_{21}\Sigma_{3}\Sigma_{4} + \Sigma_{1}\Sigma_{2}\Sigma_{3}\Sigma_{4}$$

$$- \Sigma_{1}\Sigma_{24}\Sigma_{32}\Sigma_{43} - \Sigma_{1}\Sigma_{23}\Sigma_{34}\Sigma_{42}$$

$$- \Sigma_{13}\Sigma_{21}\Sigma_{32}\Sigma_{4} - \Sigma_{14}\Sigma_{21}\Sigma_{3}\Sigma_{42}$$

$$- \Sigma_{12}\Sigma_{23}\Sigma_{31}\Sigma_{4} - \Sigma_{14}\Sigma_{2}\Sigma_{31}\Sigma_{43}$$

$$- \Sigma_{12}\Sigma_{24}\Sigma_{3}\Sigma_{41} - \Sigma_{13}\Sigma_{2}\Sigma_{34}\Sigma_{41}$$

..... (4.8)

To use these formulae in calculation of flux variation in subcritical it was necessary to replace each parameter by its appropriate equivalent values derived from real-imaginary two group model. Previously an attempt to solve these equations had been made using the two dimensional computer code SNAP, but this failed at frequencies in excess of 400 Hz and so failed to give results in the most important frequency region. Programming details referring to SNAP can be found in refs. [65,66,67,68]

$$\Sigma_{1} = \Sigma_{r_1} - 3D_1 w^2/v_1^2 \qquad = \Sigma_{3} \qquad D_3 = D_1$$

and

$$\Sigma_{2} = \Sigma_{r_2} - 3D_2 w^2/v_2^2 \qquad = \Sigma_{4} \qquad D_4 = D_2$$

$$\Sigma_{12} = \Sigma_{12}$$

$$* \Sigma_{13} = w(1+3D_1\Sigma_{r_1})/v_1$$

$$\Sigma_{14} = 0$$

$$\Sigma_{21} = \left(1 - \frac{w^2\beta}{w^2+\lambda^2}\right)\nu\,\Sigma_{f_2}$$

$$^{*}\Sigma_{23} = \frac{w\lambda\beta}{w^2+\lambda^2}\,\nu\,\Sigma_{f_2}$$

$$^{*}\Sigma_{24} = w(1+3D_2\,\Sigma_{r_2})/v_2$$

$$^{*}\Sigma_{31} = -\Sigma_{13}$$

$$\Sigma_{32} = 0$$

$$\Sigma_{34} = \Sigma_{12}$$

$$^{*}\Sigma_{41} = -\Sigma_{23}$$

$$^{*}\Sigma_{42} = -\Sigma_{24}$$

$$\Sigma_{43} = \Sigma_{21}$$

* Indicates zero value at w = 0

substitute the zero and equal cross sections into equations (4.4), (4.5), (4.6), (4.7), (4.8), the results are

$$a_1 = D_1^2\,D_2^2 \qquad \ldots\ldots\ldots \text{(4.4a)}$$

$$b_1 = 2D_1D_2(D_1\Sigma_2+\Sigma_1D_2) \qquad \ldots\ldots\ldots \text{(4.5a)}$$

$$c_1 = 4D_1\Sigma_1 D_2\Sigma_2 - 2D_1\Sigma_{12} D_2\Sigma_{21}$$

$$+ D_1^2\Sigma_2^2 + D_2^2\Sigma_1^2$$

$$+ D_1^2\Sigma_{24}^2 + D_2^2\Sigma_{13}^2 \qquad \ldots\ldots\ldots (4.6a)$$

$$d_1 = 2D_1\Sigma_{12}\Sigma_{23}\Sigma_{24} + 2\Sigma_{12}\Sigma_{13} D_2\Sigma_{23}$$

$$-2\Sigma_1\Sigma_{12} D_2\Sigma_{21} - 2D_1\Sigma_{12}\Sigma_2\Sigma_{21}$$

$$+2D_1\Sigma_1\Sigma_{24}^2 + 2D_2\Sigma_2\Sigma_{13}^2$$

$$+2D_1\Sigma_1\Sigma_2^2 + 2D_2\Sigma_2\Sigma_1^2$$

$$\ldots\ldots\ldots (4.7a)$$

$$e_1 = \Sigma_1^2\Sigma_2^2 + \Sigma_{12}^2\Sigma_{21}^2$$

$$+ \Sigma_{12}^2\Sigma_{23}^2 + \Sigma_1^2\Sigma_{24}^2$$

$$+ \Sigma_{13}^2\Sigma_{24}^2 + \Sigma_2^2\Sigma_{13}^2$$

$$-2\,\Sigma_1\,\Sigma_2\,\Sigma_{21}\,\Sigma_{12} + 2\,\Sigma_{12}\,\Sigma_{13}\,\Sigma_{21}\,\Sigma_{24}$$

$$+2\,\Sigma_{12}\,\Sigma_{13}\,\Sigma_2\,\Sigma_{23} + 2\Sigma_1\,\Sigma_{12}\,\Sigma_{23}\,\Sigma_{24}$$

..... (4.8a)

To solve the quadratic equation the Descartes-Euler solution method was used [69]. To bring the quadratic component coefficient equal to one, all coefficients were divided by $D_1^2\ D_2^2$

Therefore,

$$a_4 = \frac{b_1}{a_1} \qquad \text{..... (4.5b)}$$

$$b_4 = \frac{c_1}{a_1} \qquad \text{..... (4.6b)}$$

$$c_4 = \frac{d_1}{a_1} \qquad \text{..... (4.7b)}$$

$$d_4 = \frac{e_1}{a_1} \qquad \text{..... (4.8b)}$$

To find roots of $x^4+a_4x^3+b_4x^2+c_4x+d_4 = 0$ where $(x=B^2)$, suppose $x = (y - \frac{a_4}{4})$ and substitute in the quadratic equation, this is transformed to the "reduced form"

$$y^4 + P_4 y^2 + q_4 y + r_4 = 0$$

where $$P_4 = (b_4 - \frac{3}{8} a_4^2)$$

$$q_4 = (\frac{1}{8} a_4^3 - \frac{a_4 b_4}{2} + c_4)$$

$$r_4 = (\frac{-3}{256} a_4^4 + \frac{a_4^2 b_4}{16} - \frac{a_4 c_4}{4} + d_4)$$

The roots y_1, y_2, y_3, y_4 of the "reduced" quadratic equation are the four sums

$$\pm\sqrt{z_1} \quad \pm\sqrt{z_2} \quad \pm\sqrt{z_3}$$

with the signs of the square roots chosen so that

$$\sqrt{z_1} \cdot \sqrt{z_2} \cdot \sqrt{z_3} = \frac{-q}{8}$$

where z_1, z_2, z_3 are the roots of cubic equation

$$z^3 + \frac{P_4}{2} z^2 + \frac{P_4^2 - 4r_4}{16} z - \frac{q_4}{64} = 0$$

or $$z^3 + A_3 z^2 + B_3 z + c_3 = 0$$

where $$A_3 = \frac{P_4}{2}$$

$$B_3 = (p_4^2 - 4r_4)/16$$

$$C_3 = -q_4/64$$

The "reduced" form of cubic equation is

$$y_1^3 + py_1 + Q = 0$$

where

$$P = \frac{-A_3^2}{3} + B_3$$

$$Q = \frac{2A_3^3}{27} - \frac{A_3B_3}{3} + C_3$$

and using trigonometric solution of cubic equation finally roots of z_1, z_2, z_3 are

$$\theta = \text{Cos}^{-1} \left(\frac{-Q}{2\sqrt{+ -(\frac{p}{3})^3}} \right)$$

$$\phi = \frac{\theta}{3}$$

if

$$u = 2\sqrt{+ \frac{-p}{3}}$$

Therefore

$$z_1 = U \text{Cos}\phi - \frac{A_3}{3}$$

$$z_2 = -U \text{Cos}(60+\phi) - \frac{A_3}{3}$$

$$z_3 = -U \text{Cos}(60-\phi) - \frac{A_3}{3}$$

Four roots of Buckling $B^2 = (BU)^2$ are

$$B^2 = (BU)^2 = \alpha_1^2 \pm j\beta_1^2$$

and

$$B^2 = (BU)^2 = \alpha_2^2 \pm j\beta_2^2$$

where

$$\alpha_1^2 = -\sqrt{z_1} - \frac{a_4}{4}$$

$$\beta_1^2 = \sqrt{z_2} + \sqrt{z_3}$$

and

$$\alpha_2^2 = \sqrt{z_1} - \frac{a_4}{4}$$

$$\beta_2^2 = \sqrt{z_3} - \sqrt{z_2}$$

Once the B^2 values have been obtained it is possible to calculate the flux coupling coefficients from equations (4.1a). Take equations 2, 3, and 4 of (4.1a) and divide each by ϕ_4 and put

$$S_1 = \frac{\phi_1}{\phi_4} \qquad S_2 = \frac{\phi_2}{\phi_4} \qquad S_3 = \frac{\phi_3}{\phi_4} \qquad S_4 = 1$$

Therefore,

$$\Sigma_{12} S_1 - (D_2B^2 + \Sigma_2)S_2 + \Sigma_{32} S_3 + \Sigma_{42} = 0$$

$$\Sigma_{13} S_1 + \Sigma_{23} S_2 - (D_3B^2 + \Sigma_3)S_3 + \Sigma_{43} = 0$$

$$\Sigma_{14} S_1 + \Sigma_{24} S_2 + \Sigma_{34} S_3 - (D_4B^2 + \Sigma_4) = 0$$

..... (4.9)

also write $L_2 = (D_2B^2 + \Sigma_2)$

$L_3 = (D_3B^2 + \Sigma_3)$

$L_4 = (D_4B^2 + \Sigma_4)$

..... (4.10)

for compactness. The S_1, S_2, S_3 could be calculated and

$$S_3 = \frac{(\Sigma_{13}\Sigma_{42} - \Sigma_{12}\Sigma_{43})(\Sigma_{14}\Sigma_{23} - \Sigma_{13}\Sigma_{24}) + (\Sigma_{14}\Sigma_{43} + \Sigma_{13}L_4)(\Sigma_{13}L_2 + \Sigma_{12}\Sigma_{23})}{(\Sigma_{14}L_3 + \Sigma_{13}\Sigma_{34})(\Sigma_{13}L_2 + \Sigma_{12}\Sigma_{23}) - (\Sigma_{13}\Sigma_{32} + \Sigma_{12}L_3)(\Sigma_{14}\Sigma_{23} - \Sigma_{13}\Sigma_{24})}$$

$$S_2 = \frac{S_3(\Sigma_{13}\Sigma_{32} + \Sigma_{12}L_3) + (\Sigma_{13}\Sigma_{42} - \Sigma_{12}\Sigma_{43})}{(\Sigma_{13}L_2 + \Sigma_{12}\Sigma_{23})}$$

$$S_1 = \frac{L_2S_2 - \Sigma_{32}S_3 - \Sigma_{42}}{\Sigma_{12}}$$

$S_4 = 1$

By putting zero components and equal cross sections into the coupling coefficients:

$$S_3 = \frac{(\Sigma_{13}\Sigma_{24}+\Sigma_{12}\Sigma_{21})(\Sigma_{13}\Sigma_{24})+(\Sigma_{13}L_4)(\Sigma_{13}L_2+\Sigma_{12}\Sigma_{23})}{(\Sigma_{13}\Sigma_{12})(\Sigma_{13}L_2+\Sigma_{12}\Sigma_{23}) + (\Sigma_{12}L_3)(\Sigma_{13}\Sigma_{24})}$$

$$S_2 = \frac{S_3(\Sigma_{12}L_3) + (\Sigma_{13}\Sigma_{42} - \Sigma_{12}\Sigma_{43})}{(\Sigma_{13}L_2 + \Sigma_{12}\Sigma_{23})}$$

$$S_1 = \frac{L_2S_2 - \Sigma_{42}}{\Sigma_{12}}$$

$$S_4 = 1 \qquad \ldots\ldots\ldots\ldots \quad (4.11)$$

Having obtained B^2 (Buckling) which is a complex value the following procedures were followed to calculate the roots of B^2.

Consider $B^2 = \alpha_1^2 \pm j\beta_1^2$ $B^2 = \alpha_2^2 \pm j\beta_2^2$

assume $\alpha_1^2 + j\beta_1^2$ has two roots $\pm(c_1+jd_1)$

$\alpha_1^2 - j\beta_1^2$ has two roots $\pm (c_1-jd_1)$

Therefore $\alpha_1^2 + j\beta_1^2 = (c_1^2-d_1^2) + j2c_1d_1$

$\alpha_1^2 - j\beta_1^2 = (c_1^2- d_1^2) -j2c_1d_1$

α_1^2 and β_1^2 could be found in terms of c_1 and d_1

$$\alpha_1^2 = c_1^2 - d_1^2$$

$$\beta_1^2 = 2c_1d_1$$

so $$d_1 = \frac{\beta_1^2}{2c_1} \quad \text{and} \quad d_1^2 = \frac{\beta_1^4}{4c_1^2}$$

Substitute the d_1 and d_1^2 into the α_1^2 equation,

$$\alpha_1^2 = c_1^2 - \frac{\beta_1^4}{4c_1^2}$$

or $$4c_1^4 - 4\alpha_1^2 c_1^2 - \beta_1^4 = 0$$

The c_1^2 from this equation and corresponding d_1^2 was calculated

$$\text{For} \begin{cases} c_1^2 = (\alpha_1^2 + \sqrt{\alpha_1^4+\beta_1^4})/2 \\ d_1^2 = -(\alpha_1^2 - \sqrt{\alpha_1^4+\beta_1^4})/2 \end{cases} \quad \text{and} \quad \begin{cases} c_1^2 = (\alpha_1^2 - \sqrt{\alpha_1^4+\beta_1^4})/2 \\ d_1^2 = -(\alpha_1^2 + \sqrt{\alpha_1^4+\beta_1^4})/2 \end{cases}$$

For our system, where $k_\infty < 1$ and α^2 has to be corrected for radial leakage by adding $-B_r^2$ (α^2 is negative).

Let $$a^2 = (\sqrt{\alpha_1^4 + \beta_1^4} + \alpha_1^2)/2 \qquad \text{(positive)}$$

$$b^2 = (\sqrt{\alpha_1^4 + \beta_1^4} - \alpha_1^2)/2 \qquad \text{(positive)}$$

Therefore, $$a = \left| \sqrt{(\sqrt{\alpha_1^4 + \beta_1^4} + \alpha_1^2)/2} \right|$$

$$b = \left| \sqrt{(\sqrt{\alpha_1^4 + \beta_1^4} - \alpha_1^2)/2} \right|$$

substitute these into c_1^2 and d_1^2 equations,

$$c_1^2 = a^2 \qquad c_1 = \pm a$$

$$d_1^2 = b^2 \qquad d_1 = \pm b$$

so $c_1 + jd_1 = \pm(a+jb)$ where $B^2 = \alpha_1^2 + j\beta_1^2$ and similarly for $B^2 = \alpha_1^2 - j\beta_1^2$

$$c_1^2 = -b^2 \qquad c_1 = \pm jb$$

$$d_1^2 = -a^2 \qquad d_1 = \pm ja$$

and the roots of $c_1 - jd_1 = \pm(a-jb)$

The flux in general has the form of $\phi = e^{\pm jB_z}$ where B_z is the value of B (Buckling) when it is corrected for B_r (radial leakage correction). Assume finite height cylinder, radius R, height h, radial flux = $J_o(\frac{2.405r}{R})$ where $R = R_{core} + \lambda$, λ is reflector savings. $B_r^2 = (\frac{2.405}{R})^2$ Therefore

$$\begin{cases} \phi = e^{\pm(ja-b)z} \\ B^2 = \alpha_1^2 + j\beta_1^2 \end{cases} ; \qquad \begin{cases} \phi = e^{\pm(ja+b)z} \\ B^2 = \alpha_1^2 - j\beta_1^2 \end{cases}$$

4.1.1 Coupling Coefficients:

The coupling coefficients (4.11) are in terms of B^2, so they would be complex quantities to be determined. Supposing

$$S = R + jP \quad ; \quad S = R - jP$$

For $B^2 = \alpha_1^2 + j\beta_1^2$ we will have

$$\phi' = A' e^{(ja-b)z} + A'' e^{-(ja-b)z}$$

using boundary condition to evaluate the constants A' and A'', for $z = h$, $\phi' = 0$. Substitute into the flux equation the result is

$$A'' = -A' e^{+2(ja-b)h}$$

Therefore the flux equation is

$$\phi' = A' \left[e^{-bz} e^{jaz} - e^{-b(2h-z)} e^{ja(2h-z)} \right]$$

since $(e^{j\theta} = \cos\theta + j \sin\theta)$, the flux equation could be written in terms of sines and cosines.

$$\phi' = A' \left[e^{-bz} \cos az - e^{-b(2h-z)} \cos a(2h-z) \right]$$

$$+jA' \left[e^{-bz} \sin az - e^{-b(2h-z)} \sin a(2h-z) \right]$$

and similarly for $B^2 = \alpha_1^2 - j\beta_1^2$ the flux is

$$\phi'' = A' e^{(ja+b)z} + A'' e^{-(ja+b)z}$$

using boundary condition, $z=h$, $\phi'' = 0$, A' could be found in terms of A''

$$A' = -A'' e^{-2(ja+b)h}$$

Substitute in the flux equation (ϕ''), and using

$(e^{-j\theta} = \cos\theta - j\sin\theta)$, the result is

$$\phi'' = A'' \begin{bmatrix} e^{-bz}\cos az & -e^{-b(2h-z)}\cos a(2h-z) \end{bmatrix}$$

$$-jA'' \begin{bmatrix} e^{-bz}\sin az & -e^{-b(2h-z)}\sin a(2h-z) \end{bmatrix}$$

$\phi' + \phi''$ is real if $A' = A'' = \frac{A}{2}$

so, $$\phi' + \phi'' = A\begin{bmatrix} e^{-bz}\cos az & -e^{-b(2h-z)}\cos(2h-z)a \end{bmatrix} \quad .... \quad (4.12)$$

Consider the other flux groups, coupled to this one by the relation

$$S'_i = R_i + jP_i \quad ; \quad S''_i = R_i - jP_i$$

$$\text{So, } \phi'_i = A' (R_i + jP_i) \begin{bmatrix} e^{-bz}\cos az - e^{-b(2h-z)}\cos a(2h-z) \\ + j(e^{-bz}\sin az - e^{-b(2h-z)}\sin a(2h-z)) \end{bmatrix}$$

multiplying two complex values and rearranging it, the result is

$$\phi'_i = A' \begin{bmatrix} R_i\,(e^{-bz}\cos az - e^{-b(2h-z)}\cos a(2h-z)) \\ -P_i(e^{-bz}\sin az - e^{-b(2h-z)}\sin a(2h-z)) \\ +jR_i(e^{-bz}\sin az - e^{-b(2h-z)}\sin a(2h-z)) \\ \mp jP_i(e^{-bz}\cos az - e^{-b(2h-z)}\cos a(2h-z)) \end{bmatrix}$$

and similarly for $S_i'' = R_i - jP_i$

$$\phi_1'' = A'' \begin{bmatrix} R_i\,(e^{-bz}\cos az - e^{-b(2h-z)}\cos a(2h-z)) \\ -P_i\,(e^{-bz}\sin az - e^{-b(2h-z)}\sin a(2h-z)) \\ -jR_i\,(e^{-bz}\sin az - e^{-b(2h-z)}\sin a(2h-z)) \\ -jP_i\,(e^{-bz}\cos az - e^{-b(2h-z)}\cos a(2h-z)) \end{bmatrix}$$

again $\phi_i' + \phi_i''$ is real when $A' = A'' = \frac{A}{2}$ and the result is,

$$\phi_i' + \phi_i'' = A \begin{bmatrix} R_i\,(e^{-bz}\cos az - e^{-b(2h-z)}\cos a(2h-z)) \\ -P_i\,(e^{-bz}\sin az - e^{-b(2h-z)}\sin a(2h-z)) \end{bmatrix}$$

..... (4.13)

$e^{-bz}\cos az$ term represents outgoing wave and $-e^{-b(2h-z)}\cos a(2h-z)$ represents the reflected wave from the far boundary.

Well away from the boundary, where z=h

$$\phi' + \phi'' = A e^{-bz}\cos az \quad \text{and} \quad \phi_i' + \phi_i'' = Ae^{-bz}$$

$$[R_i \cos az - P_i \sin az]$$

4.2 ONE GROUP TREATMENT

One group treatment for time dependent subcritical is a useful example of how the calculation works. Supposing the flux has the form of $\Phi = \phi_2 + j\phi_1$

Therefore the diffusion equations are,

$$D\nabla^2\phi_2 - \Sigma_r \phi_2 + K\Sigma_r \phi_2 = \frac{-w}{V} \phi_1$$

$$D\nabla^2\phi_1 - \Sigma_r \phi_1 + K\Sigma_r \phi_1 = \frac{+w}{V} \phi_2$$

put $\frac{w}{V} = \Sigma_1$ and $(1-K)\Sigma_r = \Sigma$ $\quad (K<1)$

regarding flux with the Buckling

$$\nabla^2\phi_2 = -B^2\phi_2 \quad \text{and} \quad \nabla^2\phi_1 = -B^2\phi_1$$

Assume the solution of these has the form of $\phi = e^{\pm jBz}$

Now, substitute the values of Σ_1 and Σ into the diffusion equations,

$$-(DB^2 + \Sigma)\phi_2 + \Sigma_1\phi_1 = 0$$

$$-(DB^2 + \Sigma)\phi_1 - \Sigma_1\phi_2 = 0$$

or

$$\begin{vmatrix} -(DB^2+\Sigma) & \Sigma_1 \\ -\Sigma_1 & -(DB^2+\Sigma) \end{vmatrix} \begin{vmatrix} \phi_2 \\ \phi_1 \end{vmatrix} = 0$$

Hence the critically determinant is,

$$\begin{vmatrix} -(DB^2+\Sigma) & \Sigma_1 \\ -\Sigma_1 & -(DB^2+\Sigma) \end{vmatrix} = 0$$

Therefore $(DB^2+\Sigma)^2 + \Sigma_1^2 = 0$

When this is solved the B^2 has two complex values,

$B^2 = \frac{-\Sigma}{D} \pm j\frac{\Sigma_1}{D} = \alpha^2 \pm j\beta^2$, referring to section (4.1) two roots of B^2 could be calculated.

and coupling coefficient

$$S = \frac{\phi_1}{\phi_2} = \frac{(DB^2+\Sigma)}{\Sigma_1}$$

or $S = \pm j$

Since the coupling coefficient is obtained, real and imaginary components of flux could be very easily written using the flux equations obtained in previous section (4.12). So we have

$$\phi_2 \text{ (real)} = A\left[e^{-bz} \cos az - e^{-b(2h-z)} \cos a(2h-z)\right]$$

and imaginary component could be found by using equation (4.13)

where $R_i = 0$ $\quad P_i = \pm j$

$$\phi_1 \text{(imag)} = A\left[e^{-bz} \sin az - e^{-b(2h-z)} \sin a(2h-z)\right]$$

also for zero frequency, where a ≡ 0

$$\phi_1 = 0$$

and $$\phi_2 = A\left[e^{-bz} - e^{-b(2h-z)}\right] = Ae^{-bh}\left[e^{b(h-z)} - e^{-b(h-z)}\right]$$

or $$\phi_2 = 2Ae^{-bh} \sinh b(h-z)$$

which is the more usual form given for flux variation in an exponential system.

At $z = 0$ where frequency is not zero ($w \neq 0$)

$$\phi_2 = A(1-e^{-2bh} \cos 2ah)$$

$$\phi_1 = -A\, e^{-2bh} \sin 2ah$$

4.3 TWO NEUTRON ENERGY GROUPS:

Having obtained the Buckling coefficients, it is now necessary to return to the coupling coefficients and find the value of them. So far we have calculated, $B_1^2 = \alpha_1^2 \pm j\beta_1^2$ and roots of B_1^2 in section (4.1) where the values of a_1 and b_1 were

$$a_1 = \left| \sqrt{(\sqrt{\alpha_1^4+\beta_1^4}+\alpha_1^2)/2} \right| \text{ and } b_1 = \left| \sqrt{(\sqrt{\alpha_1^4+\beta_1^4}-\alpha_1^2)/2} \right|$$

and similarly for $B_2^2 = \alpha_2^2 \pm j\beta_2^2$ the real and imaginary components of roots of B_2^2 were,

$a_2 = \left| \sqrt{(\sqrt{\alpha_2^4+\beta_2^4}+\alpha_2^2)/2} \right|$ and $b_2 = \left| \sqrt{(\sqrt{\alpha_2^4+\beta_2^4}-\alpha_2^2)/2} \right|$

supposing the coupling coefficients are defined as $S_1, S_2,$ S_3 and $S_4 = 1$,

For $\begin{cases} B_1^2 = \alpha_1^2 \pm j\beta_1^2 \\ a_1 \ , \ b_1 \end{cases}$ we have,

$$S_1 = \begin{cases} R_{11}+jP_{11} \\ \text{or} \\ R_{11}-jP_{11} \end{cases} \quad S_2 = \begin{cases} R_{21}+jP_{21} \\ \text{or} \\ R_{21}-jP_{21} \end{cases} \quad S_3 = \begin{cases} R_{31}+jP_{31} \\ \text{or} \\ R_{31}-jP_{31} \end{cases} \quad S_4 = 1$$

and also for $\begin{cases} B_2^2 = \alpha_2^2 \pm j\beta_2^2 \\ a_2, b_2 \end{cases}$ similarly the coupling coefficients are,

$$S_1 = \begin{cases} R_{12}+jP_{12} \\ \text{or} \\ R_{12}-jP_{12} \end{cases} \quad S_2 = \begin{cases} R_{22}+jP_{22} \\ \text{or} \\ R_{22}-jP_{22} \end{cases} \quad S_3 = \begin{cases} R_{32}+jP_{32} \\ \text{or} \\ R_{32}-jP_{32} \end{cases} \quad S_4 = 1$$

generally if $B^2 = \alpha^2 \pm j\beta^2$, substitute it into equations (4.10). the L_2, L_3, L_4, ($L_2 = L_4$ because of $D_4 = D_2$ and $\underset{4}{\Sigma} = \underset{2}{\Sigma}$) will have real and imaginary components. Regarding subcripts R and I have the meaning of real and imaginary components, we have

$$L_{2_R} = D_2\alpha^2 + \Sigma_2$$

$$L_{2_I} = D_2\beta^2$$

$$L_{3_R} = D_3\alpha^2 + \Sigma_3$$

$$L_{3_I} = D_3\beta^2$$

$$L_{4_R} = L_{2_R}$$

$$L_{4_I} = L_{2_I}$$

Substituting the L values into the Equations (4.11).

Therefore if

$$E_1 = \Sigma_{13}\,\Sigma_{24}\,(\Sigma_{13}\,\Sigma_{24} - \Sigma_{12}\,\Sigma_{21}) + \Sigma_{13}\,L_{4R}\,(\Sigma_{13}\,L_{2R} + \Sigma_{12}\,\Sigma_{23}) - \Sigma_{13}^2 L_{2I} L_{4I}$$

$$E_2 = \Sigma_{13}^2\,L_{4R}\,L_{2I} + \Sigma_{13}\,L_{4I}\,(\Sigma_{13}\,L_{2R} + \Sigma_{12}\,\Sigma_{23})$$

$$E_3 = \Sigma_{13}\,\Sigma_{12}\,(\Sigma_{13}\,L_{2R} + \Sigma_{12}\,\Sigma_{23} + \Sigma_{24}\,L_{3R})$$

$$E_4 = \Sigma_{12}\,\Sigma_{13}^2\,L_{2I} + \Sigma_{12}\,\Sigma_{13}\,\Sigma_{24}\,L_{3I}$$

For compactness, the coupling coefficient S_3 is,

$$S_3 = R_3 + jP_3 = \frac{E_1 + jE_2}{E_3 + jE_4}$$

or $$(R_3 + jP_3)(E_3 + jE_4) = E_1 + jE_2$$

and finally two sides of above equation leading to two equal complex values, so by making real component of left side equal to real component of the right hand side and similarly for imaginary components, R_3 and P_3 could be found in terms of E_1, E_2, E_3 and E_4

$$R_3 = \frac{E_1 + E_4\left(\frac{E_2E_3 - E_1E_4}{E_3^2 + E_4^2}\right)}{E_3}$$

and

$$P_3 = \frac{E_2E_3 - E_1E_4}{E_3^2 + E_4^2}$$

Similarly for $S_2 = R_2 + jP_2$, if

$$F_1 = R_3 \underset{12}{\Sigma} \underset{3_R}{L} - P_3 \underset{12}{\Sigma} \underset{3_I}{L} - \underset{13}{\Sigma} \underset{24}{\Sigma} - \underset{12}{\Sigma} \underset{21}{\Sigma}$$

$$F_2 = \underset{12}{\Sigma} R_3 \underset{3_I}{L} + \underset{12}{\Sigma} P_3 \underset{3_R}{L}$$

$$F_3 = \underset{13}{\Sigma} \underset{2_R}{L} + \underset{12}{\Sigma} \underset{23}{\Sigma}$$

$$F_4 = \underset{13}{\Sigma} \underset{2_I}{L}$$

So
$$S_2 = R_2 + jP_2 = \frac{F_1 + jF_2}{F_3 + jF_4}$$

and
$$R_2 = \frac{F_1 + F_4\left[\dfrac{F_2F_3 - F_1F_4}{F_3^2 + F_4^2}\right]}{F_3}$$

$$P_2 = \frac{F_2F_3 - F_1F_4}{F_3^2 + F_4^2}$$

and similarly for S_1, where

$$G_1 = \underset{2_R}{L} R_2 - \underset{2_I}{L} P_2 + \underset{24}{\Sigma}$$

$$G_2 = \underset{2_R}{L} P_2 + \underset{2_I}{L} R_2$$

we have
$$S_1 = R_1 + jP_1 = \frac{G_1 + jG_2}{\underset{12}{\Sigma}}$$

and

$$R_1 = \frac{G_1}{\Sigma_{12}}$$

$$P_1 = \frac{G_2}{\Sigma_{12}}$$

So, if subcripts of brackets represents the corresponding Buckling coefficient, for $B_1^2 = \alpha_1^2 \pm j\beta_1^2$ and $B_2^2 = \alpha_2^2 \pm j\beta_2^2$, the following calculations will result in the corresponding coupling coefficient components.

For $B_1^2 = \alpha_1^2 \pm j\beta_1^2$

$$(L_{2_R})_1 = D_2\alpha_1^2 + \Sigma_2$$

$$(L_{2_I})_1 = D_2\beta_1^2$$

$$(L_{3_R})_1 = D_3\alpha_1^2 + \Sigma_3$$

$$(L_{3_I})_1 = D_3\beta_1^2$$

$$(L_{4_R})_1 = (L_{2_R})_1$$

$$(L_{4_I})_1 = (L_{2_I})_1$$

and $(E_1)_1 = \Sigma_{13}\ \Sigma_{24}\ (\Sigma_{13}\ \Sigma_{24} - \Sigma_{12}\ \Sigma_{21}) + \Sigma_{13}\ (L_{4_R})_1$

$$\left[\Sigma_{13}\ (L_{2_R})_1 + \Sigma_{12}\ \Sigma_{23}\right] - \Sigma_{13}^2\ (L_{2_I})_1\ (L_{4_I})_1$$

$$(E_2)_1 = \Sigma_{13}^2\ (L_{4_R})_1\ (L_{2_I})_1 + \Sigma_{13}\ (L_{4_I})_1 \left[\Sigma_{13}\ (L_{2_R})_1 + \Sigma_{12}\ \Sigma_{23}\right]$$

$$(E_3)_1 = \Sigma_{13}\ \Sigma_{12}\left[\Sigma_{13}\ (L_{2_R})_1 + \Sigma_{12}\ \Sigma_{23} + \Sigma_{24}\ (L_{3_R})_1\right]$$

$$(E_4)_1 = \Sigma_{12}\ \Sigma_{13}^2\ (L_{2_I})_1 + \Sigma_{12}\ \Sigma_{13}\ \Sigma_{24}\ (L_{3_I})_1$$

and similarly for $B_2^2 = \alpha_2^2 \pm j\beta_2^2$, we have

$$(L_{2_R})_2 = D_2\alpha_2^2 + \Sigma_2$$

$$(L_{2_I})_2 = D_2\beta_2^2$$

$$(L_{3_R})_2 = D_3\alpha_2^2 + \Sigma_3$$

$$(L_{3_I})_2 = D_3\beta_2^2$$

$$(L_{4_R})_2 = (L_{2_R})_2$$

$$(L_{4_I})_2 = (L_{2_I})_2$$

$$(E_1)_2 = \Sigma_{13}\ \Sigma_{24}\ (\Sigma_{13}\ \Sigma_{24} - \Sigma_{12}\ \Sigma_{21}) + \Sigma_{13}\ (L_{4_R})_2\left[\Sigma_{13}\ (L_{2_R})_2 + \Sigma_{12}\ \Sigma_{23}\right]$$

$$- \Sigma_{13}^2\ (L_{2_I})_2\ (L_{4_I})_2$$

$$(E_2)_2 = \Sigma_{13}^2 (L_{4R})_2 (L_{2I})_2 + \Sigma_{13} (L_{4I})_2 \left[\Sigma_{13} (L_{2R})_2 + \Sigma_{12} \Sigma_{23}\right]$$

$$(E_3)_2 = \Sigma_{13} \Sigma_{12} \left[\Sigma_{13} (L_{2R})_2 + \Sigma_{12} \Sigma_{23} + \Sigma_{24} (L_{3R})_2\right]$$

$$(E_4)_2 = \Sigma_{12} \Sigma_{13}^2 (L_{2I})_2 + \Sigma_{12} \Sigma_{13} \Sigma_{24} (L_{3I})_2$$

Therefore the coupling coefficient components are

$$R_{31} = \frac{(E_1)_1 + (E_4)_1 \left[\dfrac{(E_2)_1 (E_3)_1 - (E_1)_1 (E_4)_1}{[(E_3)_1]^2 + [(E_4)_1]^2}\right]}{(E_3)_1}$$

$$P_{31} = \frac{(E_2)_1 (E_3)_1 - (E_1)_1 (E_4)_1}{[(E_3)_1]^2 + [(E_4)_1]^2}$$

and components corresponding to B_2^2

$$R_{32} = \frac{(E_1)_2 + (E_4)_2 \left[\dfrac{(E_2)_2 (E_3)_2 - (E_1)_2 (E_4)_2}{[(E_3)_2]^2 + [(E_4)_2]^2}\right]}{(E_3)_2}$$

$$P_{32} = \frac{(E_2)_2 (E_3)_2 - (E_1)_2 (E_4)_2}{[(E_3)_2]^2 + [(E_4)_2]^2}$$

also similarly for R_2 and P_2, coupling coefficient components

$$(F_1)_1 = R_{31} \Sigma_{12} (L_{3_R})_1 - P_{31} \Sigma_{12} (L_{3_I})_1 - \Sigma_{13} \Sigma_{24} - \Sigma_{12} \Sigma_{21}$$

$$(F_2)_1 = \Sigma_{12} R_{31} (L_{3_I})_1 + \Sigma_{12} P_{31} (L_{3_R})_1$$

$$(F_3)_1 = \Sigma_{13} (L_{2_R})_1 + \Sigma_{12} \Sigma_{23}$$

$$(F_4)_1 = \Sigma_{13} (L_{2_I})_1$$

and for $B_2^2 = \alpha_2^2 \pm j\beta_2^2$

$$(F_1)_2 = R_{32} \Sigma_{12} (L_{3_R})_2 - P_{32} \Sigma_{12} (L_{3_I})_2 - \Sigma_{13} \Sigma_{24} - \Sigma_{12} \Sigma_{21}$$

$$(F_2)_2 = \Sigma_{12} R_{32} (L_{3_I})_2 + \Sigma_{12} P_{32} (L_{3_R})_2$$

$$(F_3)_2 = \Sigma_{13} (L_{2_R})_2 + \Sigma_{12} \Sigma_{23}$$

$$(F_4)_2 = \Sigma_{13} (L_{2_I})_2$$

$$R_{21} = \frac{(F_1)_1 + (F_4)_1 \left[\dfrac{(F_2)_1 (F_3)_1 - (F_1)_1 (F_4)_1}{[(F_3)_1]^2 + [(F_4)_1]^2} \right]}{(F_3)_1}$$

$$P_{21} = \frac{(F_2)_1(F_3)_1 - (F_1)_1(F_4)_1}{[(F_3)_1]^2 + [(F_4)_1]^2}$$

and

$$R_{22} = \frac{(F_1)_2 + (F_4)_2 \left[\frac{(F_2)_2(F_3)_2 - (F_1)_2(F_4)_2}{[(F_3)_2]^2 + [(F_4)_2]^2} \right]}{(F_3)_2}$$

$$P_{22} = \frac{(F_2)_2 (F_3)_2 - (F_1)_2 (F_4)_2}{[(F_3)_2]^2 + [(F_4)_2]^2}$$

Similarly for R_1 and P_1 components

if $(G_1)_1 = (L_{2R})_1 . R_{21} - (L_{2I})_1 . P_{21} + \Sigma_{24}$

$(G_2)_1 = (L_{2R})_1 . P_{21} + (L_{2I})_1 . R_{21}$

$(G_1)_2 = (L_{2R})_2 . R_{22} - (L_{2I})_2 . P_{22} + \Sigma_{24}$

$(G_2)_2 = (L_{2R})_2 . P_{22} + (L_{2I})_2 . R_{22}$

Therefore,

$$R_{11} = \frac{(G_1)_1}{\Sigma_{12}}$$

$$P_{11} = \frac{(G_2)_1}{\Sigma_{12}}$$

and

$$R_{12} = \frac{(G_1)_2}{\Sigma_{12}}$$

$$P_{12} = \frac{(G_2)_2}{\Sigma_{12}}$$

4.3.1 Neutron Flux Equations:

Having obtained the coupling coefficients, it is now necessary to return to Equations (4.12, 4.13) and find the flux equations, where the real component of B^2 is now corrected for radial leakage. (α^2 is now corrected for radial leakage).

$$\text{real thermal } \phi_4 = A_1\begin{bmatrix} e^{-b_1 z}\cos a_1 z - e^{-b_1(2h-z)}\cos a_1(2h-z) \end{bmatrix} + A_2\begin{bmatrix} e^{-b_2 z}\cos a_2 z - e^{-b_2(2h-z)}\cos a_2(2h-z) \end{bmatrix}$$

real fast

$$\phi_3 = A_1\begin{bmatrix} R_{31}(e^{-b_1 z}\cos a_1 z - e^{-b_1(2h-z)}\cos a_1(2h-z)) \\ -P_{31}(e^{-b_1 z}\sin a_1 z - e^{-b_1(2h-z)}\sin a_1(2h-z)) \end{bmatrix} + A_2\begin{bmatrix} R_{32}(e^{-b_2 z}\cos a_2 z - e^{-b_2(2h-z)}\cos a_2(2h-z)) \\ -P_{32}(e^{-b_2 z}\sin a_2 z - e^{-b_2(2h-z)}\sin a_2(2h-z)) \end{bmatrix}$$

Imaginary thermal,

$$\phi_2 = A_1 \begin{bmatrix} R_{21}(e^{-b_1 z}\cos a_1 z - e^{-b_1(2h-z)}\cos a_1(2h-z)) \\ -P_{21}(e^{-b_1 z}\sin a_1 z - e^{-b_1(2h-z)}\sin a_1(2h-z)) \end{bmatrix}$$

$$+ A_2 \begin{bmatrix} R_{22}(e^{-b_2 z}\cos a_2 z - e^{-b_2(2h-z)}\cos a_2(2h-z)) \\ -P_{22}(e^{-b_2 z}\sin a_2 z - e^{-b_2(2h-z)}\sin a_2(2h-z)) \end{bmatrix}$$

Imaginary fast,

$$\phi_1 = A_1 \begin{bmatrix} R_{11}(e^{-b_1 z}\cos a_1 z - e^{-b_1(2h-z)}\cos a_1(2h-z)) \\ -P_{11}(e^{-b_1 z}\sin a_1 z - e^{-b_1(2h-z)}\sin a_1(2h-z)) \end{bmatrix}$$

$$+A_2 \begin{bmatrix} R_{12}(e^{-b_2 z}\cos a_2 z - e^{-b_2(2h-z)}\cos a_2(2h-z)) \\ -P_{12}(e^{-b_2 z}\sin a_2 z - e^{-b_2(2h-z)}\sin a_2(2h-z)) \end{bmatrix}$$

Two constants A_1 and A_2 are determined by using the boundary conditions.

4.3.2 Boundary Conditions

To determine the flux equations two constants of A_1 and A_2 were needed to be evaluated. This was done by using boundary conditions. At z=0 three options are available,

1) $\phi_4 = 0$, $-D_1 \frac{d\phi_3}{dz} = J_1$

2) $\phi_3 = 0$, $-D_2 \frac{d\phi_4}{dz} = J_2$

3) $-D_1 \frac{d\phi_3}{dz} = J_1$ and $-D_2 \frac{d\phi_4}{dz} = J_2$ where the relative strength of J_1 and J_2 should be decided by reference to previous calculations. It will be seen that

differentials of F and G will be needed, where F and G are,

$$F = [e^{-bz}\cos az - e^{-b(2h-z)}\cos a(2h-z)]$$

$$G = [e^{-bz}\sin az - e^{-b(2h-z)}\sin a(2h-z)]$$

The differentials are

$$\frac{dF}{dz} = F' = -e^{-bz}(b\cos az + a\sin az)$$

$$-e^{-b(2h-z)}[b\cos a(2h-z) + a\sin a(2h-z)]$$

and $(\frac{dF}{dz})_0 = F_0' = -b - e^{-2bh}(b\cos 2ah + a\sin 2ah)$

Similarly differential of G

$$\frac{dG}{dz} = G' = -e^{-bz}(b\sin az - a\cos az)$$

$$-e^{-b(2h-z)}[b\sin a(2h-z) - a\cos a(2h-z)]$$

and $(\frac{dG}{dz})_0 = G_0' = a - e^{-2bh}[b\sin 2ah - a\cos 2ah]$

Now consider first option,

1) $(\phi_4)_0 = 0$

Therefore, substitute z=0 and $\phi_4 = 0$ in flux equation representing ϕ_4 in section (4.3.1), A_2 could be found in terms of A_1,

$$A_2 = -A_1 \frac{[1-e^{-2b_1h} \cos 2a_1h]}{[1-e^{-2b_2h} \cos 2a_2h]}$$

or $$A_2 = -A_1 \frac{F_{10}}{F_{20}}$$

where F_{10} is the value of F for (a_1, b_1 and z=0) and F_{20} has the similar meaning. i.e. value of F for (a_2,b_2, z=0)

and $$-\left[\frac{d\phi_3}{dz}\right]_0 = \frac{J_1}{D_1}$$

Therefore,

$$A_1 = \frac{-J_1/D_1}{\left[R_{31}F'_{10}-P_{31}G'_{10}- \frac{1-e^{-2b_1h}\cos 2a_1h}{1-e^{-2b_2h}\cos 2a_2h}(R_{32}F'_{20}-P_{32}G'_{20})\right]}$$

and finally

$$A_1 = \frac{-J_1/D_1}{R_{31}F'_{10}-P_{31}G'_{10} - \frac{F_{10}}{F_{20}}(R_{32}F'_{20} - P_{32}G'_{20})}$$

where F'_{10} is the value of F' for (a_1, b_1 and z=0).

G'_{10}, F'_{20}, G'_{20} have the similar meanings.

2) Second option of boundary is,

$(\phi_3)_0 = 0$

Therefore $$A_2 = -A_1 \left[\frac{R_{31}F_{10}-P_{31}G_{10}}{R_{32}F_{20}-P_{32}G_{20}} \right]$$

and $$\frac{J_2}{D_2} = - \left(\frac{d\phi_4}{dz}\right)_0$$

so $$A_1 = \frac{-J_2/D_2}{F'_{10} - \left[\frac{R_{31}F_{10}-P_{31}G_{10}}{R_{32}F_{20}-P_{32}G_{20}}\right] F'_{20}}$$

3) The third option is,

$$\frac{J_2}{D_2} = -A_1 F'_{10} - A_2 F'_{20}$$

$$\frac{J_1}{D_1} = -A_1(R_{31} F'_{10}-P_{31}G'_{10}) - A_2(R_{32}F'_{20}-P_{32}G'_{20})$$

By solving these two equations A_1 and A_2 can be found.

$$A_1 = - \frac{J_2/D_2 + A_2F'_{20}}{F'_{10}}$$

substitute into the second equation, A_2 could be evaluated.

$$A_2 = \frac{J_1/D_1 - \frac{J_2/D_2}{F'_{10}} (R_{31}F'_{10} - P_{31}G'_{10})}{(F'_{20}/F'_{10})(R_{31}F'_{10}-P_{31}G'_{10}) - (R_{32}F'_{20}-P_{32}G'_{20})}$$

4.4 COMPUTER PROGRAM ATEST

The theoretical frequency response characteristics of the subcritical assembly were obtained by means of computer program ATEST. This program was written in

FORTRAN. The second option of Boundary condition (at z=0, all neutrons assumed thermal) were taken into the calculations. The program after calculating real (ϕ_R) and imaginary (ϕ_I) components of thermal flux for a given height of core, calculates the amplitude response and phase shift by following relations.

$$\text{Amplitude response} = \frac{\sqrt{\phi_R^2 + \phi_I^2}}{\text{thermal neutron flux at zero frequency and same height}}$$

$$\text{phase} = \frac{\phi_I}{\phi_R}$$

These were repeated for different heights of the core, and for different frequencies. The program is represented in Appendix C. It also gives the thermal flux amplitude in different layers of the core.

4.5 CALCULATION OF GAMMA RESPONSE

Having obtained the thermal neutron flux in different layers of subcritical core, it was possible to calculate the prompt fission gamma produced in outside the subcritical where the detector was located. This was done by adding the all gamma rays produced from different layers of the core on that point.

Suppose point D is outside the subcritical where gamma detector was located. Let us first consider one layer of the core and then extend it to the whole core

(R is the radius of the core). Assuming P is one of the points of fission (r distance from centre of the core), where the fission has occurred. To determine the fission gamma at point D, it was necessary to calculate the attenuation coefficient.

The gamma rays produced at point P has to travel through two media to get to the point D. If ℓ_1 is the distance travelled inside the uranium and ℓ_2 is the distance in water, so

$$\ell = \ell_1 + \ell_2$$

where ℓ is the distance between points P and D. For convenience in making calculations let us consider Fig. (4.1).

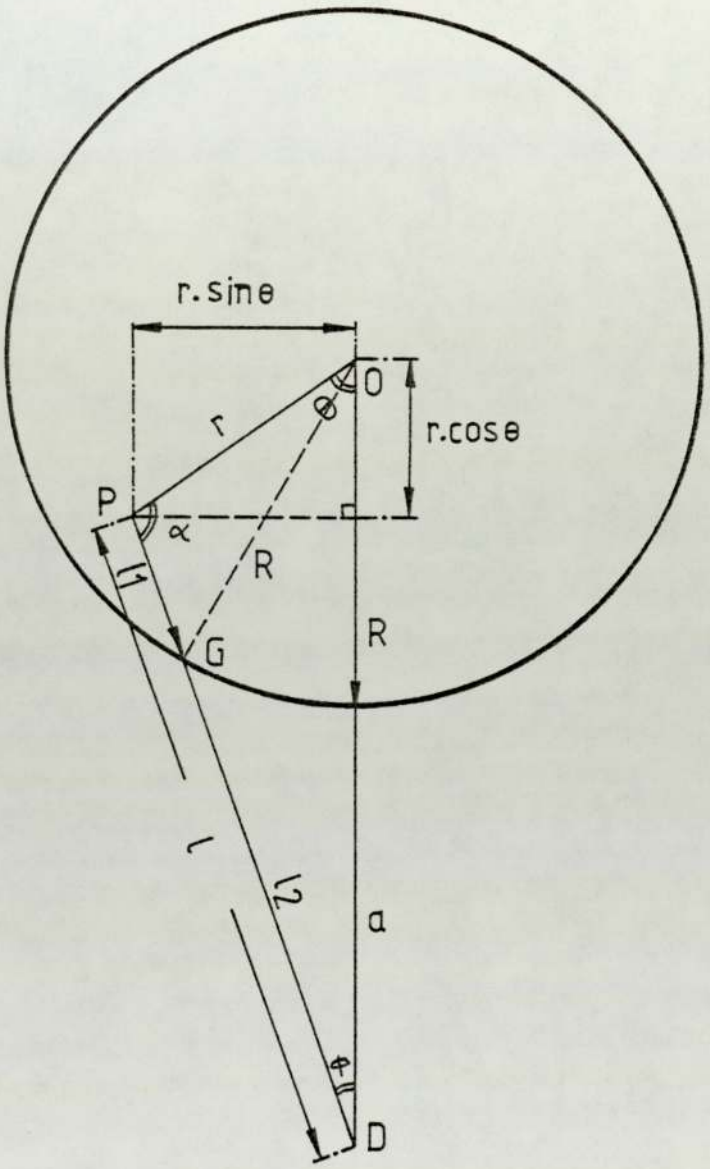

Fig. (4.1)

Regarding triangular DPO and GPO, it could be written

$$\ell^2 = r^2 + (R+a)^2 - 2r(R+a)\cos\theta \quad \text{and}$$

$$R^2 = \ell_1^2 + r^2 - 2\ell_1 r \cos\alpha$$

from second equation, ℓ_1 could be found.

Therefore $\ell_1 = r \cos \alpha + \sqrt{R^2 - r^2 \sin^2 \alpha}$ and ℓ could be obtained from the first equation, and finally $\ell_2 = \ell - \ell_1$. Suppose D has a distance of h above or below the considered layer (plane). Therefore the total path length L could be calculated from Fig. (4.2).

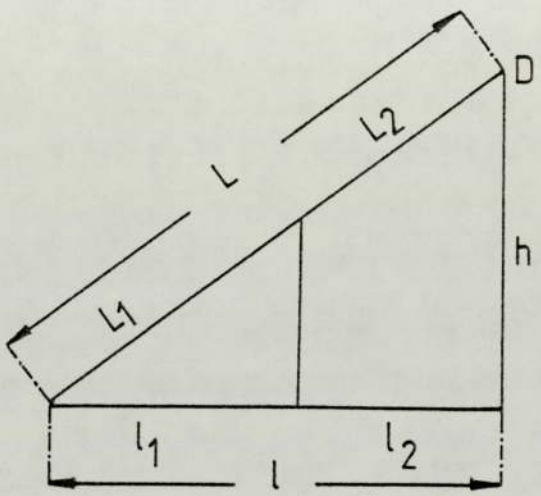

Fig. (4.2)

$$L = \sqrt{\ell^2 + h^2}$$

and also $$L_1 = \ell_1 . \frac{L}{\ell}$$

$$L_2 = L - L_1$$

So, the exponential attenuation coefficient from point P is

$$e^{-\mu_1 L_1} \cdot e^{-\mu_2 L_2} = e^{-(\mu_1 L_1 + \mu_2 L_2)}$$

where μ_1 and μ_2 are the absorption coefficients of the core and water respectively.

There is also an inverse square factor, therefore

$$\text{attenuation from point P at D} = \frac{e^{-(\mu_1 L_1 + \mu_2 L_2)}}{L^2}$$

Now considering fuel (core) as summation of unit cells with areas of δA, attenuating coefficient could be found for each unit cell. Consider Fig. (4.3), to calculate unit cell area.

The unit cell area = $r.\ \delta\theta.\delta r$ where $\delta\theta$ is the angle and δr is the unit cell width.

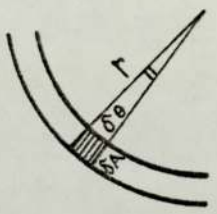

Fig. (4.3)

Therefore the total attenuation coefficient for each layer of gamma ray production at point D is,

$$\text{total attenuation for each layer} = \sum_{\theta,r} \delta_A . \frac{e^{-(\mu_1 L_1 + \mu_2 L_2)}}{L^2}$$

which is the summation over the attenuations of gamma rays at point D from each layer, where

$$\delta\theta = \frac{\pi}{m}$$

and

$$\delta r = \frac{R}{n} \qquad m = 20 \text{ and } n = 8$$

as the thermal neutron flux contribution in each layer was not completely plane, the Bessel functions corrections were introduced to the total attenuation coefficient.

Therefore,

$$\text{total attenuation for each layer} = \sum_{\theta,r} \delta A . \frac{e^{-(\mu_1 L_1 + \mu_2 L_2)}}{L^2} .$$

$$J_o\left(2.405 \frac{R}{R_{EXT}}\right)$$

where R_{EXT} is the extra polated length and is equal to

$$R_{EXT} = R_{core} + \text{Reflector savings}$$

Values of J_o, later were introduced inside the computer progamming by means of subroutine (LIB NAGF) in which J_o is defined as (S17AAF(R)).

Having obtained the amplitude ϕ_h and phase shift λ_h of thermal neutrons in different layers of the core by computer program code (ATEST), the flux for each layer is $\phi_h \sin(wt + \lambda_h)$, supposing each thermal neutron is production of fission, the gamma rays produced from each layer at point D is

$$\phi_h \sin(wt + \lambda_h) \text{ x total attenuation at h}$$

Summations of this over the total height of the core will give the total gamma rays introduced in point D by the core of subcritical assembly for each given frequency.

Therefore,

$$\Phi(wt + \lambda) = \sum_h \phi_h \sin(wt + \lambda_h) \text{ x total attenuation at h and for zero frequency}$$

$$\Phi(O) = \sum_{h} \phi_h(O) \times \text{total attenuation at h}$$

and finally fission gamma rays response function is

$$G.R.R.F. = \frac{\Phi(wt+\lambda)}{\Phi(O)}$$

4.6 COMPUTER PROGRAM GAMMARESFU

The theoretical frequency response characteristics of the subcritical assembly by prompt fission gamma rays were obtained by means of computer program GAMMARESFU. This program was written in FORTRAN, and performs the following operations for a given detector height, frequency and gamma ray energy (absorption coefficients are dependent on gamma rays energy).

a) Calculates the gamma rays introduced at detector location from different layers of the core (varying z=5cm to maximum of 80cm with 5cm interval). These calculations are done for zero and given frequency.

b) Summation of these gamma rays to obtain the final gamma rays introduced at detector location by the core. To simplify the summation of these the following procedures were performed in programming.
Suppose $A_1 \sin(wt+\lambda_1)$ is the gamma rays of first core layer at detector point and $A_2 \sin(wt+\lambda_2)$ is from second layer.
The program adds these two as follows:

if $A_3 \sin(wt+\lambda_3) = A_1 \sin(wt+\lambda_1) + A_2 \sin(wt+\lambda_2)$

Therefore $$A_3 = \sqrt{A_1^2 + A_2^2 + 2A_1A_2 \cos(\lambda_1-\lambda_2)}$$

and $$\lambda_3 = \text{ATAN}\frac{A_1 \sin\lambda_1 + A_2 \sin\lambda_2}{A_1 \cos\lambda_1 + A_2 \cos\lambda_2}$$

Having obtained A_3 and λ_3, it calculates the gamma rays of the third layer and adds on $A_3 \sin(wt+\lambda_3)$ in the same way.

c) The amplitude response function is obtained by dividing amplitude of total gamma rays of given frequency to zero frequency amplitude and phase shift will be the last calculated phase.

d) Program repeats this calculation to all given frequencies and also for detector location with 20cm interval.

The program is represented in Appendix D. The calculations were done for different axial gamma detector locations (H) and also for gamma ray energies varying from 3 Mev up to 10 Mev (these are the most expected range of fission gamma rays energies). The theoretical amplitude response obtained from these calculations are shown in Fig.s (4.4-4.9), and phase responses are represented in fig. (4.10-4.11).

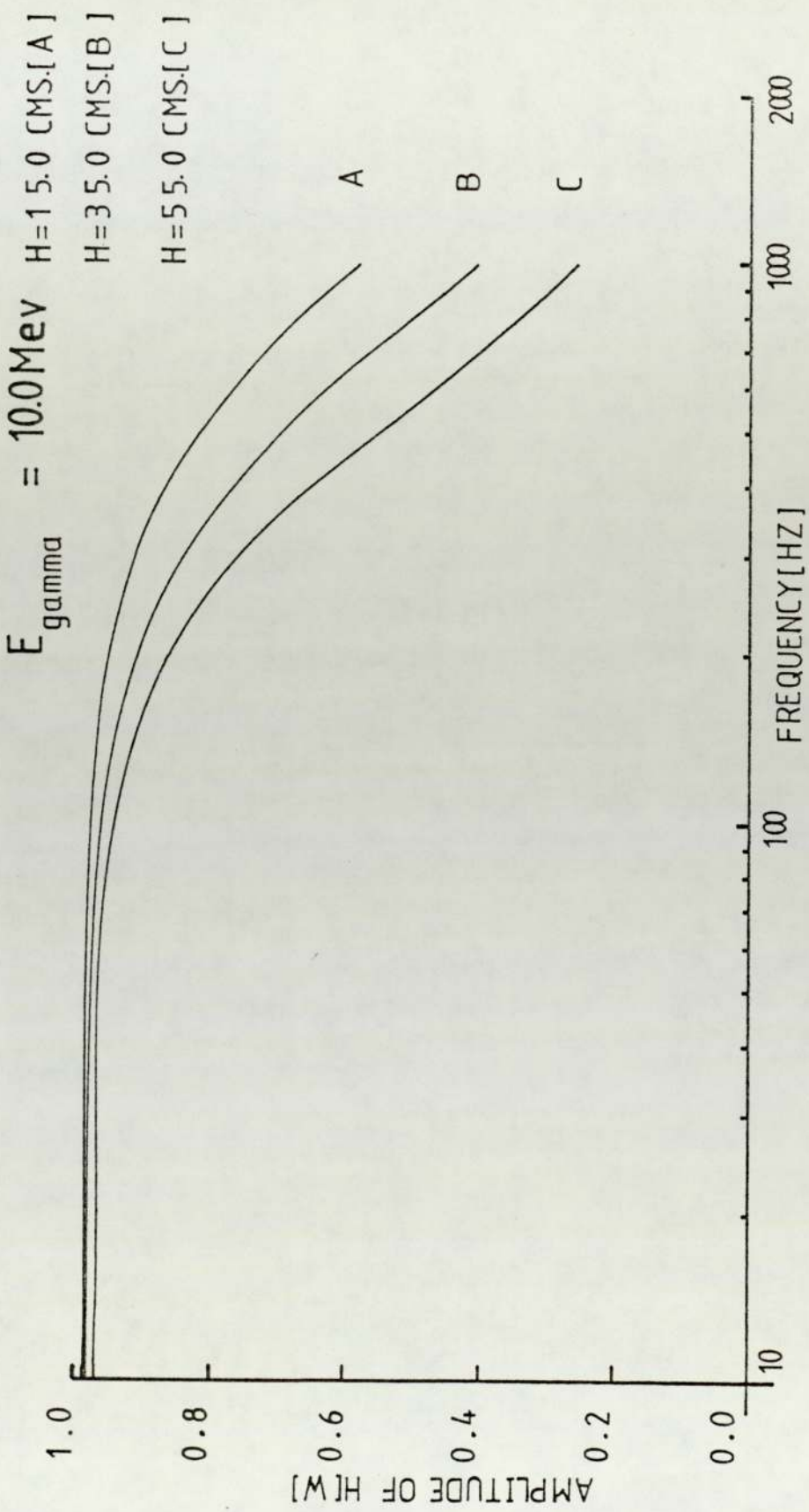

FIG.(4.4) THEORETICAL AMPLITUDE RESPONSE FOR DIFFERENT AXIAL POSITIONS

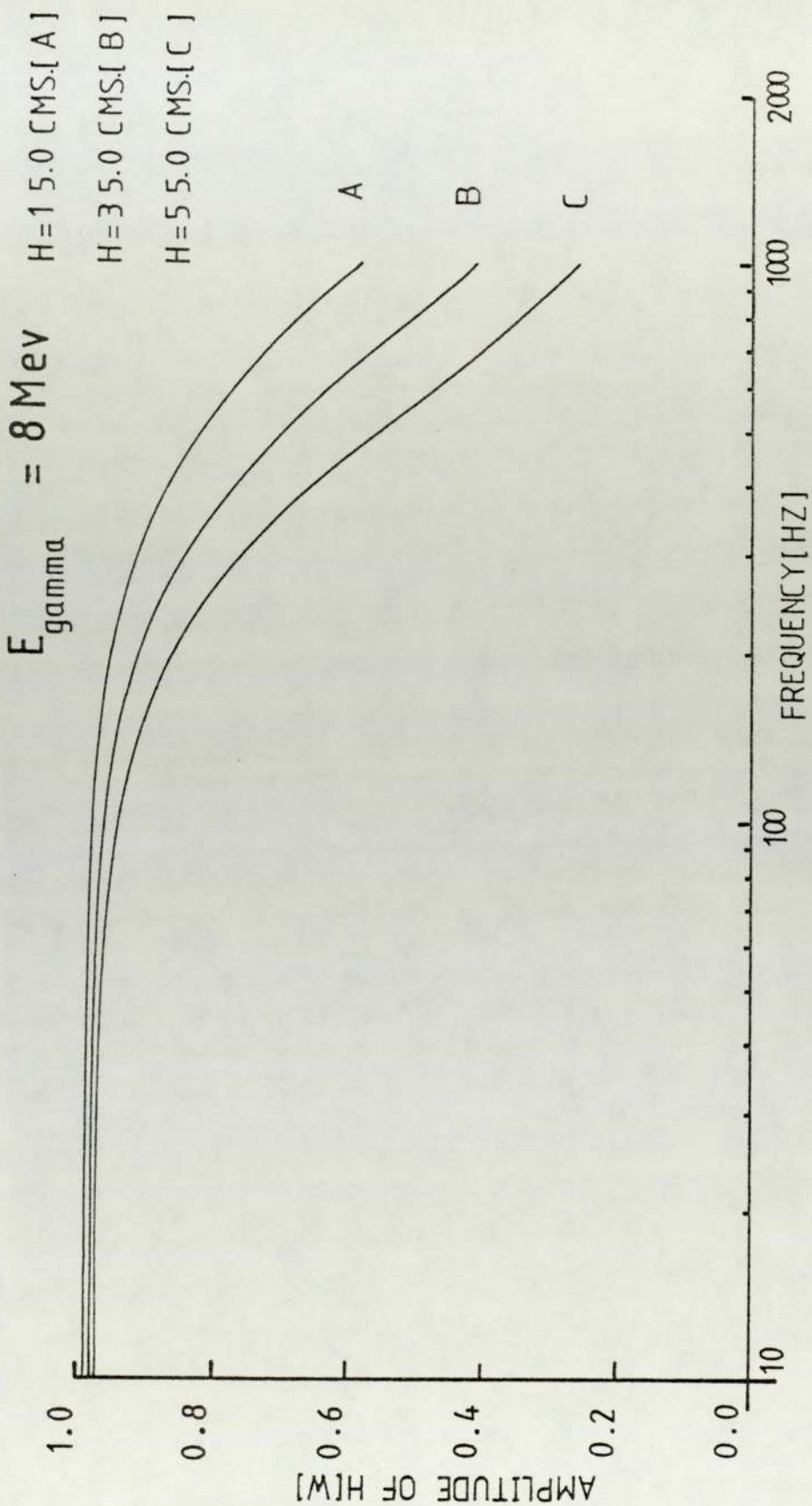

FIG.(4.5) THEORETICAL AMPLITUDE RESPONSE FOR DIFFERENT AXIAL POSITIONS

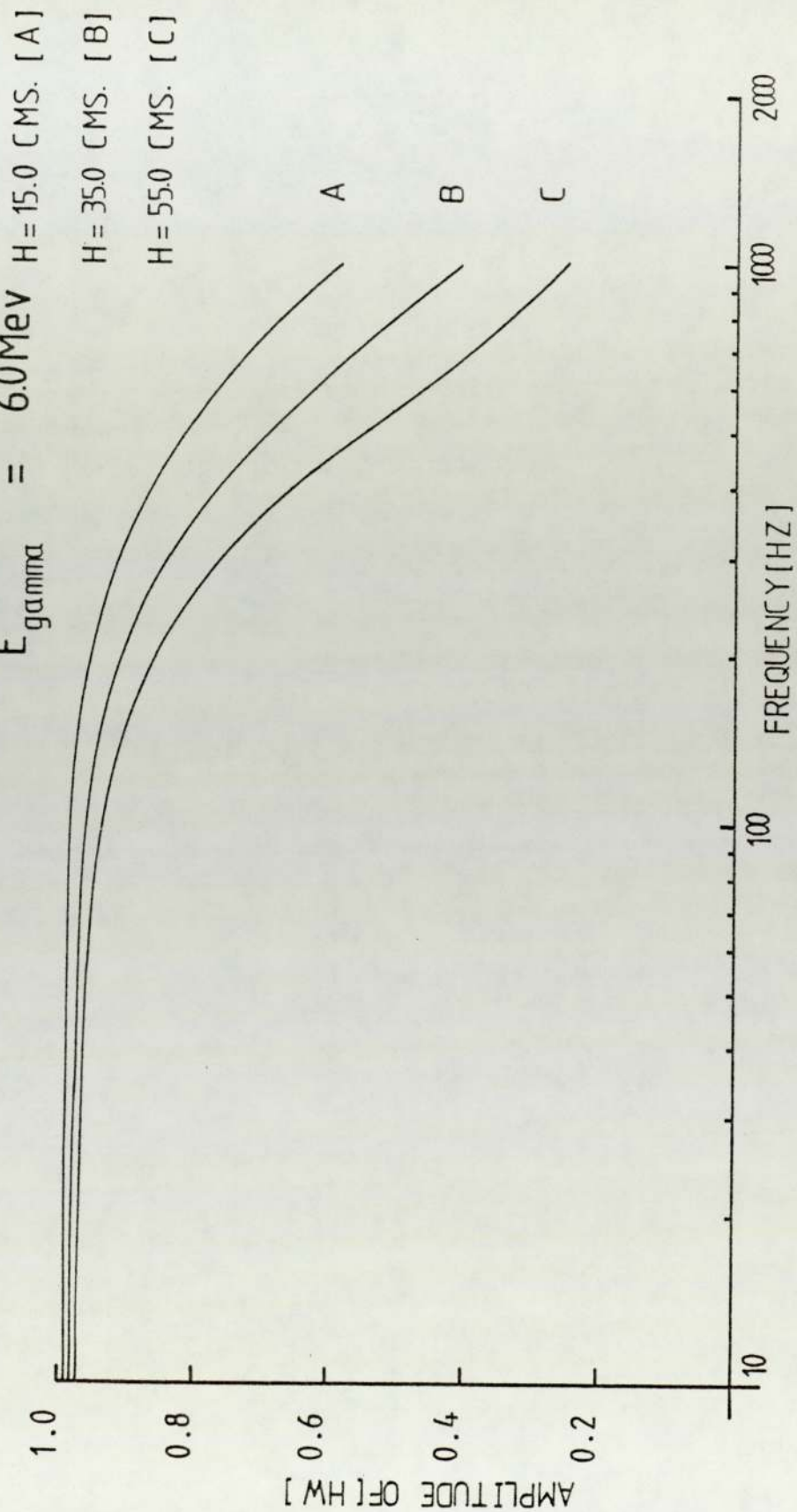

FIG.(4.6) THEORETICAL AMPLITUDE RESPONSE FOR DIFFERENT AXIAL POSITIONS

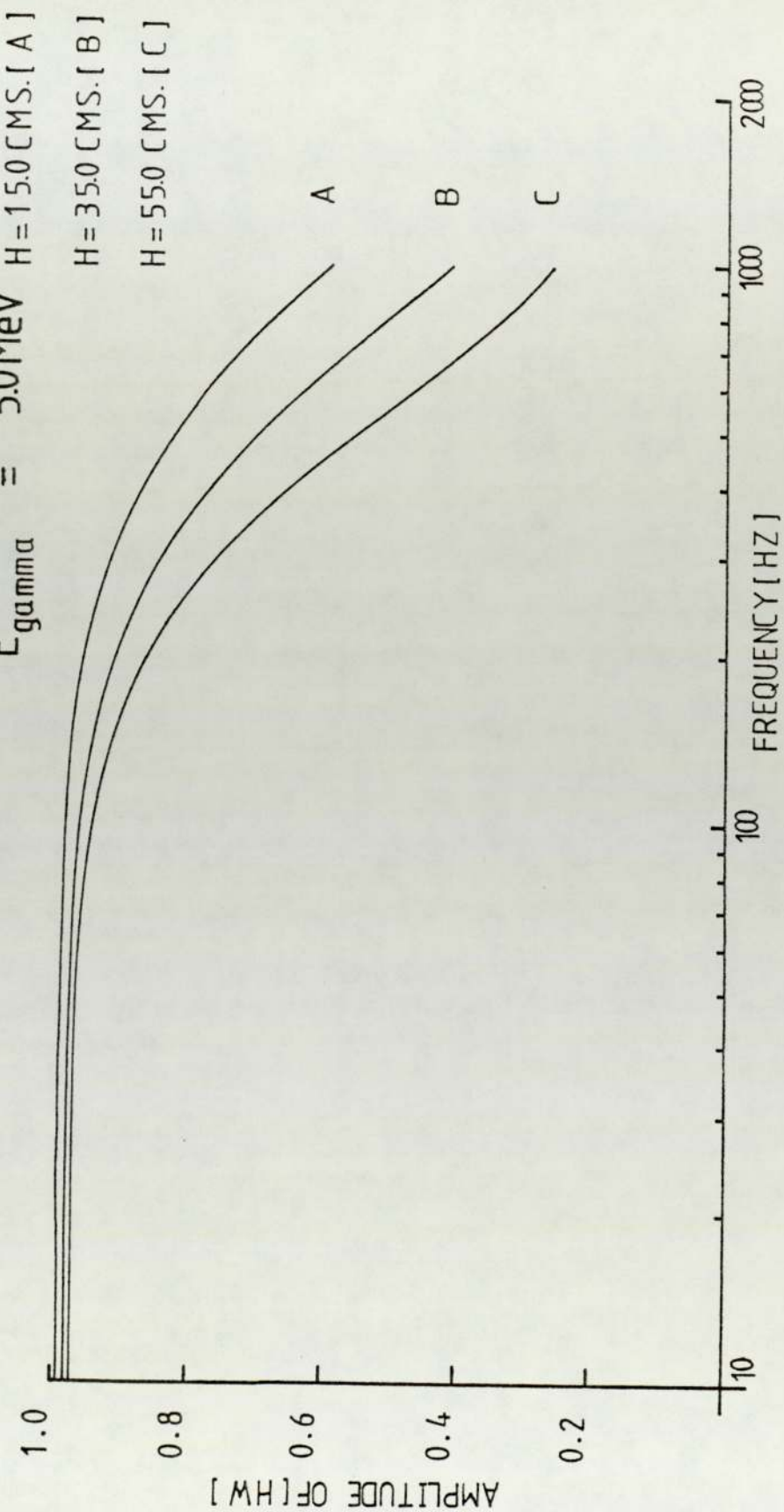

FIG.(4.7) THEORETICAL AMPLITUDE RESPONSE FOR DIFFERENT AXIAL POSITIONS

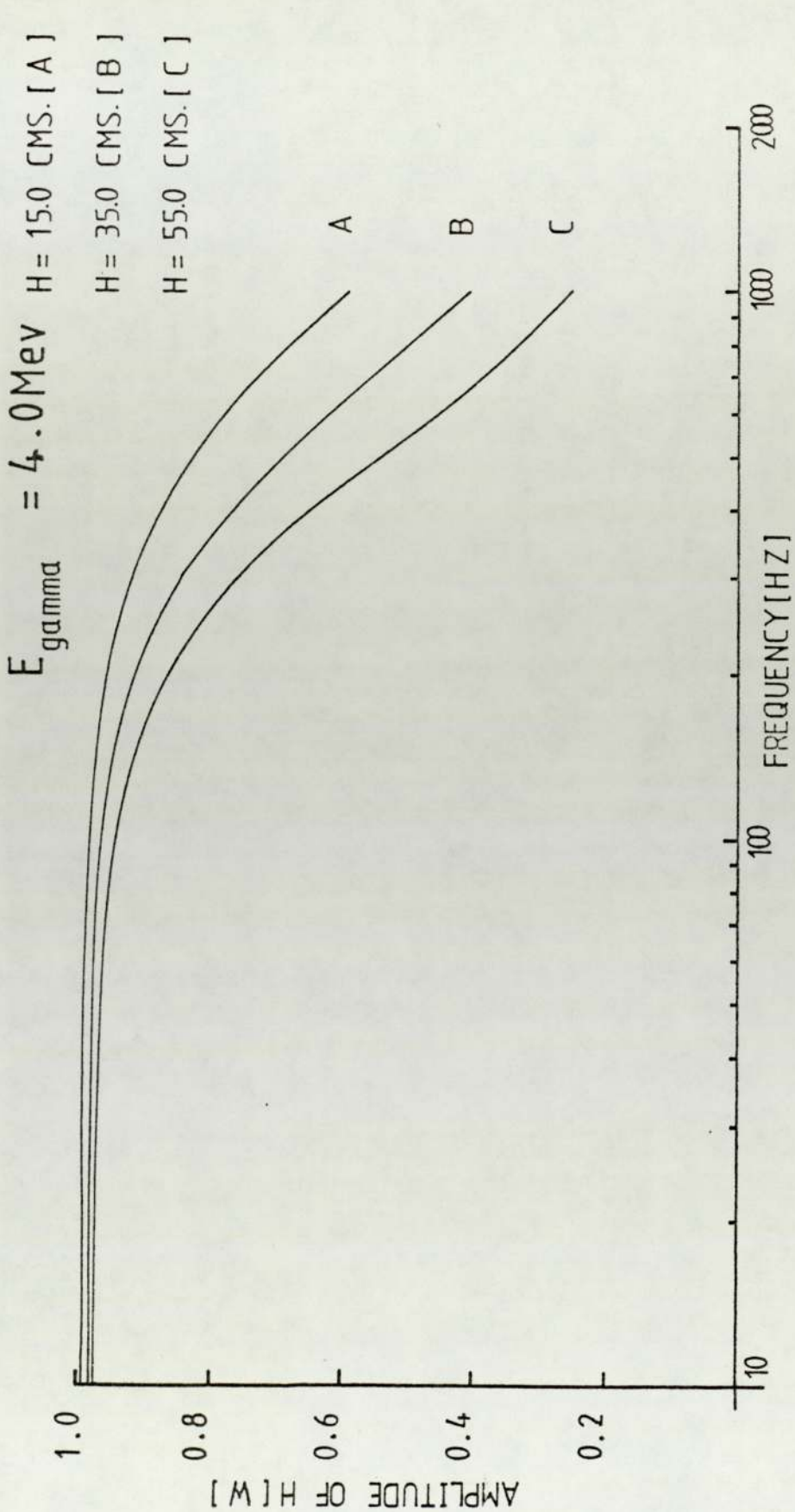

FIG.(4.8) THEORETICAL AMPLITUDE RESPONSE FOR DIFFERENT AXIAL POSITIONS

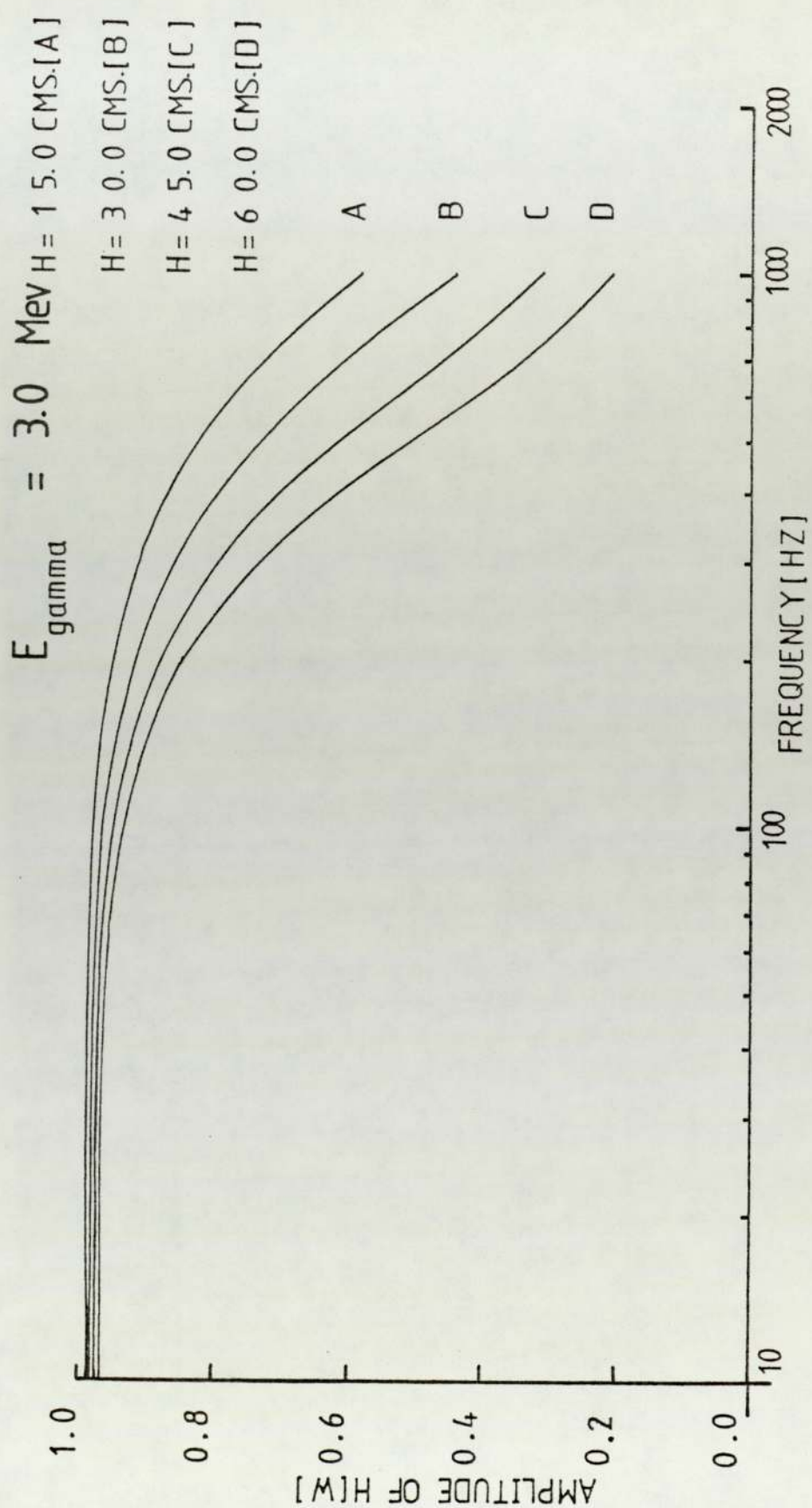

FIG.(4.9) THEORETICAL AMPLITUDE RESPONSE FOR DIFFERENT AXIAL POSITIONS

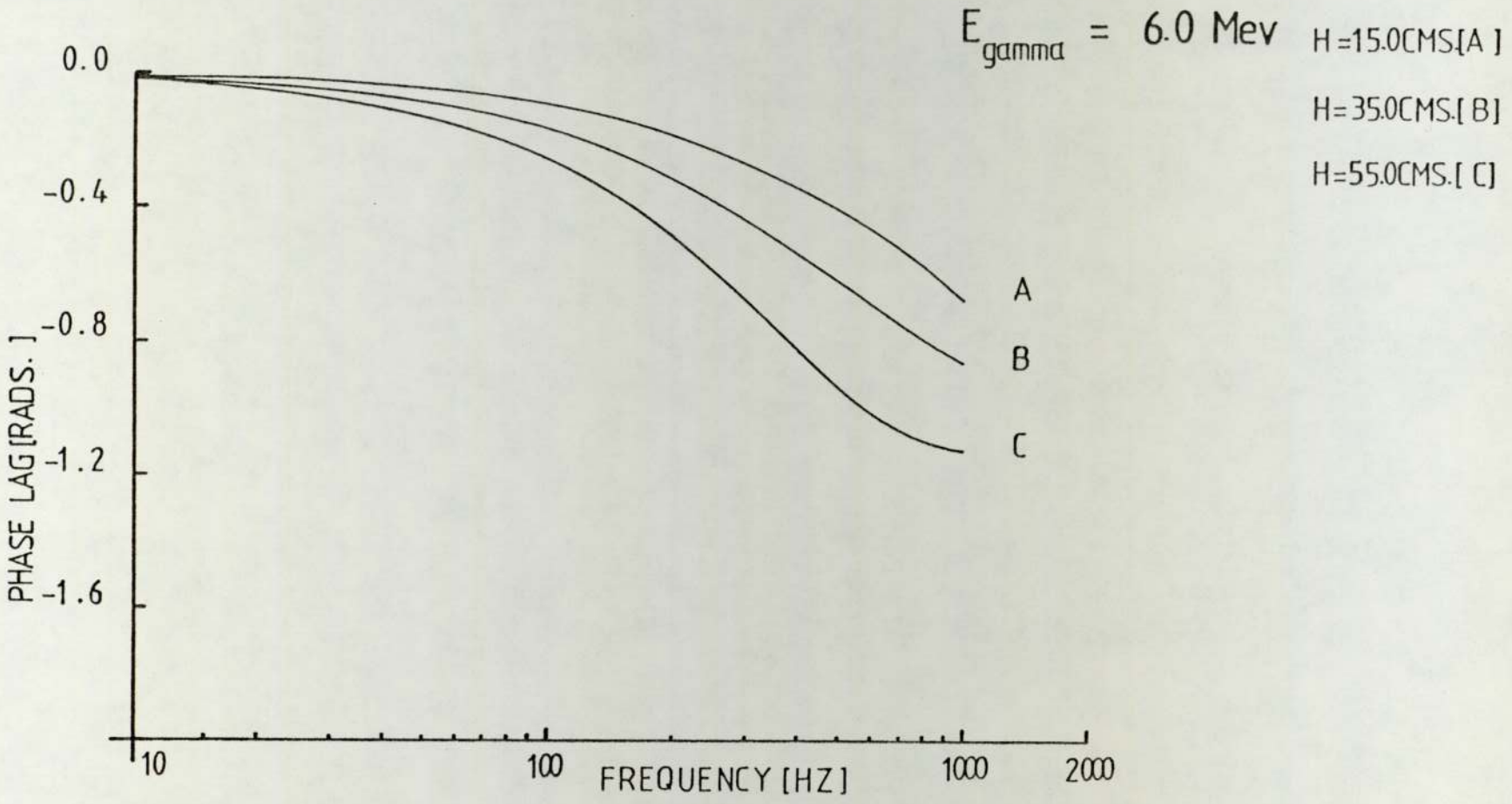

FIG.(4.10) THEORETICAL PHASE RESPONSE FOR DIFFERENT AXIAL POSITIONS

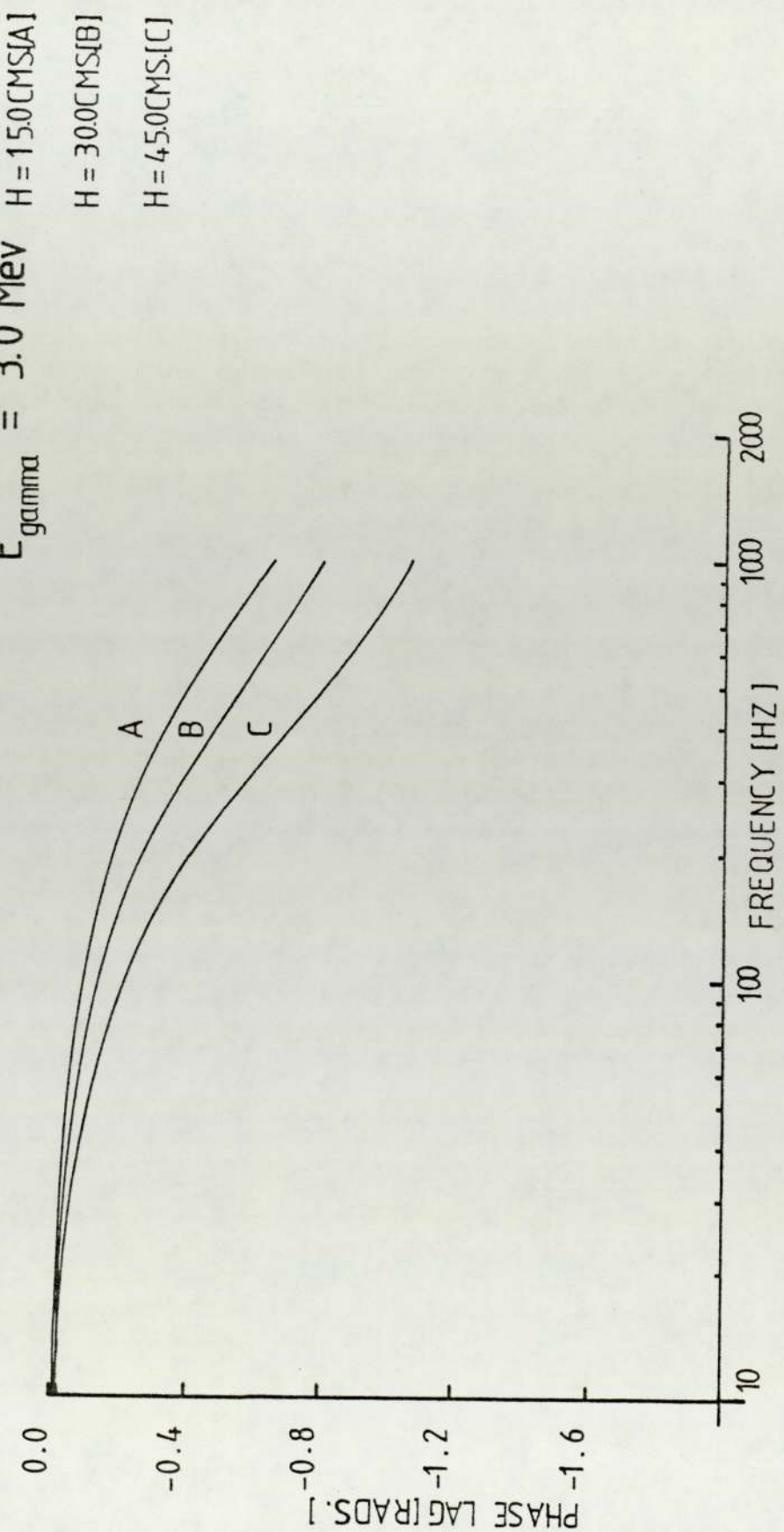

FIG.(4.11) THEORETICAL PHASE RESPONSE FOR DIFFERENT AXIAL POSITIONS

CHAPTER 5

DETECTOR EFFICIENCY

In this chapter the NaI(Tℓ) detector efficiency was calculated for different gamma ray energies to find which gamma ray energies are most efficiently detected.

If Σ_T is the total macroscopic cross-section of the NaI(Tℓ) crystal for a given gamma ray energy, the relative detector efficiency could be calculated from the following relation,

$$\text{relative efficiency} \propto \left[\text{mean number of photons per fission per Mev.}\right] . A(1-e^{-\Sigma_T . t}) \quad \ldots\ldots\ldots\ldots (5.1)$$

where A is the crystal front area,
and t is the thickness (for our NaI(Tℓ) crystal A=15.165 CM^2 and t is 2.54CMS).

Therefore both Σ_T and the mean number of photons per fission per Mev for each gamma ray energy should be evaluated to calculate detector efficiency.

5.1 TOTAL MACROSCOPIC CROSS-SECTION

The total macroscopic cross section is defined as

$$\Sigma_T = \Sigma_{pp} + \Sigma_{cc} + \Sigma_{PE} \quad \ldots\ldots\ldots\ldots (5.2)$$

where, Σ_{pp} is the macroscopic pair production cross-section, and Σ_{cc} is the macroscopic Compton scattering cross-section and Σ_{PE} is the macroscopic photoelectric cross-section. These cross-sections for different gamma ray energies were calculated with following procedure.

(i) Pair production

For creation of pairs by a gamma ray in the field of a nucleus the differential cross-section for the production of a positron of kinetic energy T_+ and therefore an electron of energy $(E_\gamma - 2mc^2 - T_+)$ could be written as[70,71]

$$d\sigma_{pp} = \frac{\delta_o z^2 P}{E_\gamma - 2mc^2} \, dT_+ \qquad \ldots\ldots\ldots\ldots \quad (5.3)$$

where $\delta_0 = \frac{1}{137} \left(\frac{\mu_0 e^2}{4\pi m}\right)^2 = 5.8 \times 10^{-32} \ m^2$

and E_γ is the incident gamma ray energy.

P is slowly varying function of E_γ and Z.

The variation of pair total cross section with energy for lead is shown in Fig. (5.1.a). This is obtained by integrating the expression (5.3) over the energy spectrum. The cross-section increases at first with energy, as the pair production takes place at larger distance from the nucleus, but a limit is set to

the increase by the screening of the nuclear charge by the atomic electrons. In the absence of screening the pair production cross-section is proportional to Z^2. Therefore

$$\frac{\sigma_{pp} \text{ (for iodine)}}{\sigma_{pp} \text{ (for lead)}} = \left[\frac{Z_{iodine}}{Z_{lead}}\right]^2$$

by using this relation and Fig. (5.1.a) the pair production cross section for iodine is obtained Fig. (5.1.b).

Similarly, pair production cross section for NaI is,

$$\sigma_{pp} \text{ (NaI)} = \sigma_{pp}\text{(iodine)} \left[1 + \left[\frac{Z_{sodium}}{Z_{iodine}}\right]^2\right]$$

and is shown in Fig. (5.1.c).

Therefore the macroscopic pair production cross-section per atom of NaI is given by,

$$\Sigma_{pp} = N. \sigma_{pp}$$

where N is the number density and is given by,

$$N = \frac{N_o . \rho}{\text{Mol.wt}}$$

where N_o is the avogadro's number 6.025×10^{23}

and ρ is the crystal density $3.667\ gcm^{-3}$

Mol.wt = 150 for sodium iodide.

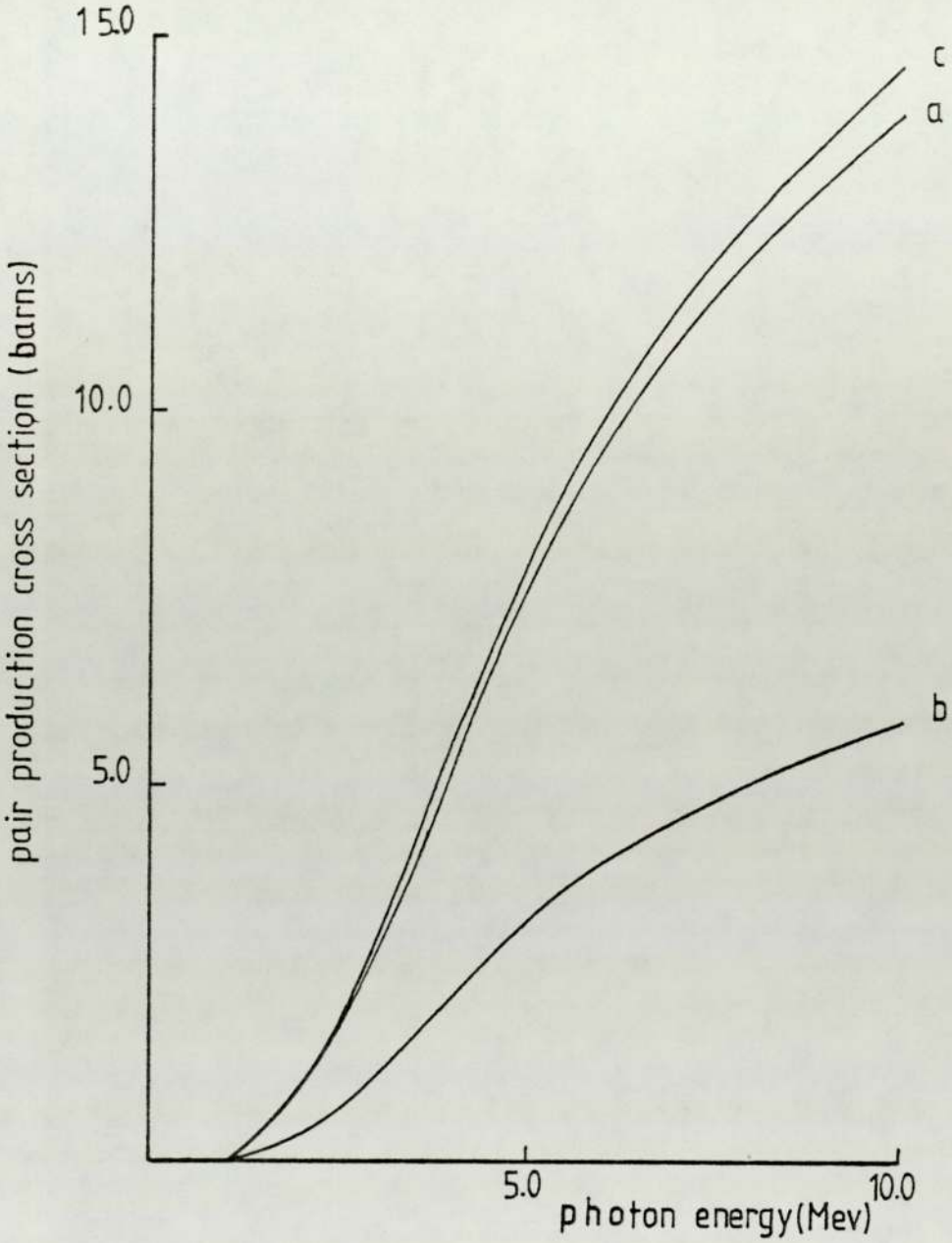

FIG. 5.1

ref.(38) (a) variation of pair total cross section σ_{pp} with energy for lead

(b) " " " " " " " " " " iodine

(c) " " " " " " " " " " Na I

Calculated pair production cross sections of NaI for different gamma ray energies is represented in table (5.1).

(ii) Compton scattering

Differentiated Compton cross section derived from Klein-Nishina expression is given by

$$\sigma_{cc} = \frac{\pi r^2}{\alpha^2 mc^2}\left[(T-E_\gamma)\left(\frac{1}{\alpha^2}+\frac{2}{\alpha}\right)+E_\gamma\left(\frac{2}{\alpha^2}+\frac{2}{\alpha}-1\right)\mathrm{Ln}(E_\gamma-T)+\frac{1}{\alpha^2}\cdot\frac{E_\gamma^2}{E_\gamma-T}-\frac{(E_\gamma-T)^2}{2E_\gamma}\right]_{T_{min}}^{T_{max}}$$

where $\alpha = \dfrac{E_\gamma}{mc^2}$

r is the classical electron radius = 2.81777×10^{-15} metres

$T_{max} = E_\gamma \cdot \dfrac{2\alpha}{1+2\alpha}$ maximum electron energy.

Using these equations the Compton cross-sections were calculated for different incident gamma ray energies.

The Compton scattering cross section per electron for scattered electrons of energy >2.50 Mev is given in Fig. (5.2). Macroscopic Compton scattering cross sections are calculated by expression,

$$\Sigma_{cc} = N\,\sigma_{cc}$$

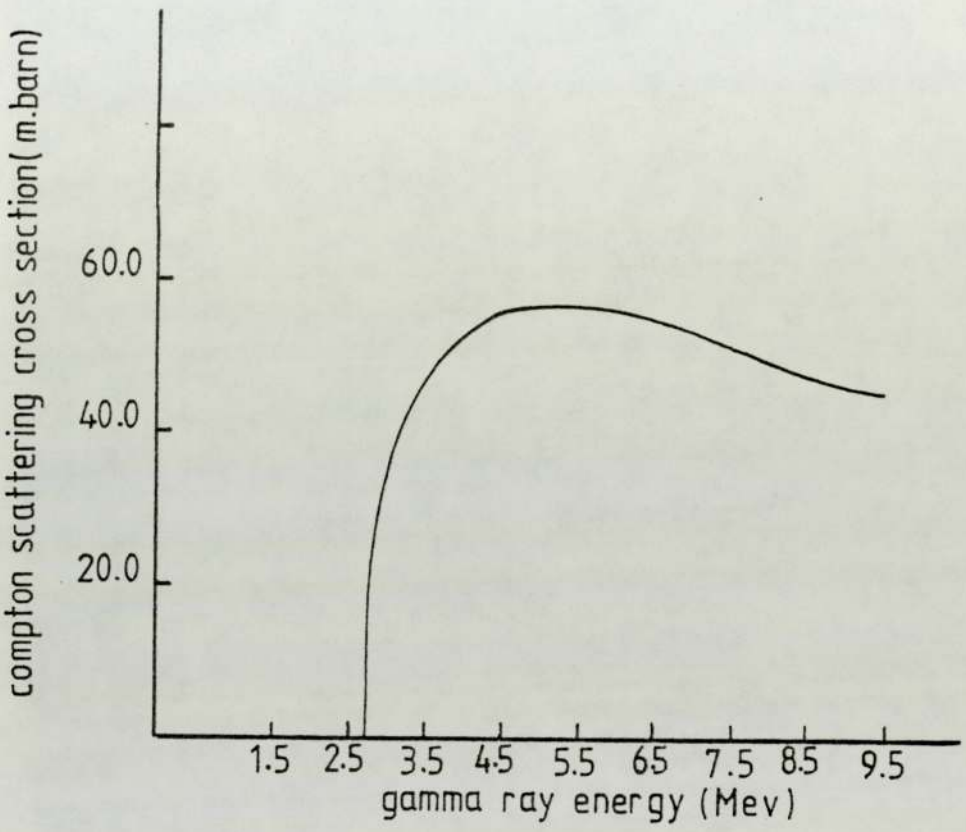

FIG.5.2 variation of Compton scattering cross section per electron with energy of gamma ray.

where N is the number density. To obtain the macroscopic Compton scattering cross-sections per atom of NaI crystal, the macroscopic Compton scattering cross-sections per electron were multiplied to the number of assumed free electrons per atom of sodium iodide (for sodium, electrons of K shell and for iodine, the electrons of K and L shells considered to be most bounded). The obtained macroscopic Compton scattering cross-sections per molecule of sodium iodide are represented in table (5.1).

(iii) Photoelectric

Macroscopic photoelectric cross sections are obtained by,

$$\Sigma_{PE} \simeq \mu_e$$

where μ_e is the energy absorption coefficient. It was calculated by multiplying the mass absorption coefficient of sodium iodide ($\frac{\mu_e}{\rho}$, values given in ref.[27]) to its density. The macroscopic photoelectric cross sections for sodium iodide is also given in table (5.1).

Having obtained the macroscopic pair production, Compton scattering, photoelectric cross sections the total macroscopic cross section (Σ_T) of sodium iodide for different gamma ray energies are determined by expression (5.2). The values of Σ_T are also given in table (5.1).

5.2 MEAN NUMBER OF PHOTONS PER FISSION PER Mev

The energy spectrum of prompt fission gamma rays was obtained by Maienschein [28]. This spectrum is shown in Fig. (5.3). To find the mean number of photons per fission per Mev, the spectrum was divided between energy intervals of 1 Mev. and replotted to calculate area concerning each energy interval (Figs. 5.4 and 5.5) and therefore the mean number of photons per fission per Mev was obtained by dividing each of these subarea to total area under the energy spectrum. The mean number of photons per fission per Mev is shown in Fig. (5.6) and given in table (5.1).

Having obtained the total macroscopic cross section for sodium iodide and also mean number of photons per fission per Mev, the relative efficiency for the detector used is obtained by using equation (5.1) described earlier in this chapter.

Finally, the relative efficiency for the gamma detector used is shown in Fig. (5.7). It is clear that the efficiency curve peak is between 3 to 4 Mev gamma rays, so the theoretical results at 3 and 4 Mev should best match the experiment.

The attenuation coefficient in the core and reflector are also given in table (5.1). It could be seen that they are varying very slowly with energy range of 3-10 Mev. The effect of these on the result are given

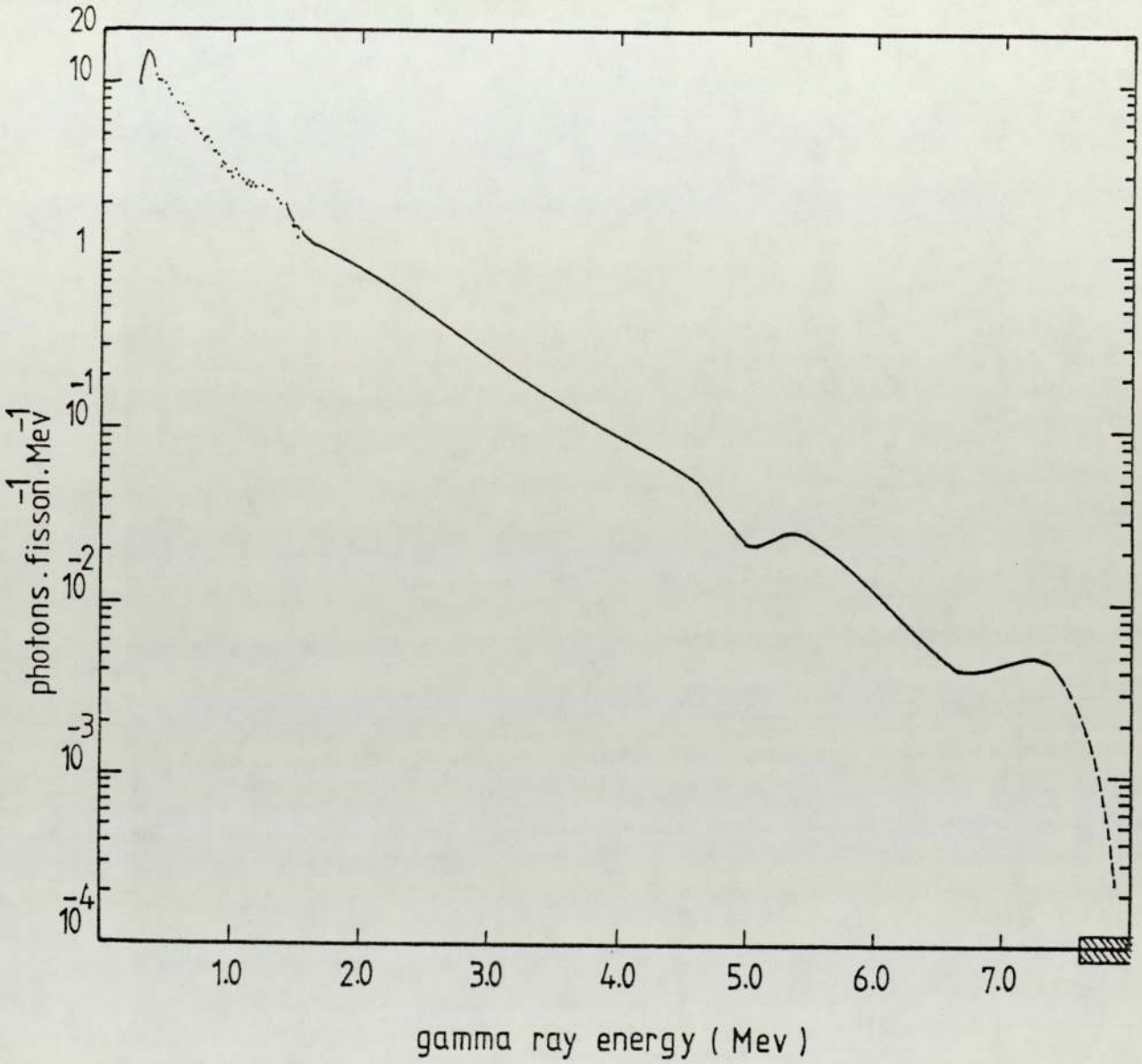

FIG. 5.3. The energy spectrum of promt gamma rays of fisson. Ref. (28).

▨ Average photons. fission^{-1}. Mev^{-1}. from 7.7 to 10.5 Mev

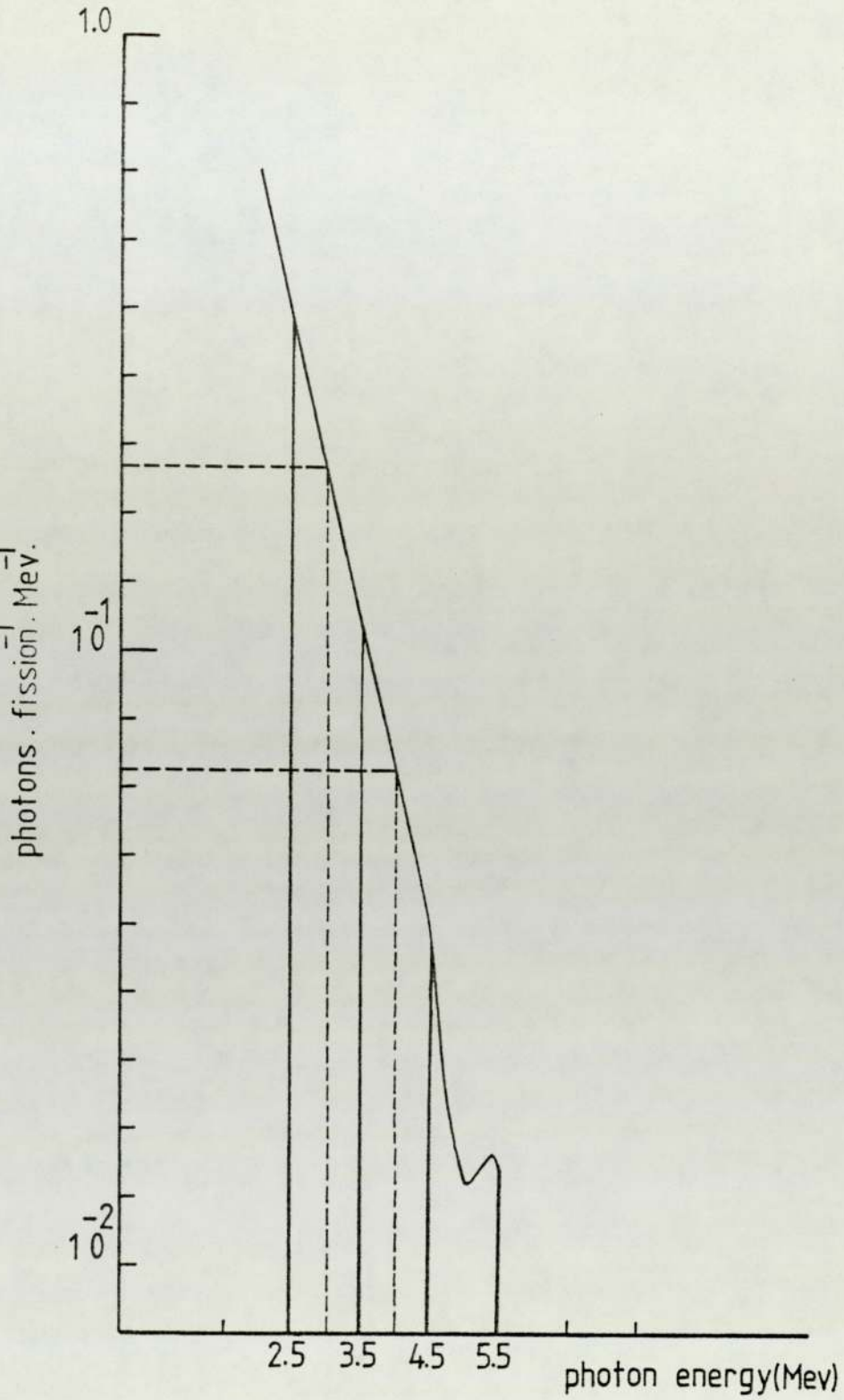

FIG.5.4 block area between 2.5 – 3.5 Mev = 1266×10^{-3} photons.fisson^{-1}

" " " 3.5 – 4.5 Mev = 818.5×10^{-3} " "

" " " 4.5 – 5.5 Mev = 305.5×10^{-3} " "

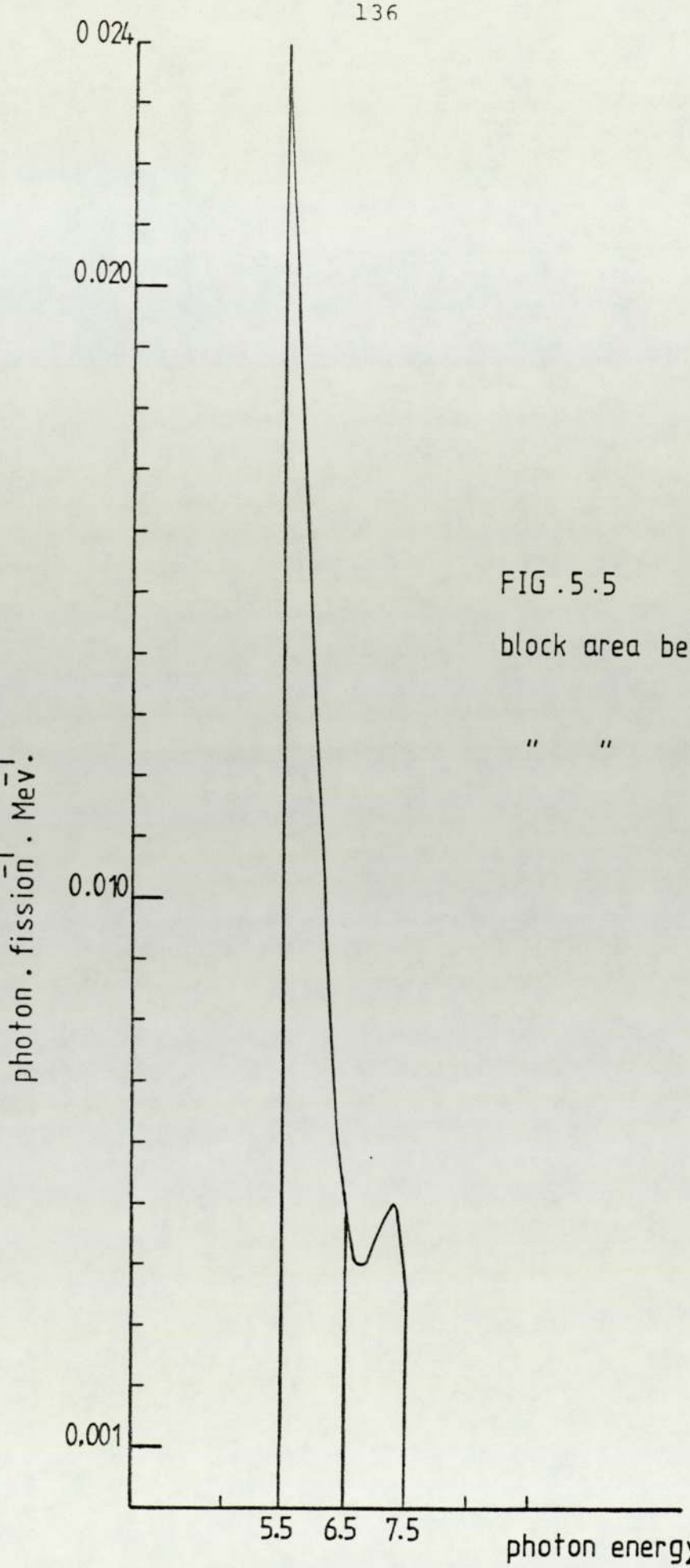

FIG . 5 . 5

block area between 5.5–6.5 Mev $= 134.15 \times 10^{-3}$

" " " 6.5–7.5 $= 43.7 \times 10^{-3}$

photons fission^{-1}

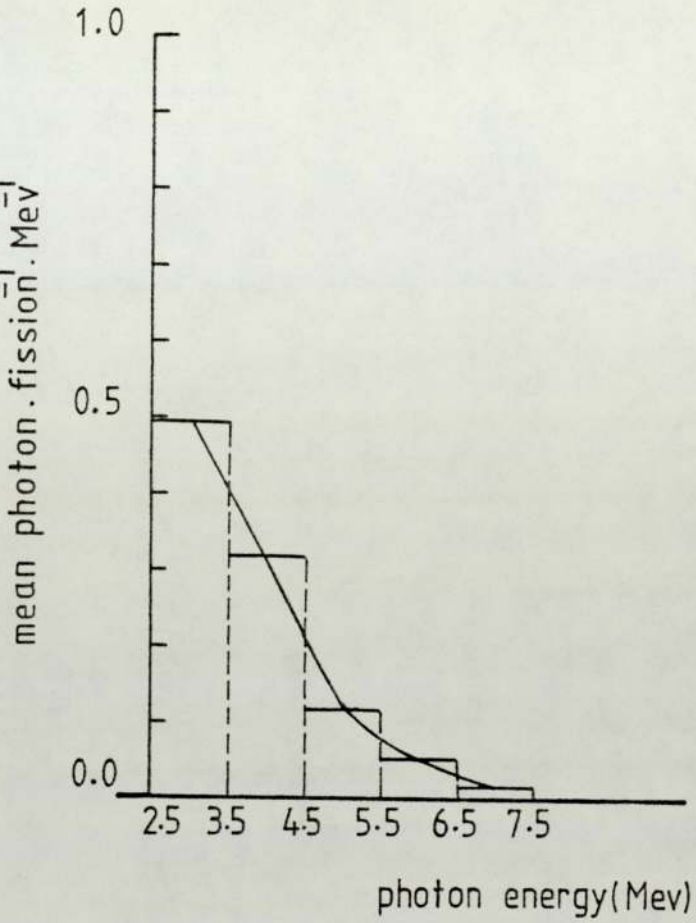

FIG.5.6

Total area of energy spectrum of gamma rays between 2.5 - 7.5 Mev $= 2567.85 \times 10^{-3}$ photons fisson^{-1}

energy range	area of block to total area
2.5-3.5	0.493
3.5-4.5	0.318
4.5-5.5	0.118
5.5-6.5	0.052
6.5-7.5	0.017

E (Mev) Gamma ray energy	Σ (cm^{-1}) pp	Σ (cm^{-1}) cc	Σ (cm^{-1}) PE	Σ (cm^{-1}) T	Mean number of photons $fission^{-1}.Mev^{-1}$	μ (cm^{-1}) core	μ (cm^{-1}) ref.
3	0.044	0.027	0.088	0.159	0.493	0.34265	0.03950
4	0.078	0.040	0.093	0.211	0.318	0.33528	0.03390
5	0.118	0.0431	0.098	0.259	0.118	0.33700	0.03010
6	0.144	0.0426	0.103	0.289	0.052	0.34165	0.02750
7	0.167	0.0505	0.108	0.3155	0.017	-	-

TABLE 5.1

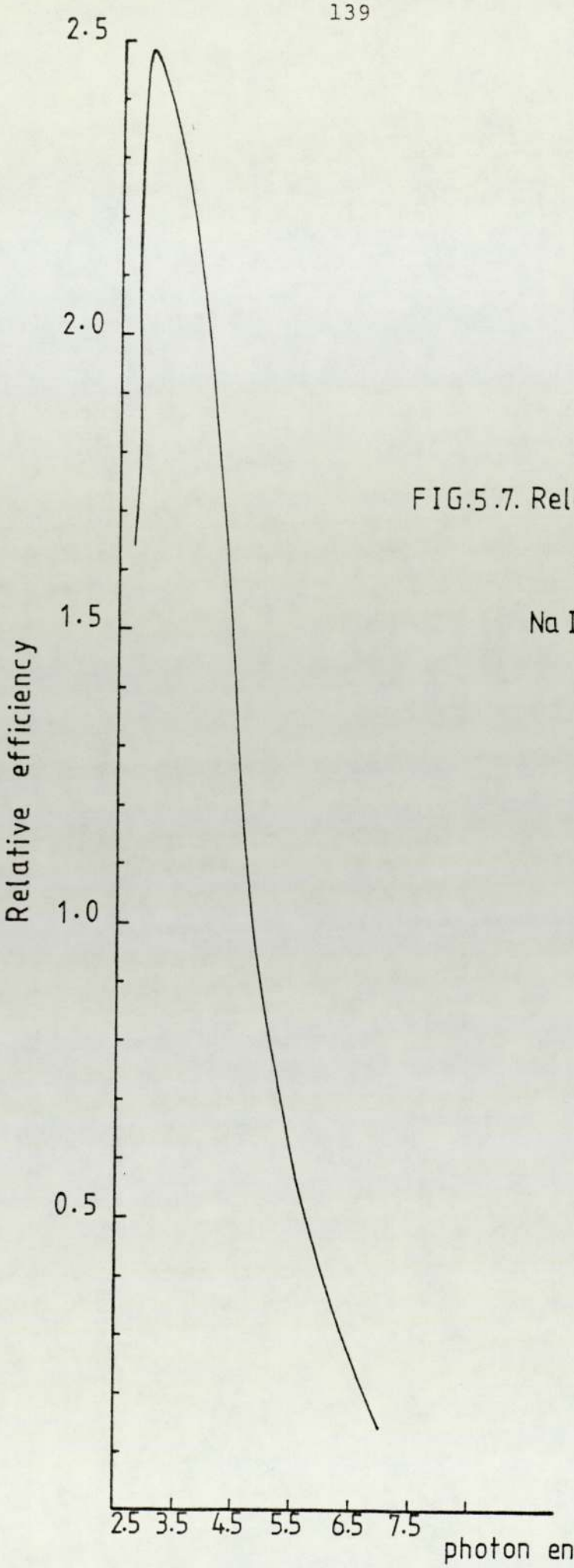

FIG.5.7. Relative efficiency of the NaI(Tl) detector used.

in detail in the conclusion.

CHAPTER 6

COMPARISON BETWEEN THEORETICAL AND EXPERIMENTAL RESULTS

In this chapter, the results obtained with theoretical method are compared with those obtained experimentally in order to test the validity of the theoretical method.

In Figures (6.1) to (6.6), the amplitude response of the nuclear system as given by the theoretical method for different gamma rays energies are compared with that obtained experimentally.

This comparison was done for different axial positions (H). Three measurements were taken in every position for every frequency of interest, the error bars in the graphs represents the deviations [72] in the values of both the amplitude and phase lag. The mean deviations were calculated by means of the numerical values of the deviations,

$$\frac{|d_1| + |d_2| + |d_3| + \text{------} + |d_n|}{n} = \frac{1}{n} \sum_{s=1}^{n} |d_s|$$

where d_1, d_2, d_3, ------- d_n are the deviations of the results obtained in every position for every frequency of interest from the mean of the results and n is the number of experiments (results). The points related to harmonics of the fundamental generally show a larger

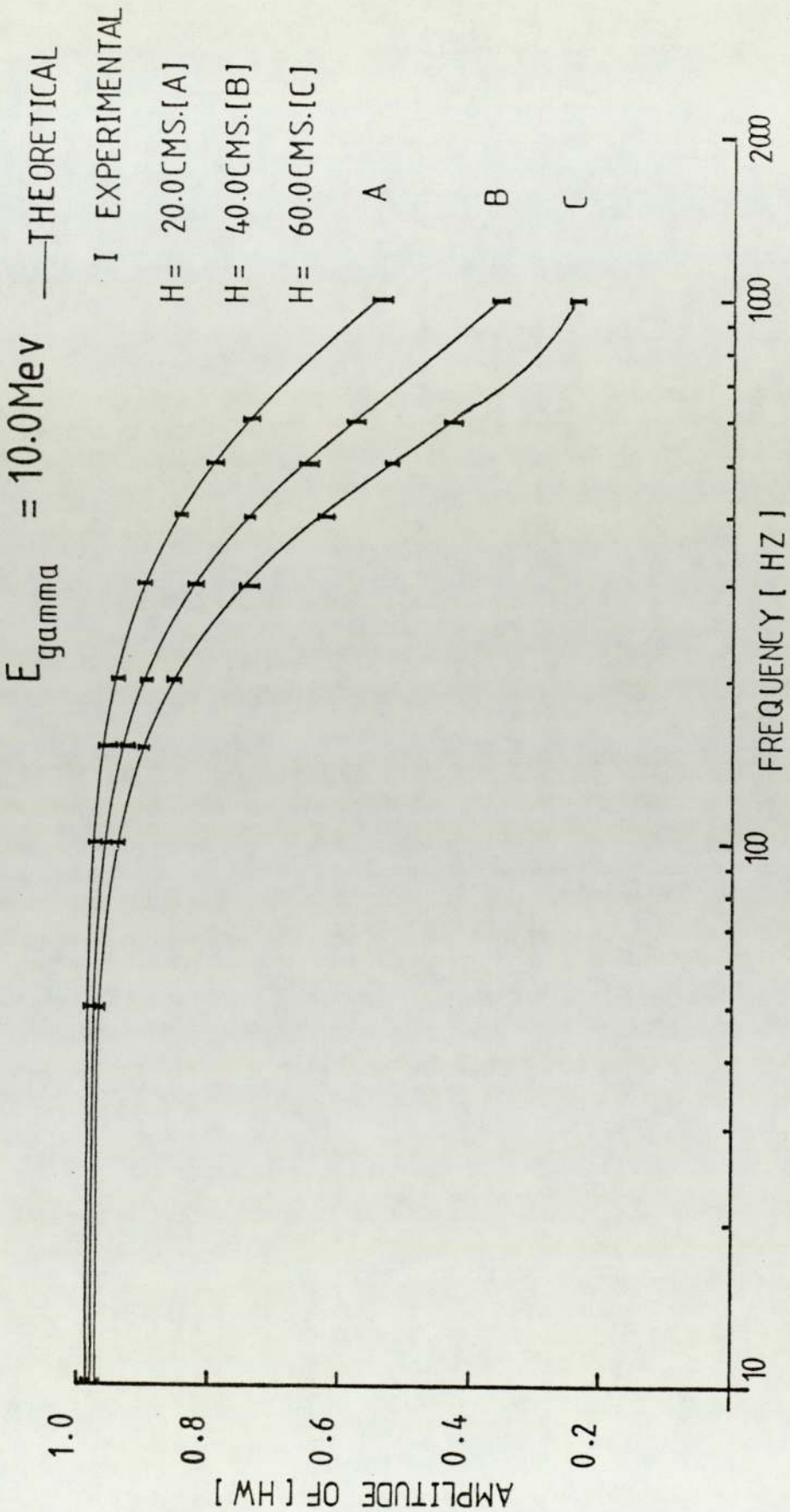

FIG.(6.1) COMPARISON BETWEEN THEORETICAL(10.0 Mev Gama rays energy)AND EXPERIMENTAL RESULTS.

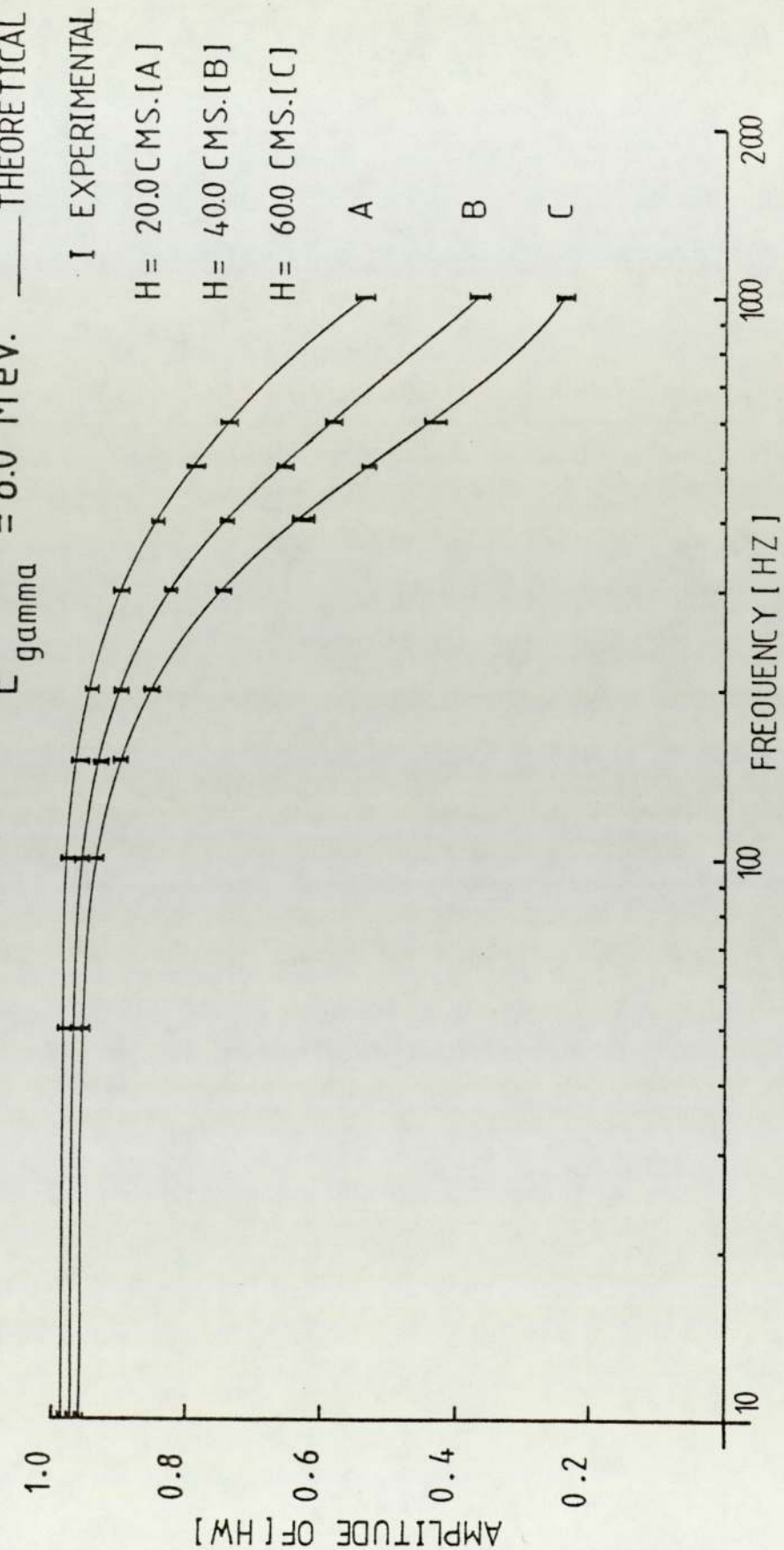

FIG.(6.2) COMPARISON BETWEEN THEORETICAL (8.0 Mev Gamma rays)AND EXPERIMENTAL RESULTS.

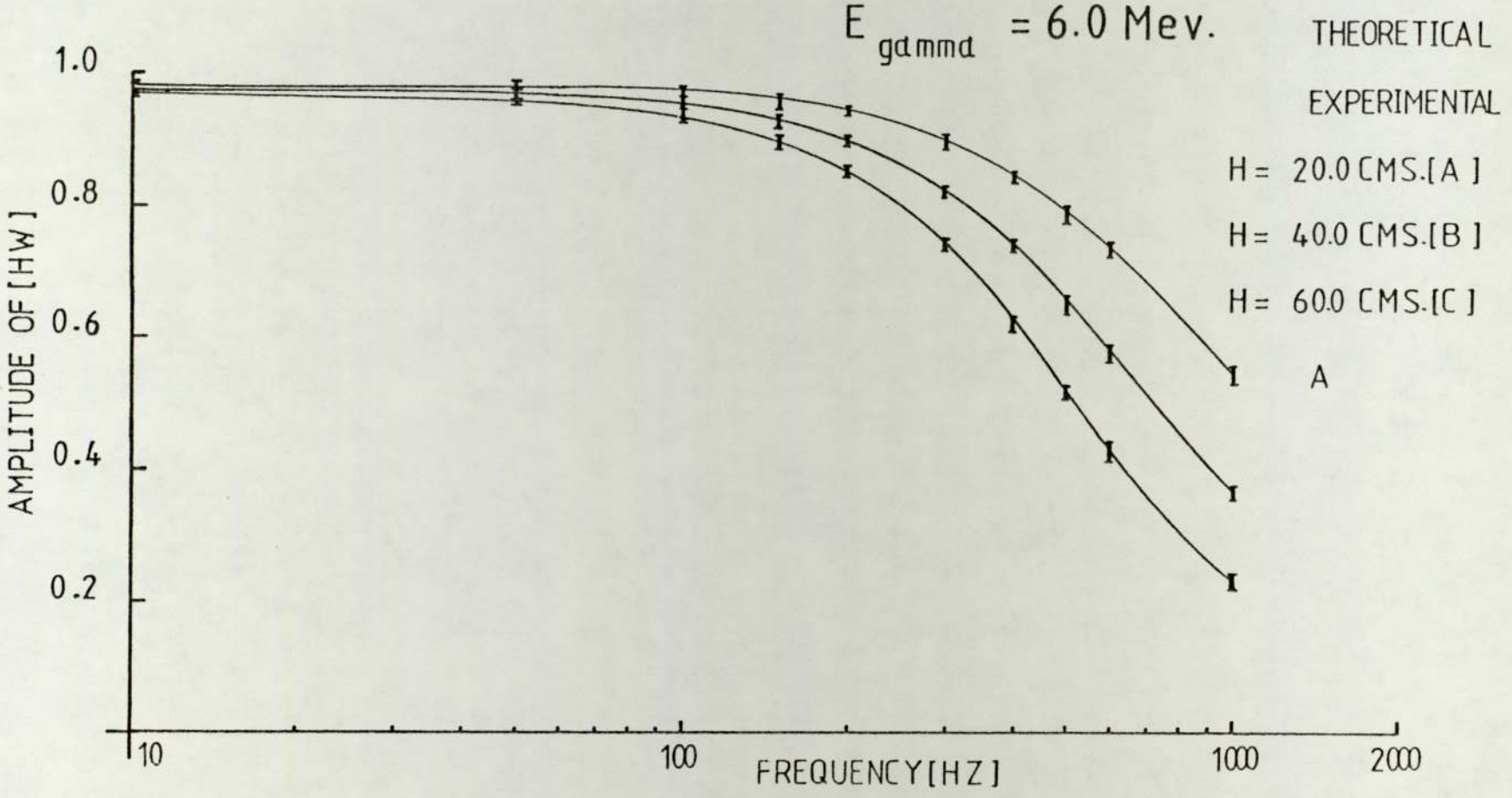

FIG.(6.3) COMPARISON BETWEEN THEORETICAL(6.0 Mev Gamma rays energy)AND EXPERIMENTAL RESULTS.

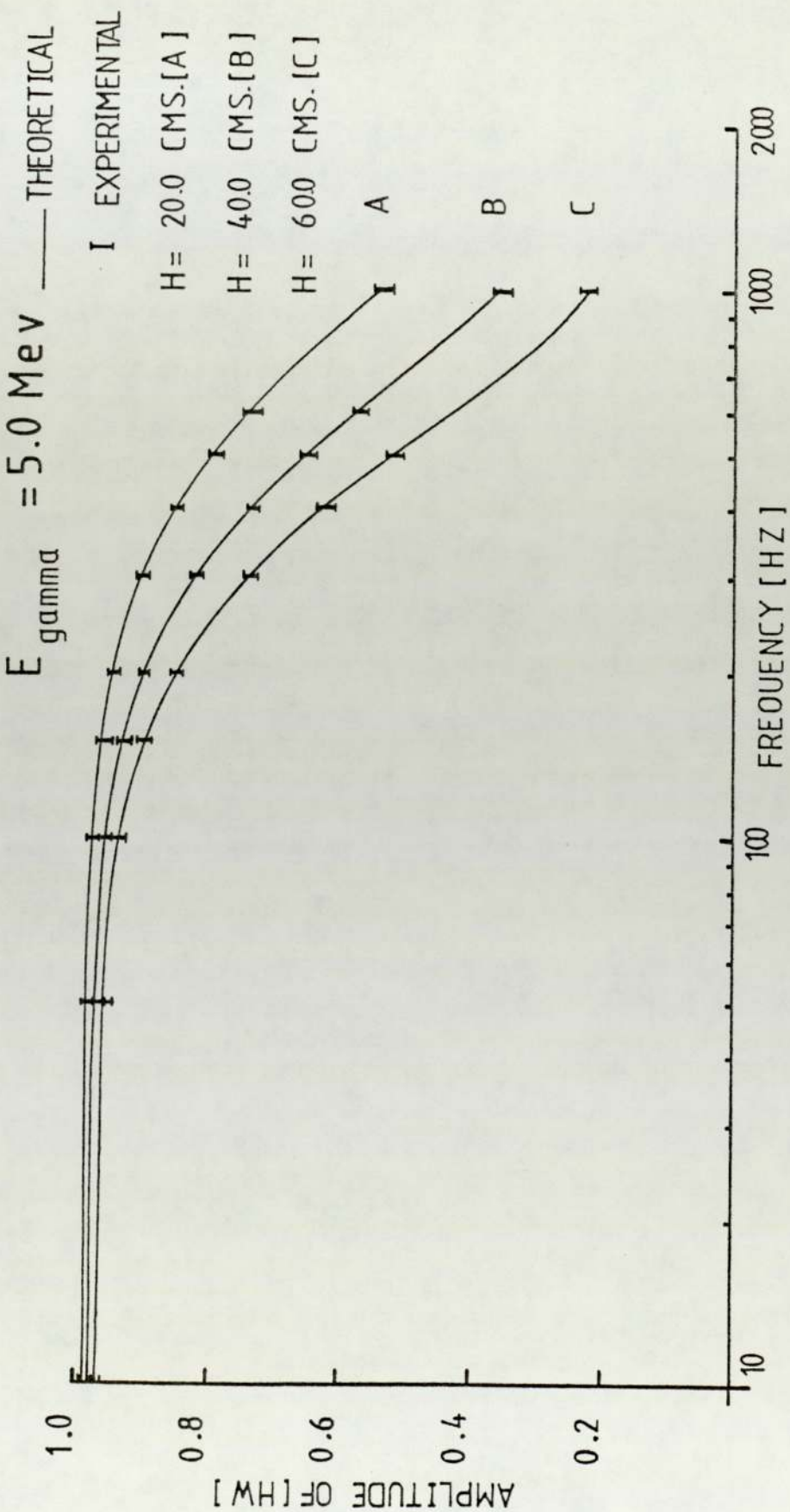

FIG.(6.4) COMPARISON BETWEEN THEORETICAL(5.0 Mev Gamma rays energy)AND EXPERIMENTAL RESULTS.

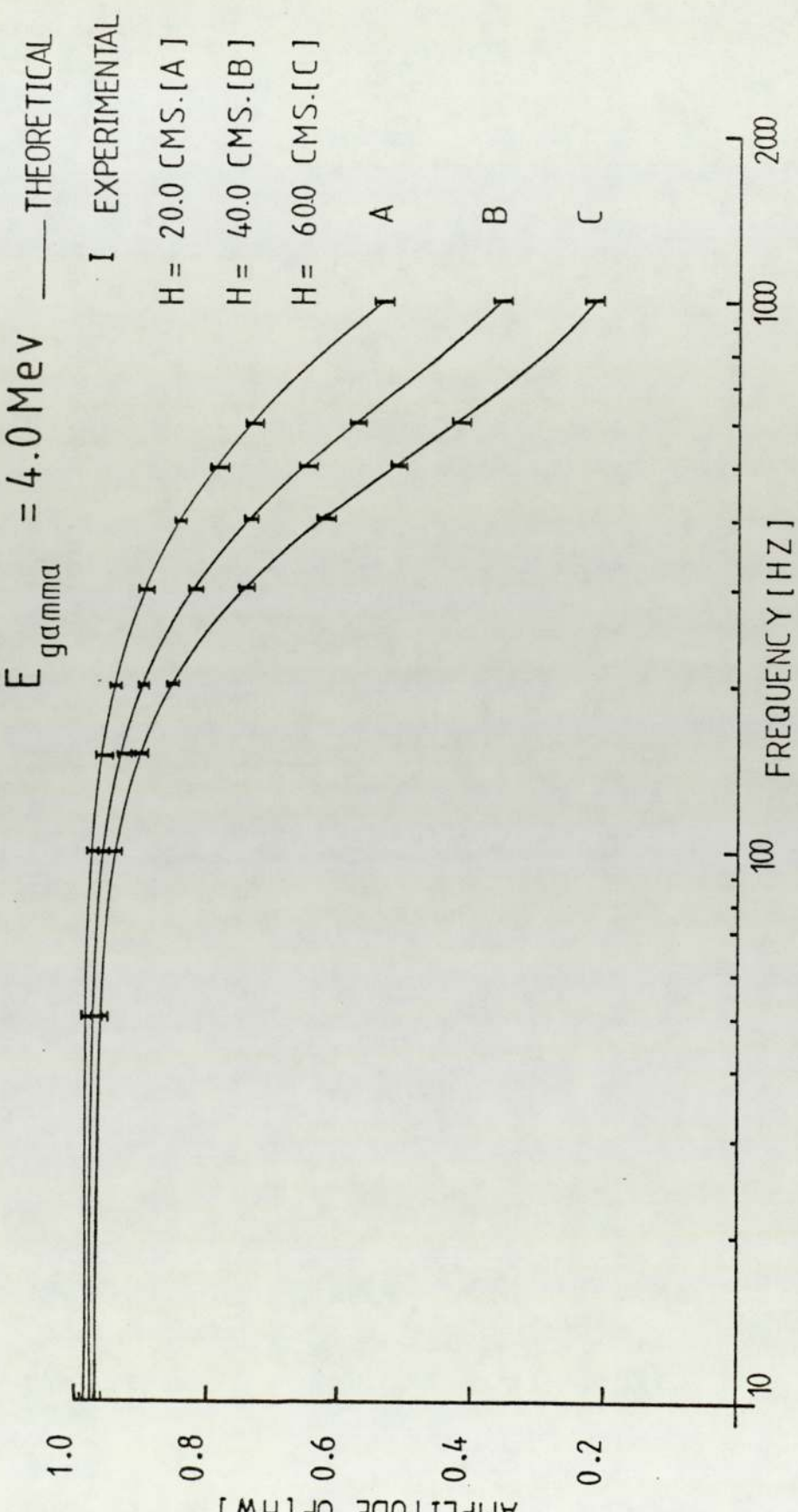

FIG.(6.5) COMPARISON BETWEEN THEORETICAL(4.0 Mev Gamma rays energy)AND EXPERIMENTAL

RESULTS

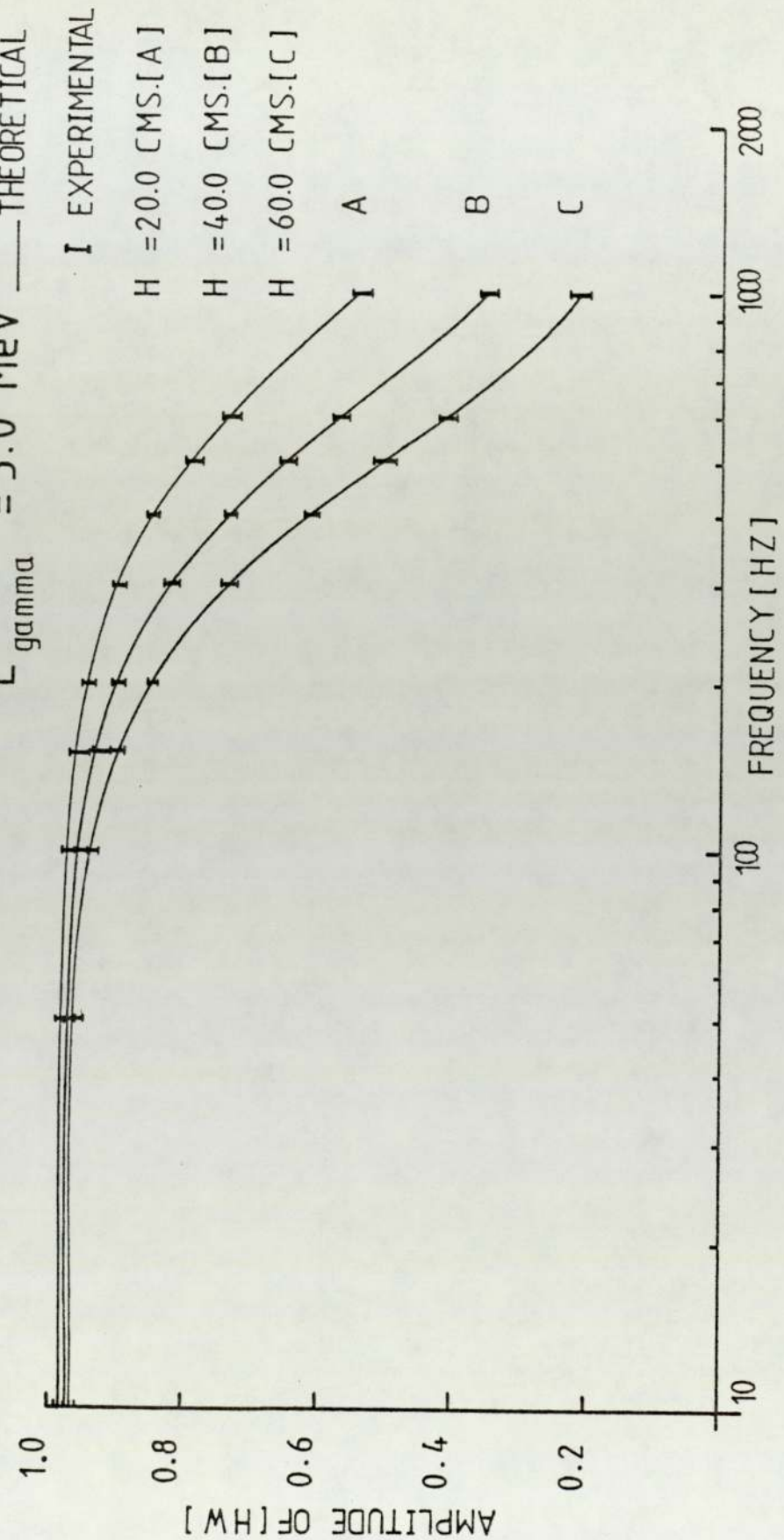

FIG.(6.6) COMPARISON BETWEEN THEORETICAL(3.0 Mev Gamma rays energy)AND THEORETICAL

RESULTS.

spread (deviation) in values than those obtained from the fundamental.

As a conclusion it can clearly be seen how the agreement is fairly good over the entire range of frequencies for each output position, the amplitude and therefore the spatial differences remain practically constant for frequencies of up to nearly 100 HZ. At the higher end of the system, the amplitude starts to decrease before this frequency. Beyond 100HZ, the amplitude decreases rather rapidly and spatial differences become much more noticeable.

Therefore, the theoretical method described in Chapter four is able to predict with fairly good accuracy the source transfer function in the present nuclear system for the entire range of frequencies by prompt fission gamma rays calculation outside the system provided that an appropriate value of the thermal neutron lifetime ($\ell = \frac{1}{V\Sigma_a}$) is selected.

The nuclear system is made up of two regions with quite different thermal neutron life times, on one hand the life time for thermal neutrons in the core is around 40 microseconds, while in the reflector it is 210 microseconds. Therefore, we should expect the thermal life time for the system as a whole to have an intermediate value between these.

Simple perturbation theory shows that the statistical weight of a neutron is proportional to ϕ^2. This suggests that the effective thermal neutron life time of the system as a whole could be calculated as follows,

$$\ell_{eff} = \frac{\ell_c \int_{core} \phi^2 . dv + \ell_r \int_{reflector} \phi^2 . dv}{\int_{core + reflector} \phi^2 . dv} \quad \ldots\ldots\ldots\ldots \quad (6.1)$$

The previous work [26] based on experimental determinations of the relative fluxes inside the core and the reflector by using indium foils, and applying equation (6.1), a value of 78 microseconds was found for thermal neutron life time of the subcritical facility. This value of 78 μsecs. is not quite the same as 84 μsecs. used in the present calculations. However, with a thermal life time of 84 μsecs. a good agreement between the amplitude response of theoretical model and the experimentally measured amplitude response was achieved both here and in previous work [26]. Also a good agreement was found between the experimental and theoretical phase response as shown in Fig.s (6.7) and (6.8).

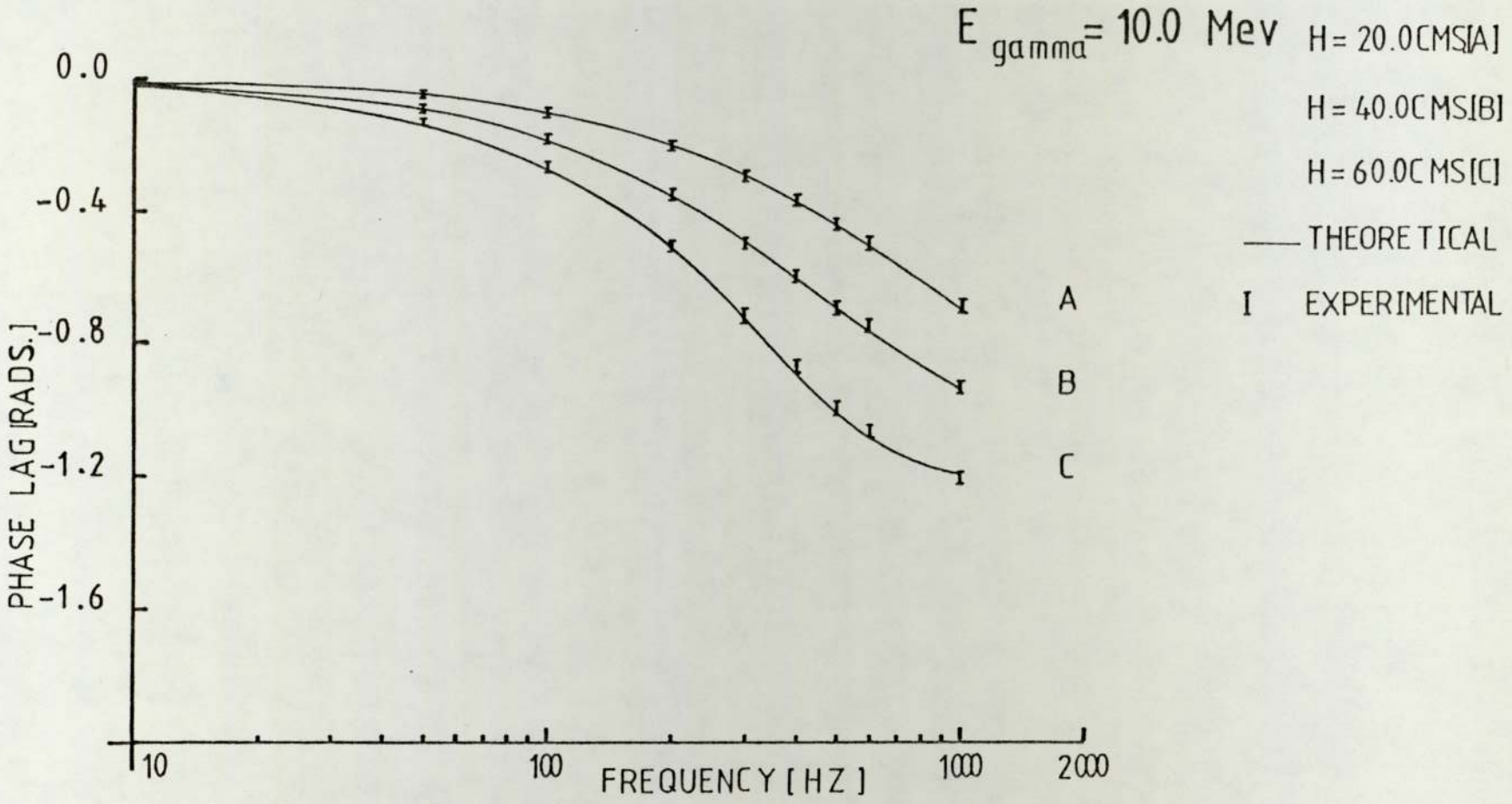

FIG.(6.7) COMPARISON BETWEEN THEORETICAL(10.0 Mev Gamma rays energy)AND THEORETICAL RESULTS.

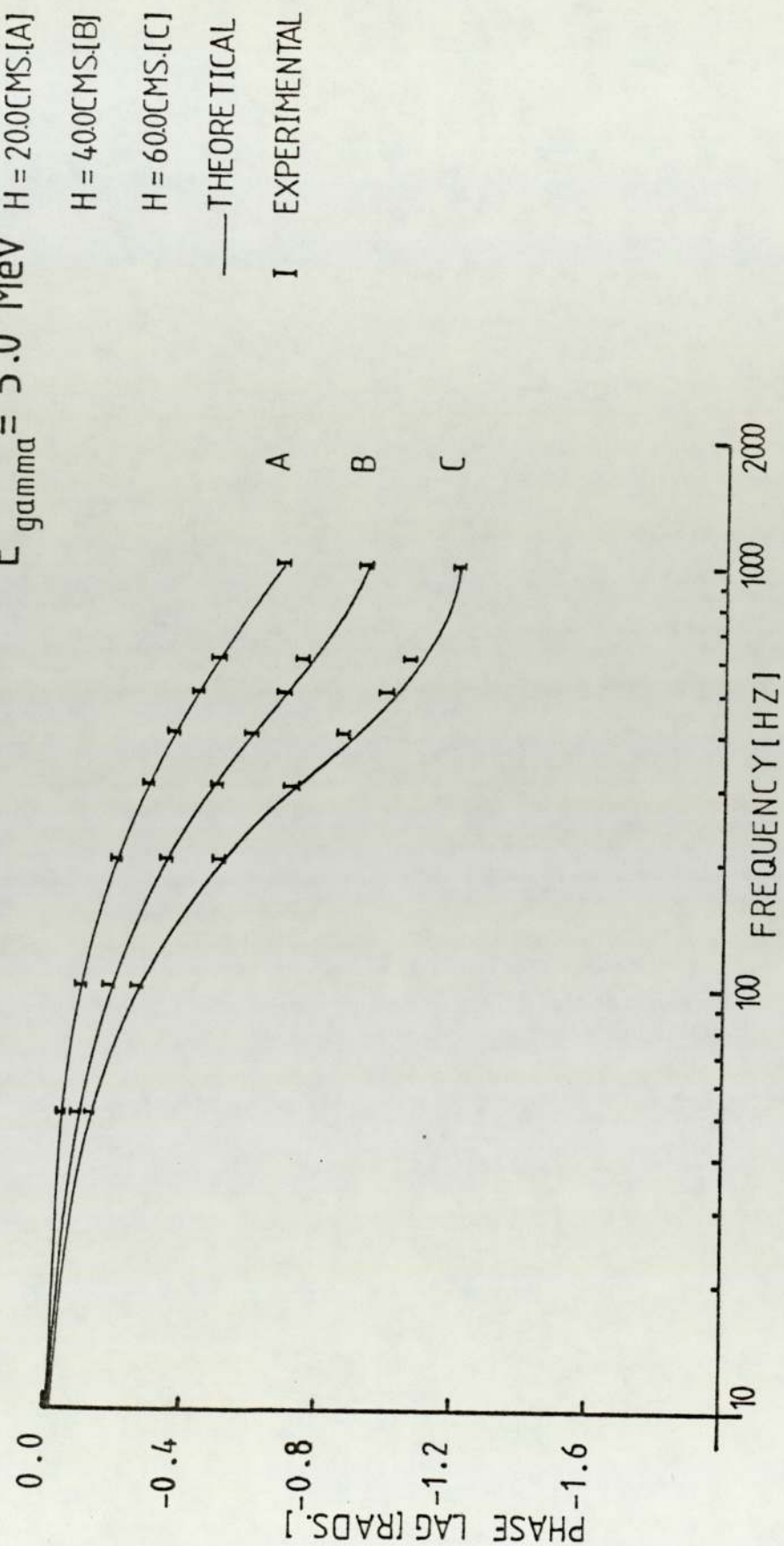

FIG.(6.8) COMPARISON BETWEEN THEORETICAL(5.0 Mev Gamma rays energy)AND EXPERIMENTAL RESULTS.

CHAPTER 7

CONCLUSIONS AND RECOMMENDATIONS

In this chapter, a summary of the conclusions reached and some possible extensions to the present work, are presented.

7.1 CONCLUSIONS

The use of two group diffusion theory with its real and imaginary components was able with farily good accuracy to determine the spatial dependent transfer function of the nuclear system studied. It was also able to give information for frequencies beyond 400 HZ, while the previous attempt to solve these equations using the two dimensional finite difference code SNAP, failed at frequencies in excess of 400 HZ. Also the size of the codes (ATEST, and GAMMARESFU) are small compared to SNAP (200K of core plus three discs), so it does not limit their use to very powerful computers.

With respect to the experimental side of the present work, a great deal of improvement has been achieved regarding the pulsing system of the S.A.M.E.S. accelerator. This method of pulsing the system eliminates the uncertainty of the beam being in phase with the starting command of the P.H.A.

Also, the electronic network developed to simultaneously use two detectors can be used in any further experiments where two detector correlations are required.

As it was shown that the detector efficiency curve peak lies between 3-4 Mev gamma rays, so theoretical results at 3 and 4 Mev should best match the experiment. However, it was also seen that the μ (linear absorption coefficient) for core and reflector is roughly independent of E_γ , therefore the gamma ray energy does not affect the match for gamma ray energies between 3-10 Mev.

Both theory and experiment have shown that even a small system such as the one used in the experimental work can not be regarded as a point reactor or a lumped parameter model.

It is also shown that how the spatial dependent transfer function of the system theoretically and experimentally could be determined by looking at the prompt fission gamma rays outside the system, while previous studies with thermal neutrons have shown that the detector must be located inside the nuclear system since the reflector attenuates and modifies the thermal neutron signal.

One further conclusion is that although an outside core detector can be used, space dependence of the nuclear system is still observed.

7.2 RECOMMENDATIONS FOR FUTURE WORK

An extension of the present work should be possible on the following lines:

(1) Improvement to the theoretical neutron flux calculations by expanding it to a two region geometry.

(2) Effect of different reflectors on the neutron life time and therefore on the transfer function.

APPENDIX A

Summary of nuclear parameters

Parameter	Value	Units
K	0.996	---
B_r^2	0.004135	Cm^{-2}
D_2	0.2020	Cm
Σ_{r_2}	0.1053	Cm^{-1}
L_{th}^2	1.9183	Cm^2
D_1	1.0020	Cm
Σ_{r_1}	0.0247	Cm^{-1}
L_F^2	40.56	Cm^2
λ	0.0790	Sec^{-1}
β	0.0064	---

APPENDIX B

COMPUTER PROGRAM

(FOURIDL)

```
 0    0      'BEGIN'
 1    1      'INTEGER' J1,J2,J3,J4,J5,J6,J7,J8,J9,J10,STEP,K,NXE1,PLOT,PRIN,NG,NXE,
 2    1      NVE,P,N,M,L,I,J,NUMBER,DETNUM,ORDER1,ORDER2;
 3    1      'REAL'T1,T2,TIMCHAN,AMPLITUDE,AVERAL,MAXIAV,MAXI,MAX,SUM,TRANSFERT,
 4    2      DEADT,T,FACTOR,TRUBACK,UNIBACK,FREQ,C,AMP,NORM,GAIN,RATIO,UNIBACK1,
 5    2      UNIBACK2,X,Y,LOG,PHASE,YMAX,YMIN;
 6    2      'REAL''ARRAY'FR,AM,GA,TEXT4[1:4];



 7    3      'REAL''ARRAY'TEXT1,TEXT2,TEXT3,TEXT5,TEXT6[1:2];
 8    4      'REAL''ARRAY'DATA,DATA1,DATA2[1:80];
 9    5
10    5      'PROCEDURE'ARRANGE(TRUE,CONVAL);
11    7      'ARRAY'TRUE,CONVAL;
12    8      'BEGIN'
13    8      'FOR'I:=0'STEP'1'UNTIL'NUMBER-1'DO'
14   10      CONVAL[I]:=0;
15   11      'FOR'I:=0'STEP'1'UNTIL'NUMBER-1'DO'
16   12      'FOR' J:=I 'STEP' NUMBER 'UNTIL' N 'DO'
17   13      CONVAL[I]:=CONVAL[I]+TRUE[J];
18   14      'FOR'I:=0'STEP'1'UNTIL'NUMBER-1'DO'
19   15      CONVAL[I]:=CONVAL[I]/TIMCHAN;
20   16      'END' OF PROCEDURE ARRANGE;
21   16
22   16      'PROCEDURE' CORRECT(CONVAL,CONVAL1);
23   18      'ARRAY' CONVAL,CONVAL1;
24   19      'BEGIN'
25   19      TRANSFERT:=0,0000125;
26   21      DEADT:=0,000001;
27   22      FACTOR:=TRANSFERT*NUMBER*FREQ;
28   23      'FOR' I:=0 'STEP' 1 'UNTIL' NUMBER-1 'DO'
29   24      'BEGIN'
30   24      X:=CONVAL[I]/((1-FACTOR)*(1-CONVAL[I]*DEADT)+
```

```
31  25      FACTOR*((1-EXP(-CONVAL[I]*TRANSFERT))/(CONVAL[I]*TRANSFERT));
32  26      AGAIN:
33  26      Y:=CONVAL[I]/((1-FACTOR)*(1-CONVAL[I]*DEADT)+
34  26      FACTOR*((1-EXP(-X*TRANSFERT))/(X*TRANSFERT)));
35  27      'IF' ABS((Y-X)/Y) 'GE' 0,001 'THEN'
36  27      'BEGIN' X:=Y; 'GOTO' AGAIN; 'END';
37  31      CONVAL1[I]:=Y;
38  32      'END';
39  33      'END' OF PROCEDURE CORRECT;
40  33
41  33      'PROCEDURE' FOURHEAD;
42  34      'BEGIN'
43  34      NEWLINE(2);
44  36      SPACE(48);
45  37      WRITETEXT('('****FOURIERANALYSIS****')');
46  38      NEWLINE(1);
47  39      SPACE(48);
48  40      WRITETEXT('('**********************')');
49  41      NEWLINE(2);

50  42      SPACE(5);
51  43      WRITETEXT('('HARMONIC')');
52  44      SPACE(13);
53  45      WRITETEXT('('A')');
54  46      SPACE(16);
55  47      WRITETEXT('('B')');
56  48      SPACE(12);
57  49      WRITETEXT('('AMPLITUDE')');
58  50      SPACE(10);
59  51      WRITETEXT('('H[W]')');
60  52      SPACE(10);
61  53      WRITETEXT('('GAIN[DB]')');
62  54      SPACE(10);
63  55      WRITETEXT('('PHASE')');
64  56      NEWLINE(1);
```

```
65  57      'END' OF PROCEDURE FOURHEAD;
66  57
67  57      'PROCEDURE'FOURIER(NUMBER,CONVAL,A,B);



68  59      'ARRAY' CONVAL,A,B;
69  60      'INTEGER'NUMBER;
70  61      'BEGIN'
71  61      'REAL''ARRAY'S,C[1:2],U[0:2];
72  61      'REAL' TEMP,PI;
73  62      'INTEGER' P,I;
74  63      PI:=3.14159265;
75  65      C[2]:=1;
76  66      S[2]:=0;
77  67      C[1]:=COS(2*PI/NUMBER);
78  68      S[1]:=SIN(2*PI/NUMBER);
79  69      'FOR' P:=0'STEP'1'UNTIL'NUMBER/2'DO'
80  70      'BEGIN'
81  70      U[1]:=0;
82  72      U[2]:=0;
83  73      'FOR' I:=NUMBER-1'STEP'-1'UNTIL'1'DO'
84  74      'BEGIN'
85  74      U[0]:=CONVAL[I]+2*C[2]*U[1]-U[2];
86  76      U[2]:=U[1];
87  77      U[1]:=U[0];
88  78      'END';
89  79      A[P]:=2*(CONVAL[0]+U[1]*C[2]-U[2])/NUMBER;
90  80      B[P]:=2*(U[1]*S[2])/NUMBER;
91  81      TEMP:=C[1]*C[2]-S[1]*S[2];
92  82      S[2]:=C[1]*S[2]+S[1]*C[2];
93  83      C[2]:=TEMP;
94  84      'END';
95  85      'END' OF PROCEDURE FOURIER;
```

```
 96    85
 97    85        'PROCEDURE' FOUREXIT(A,B);
 98    87        'ARRAY'A,B;
 99    88        'BEGIN'
100    88        I:=0;
101    90        SPACE(7);
102    91        PRINT(I,2,0);
103    92        SPACE(8);
104    93        PRINT(A[0],5,2);
105    94        SPACE(6);
106    95        PRINT(B[0],5,2);
107    96        SPACE(6);
108    97        PRINT(A[0],5,2);
109    98        NEWLINE(1);

110    99        'FOR'I:=1'STEP'1'UNTIL'7'DO'
111   100        'BEGIN'
112   100        C:=3.1415926*I/(2.0*A[0]);
113   102        AMP:=SQRT(A[I]*A[I]+B[I]*B[I]);
114   103        NORM:=AMP*C;
115   104        GAIN:=4.343*LN(NORM*NORM);
116   105        PHASE:=ARCTAN(A[I]/B[I]);
117   106        'IF' A[I]>0 'AND' B[I]<0 'THEN' PHASE:=PHASE+3.1416;
118   107        'IF' A[I]<0 'AND' B[I]<0 'THEN' PHASE:=PHASE-3.1416;
119   108        SPACE(7);
120   109        PRINT(I,2,0);
121   110        SPACE(8);
122   111        PRINT(A[I],5,2);
123   112        SPACE(6);
124   113        PRINT(B[I],5,2);
125   114        SPACE(6);
126   115        PRINT(AMP,5,2);
127   116        SPACE(7);
128   117        PRINT(NORM,1,5);
```

```
129  118        SPACE(6);
130  119        PRINT(GAIN,2,3);
131  120        SPACE(7);
132  121        PRINT(PHASE,2,3);
133  122        NEWLINE(1);
134  123        'END';
135  124        'END' OF PROCEDURE FOUREXIT;
136  124
137  124        M:=0;  N:=49;  L:=1;
138  128        LEVEL1:
139  128        T1:=READ;
140  129        'IF' T1<0 'THEN' 'GOTO' FIN;
141  130        UNIBACK:=READ;
142  131        UNIBACK:=UNIBACK/(T1*60);
143  132        NUMBER:=READ;
144  133        FREQ:=READ;
145  134        NEWLINE(1);
146  135        WRITETEXT('('FREQUENCY%%%=')');
147  136        PRINT(FREQ,4,2);
148  137        WRITETEXT('('%HZ')');
149  138        T2:=READ;
150  139        TIMCHAN:=T2*60/NUMBER;
151  140        'BEGIN'
152  140        'REAL' 'ARRAY' TRUE[M:N],CONVAL,CONVAL1[0:NUMBER-1],A,B[0:NUMBER/2];
153  140        'FOR' I:=M 'STEP' L 'UNTIL' N 'DO'
154  142        TRUE[I]:=READ;
155  143        ARRANGE(TRUE,CONVAL);
156  144        CORRECT(CONVAL,CONVAL1);
157  145        'FOR'I:=0'STEP'1'UNTIL'NUMBER-1'DO'
158  146        CONVAL[I]:=CONVAL1[I]-UNIBACK;
159  147        FOURHEAD;
160  148        FOURIER(NUMBER,CONVAL,A,B);
161  149        FOUREXIT(A,B);
162  150        'END';
163  151        NEWLINE(5);
```

```
164  152          !GOTO'LEVEL1;
165  153          FIN:
166  153          !END!;
```

AN INPUT EXAMPLE

```
   8         3811        50         10         7.5
018387     016424     019545     020978     022381     023055     023011     023620     023418
023537     023340     023465 ....................
022784     023021 ...................
00603 ..................
..............
up to 100
   8         3811        50         50         7.5
020762     020192     022855     024573     024872 ............
026427     026733     026709     ...................
026588     026508     ..................
001511     .........
.......
up to 100
........
........
-1
****
```

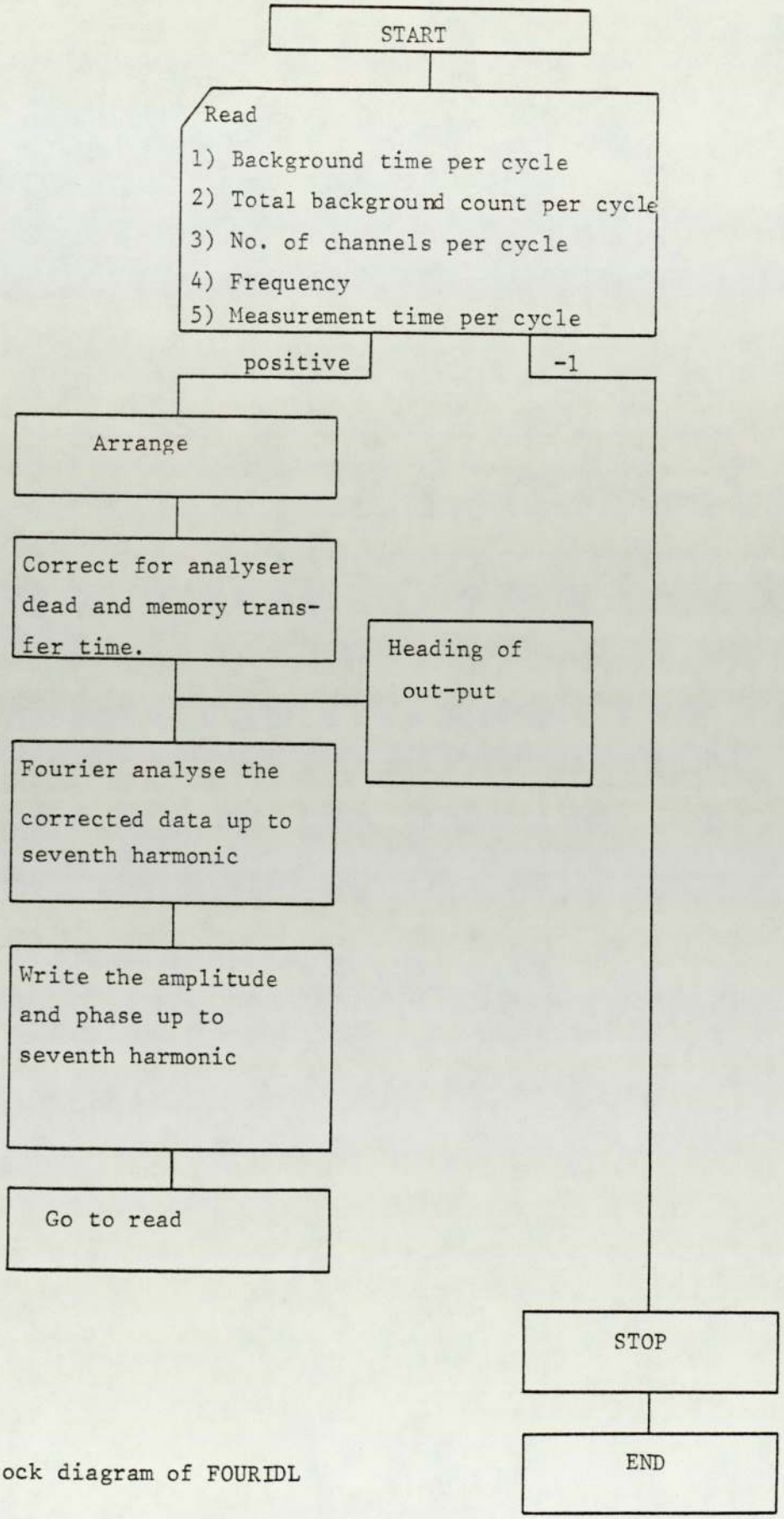

Block diagram of FOURIDL

AN EXAMPLE OF OUTPUT

FREQUENCY = 10.00 Hz

****FOURIER ANALYSIS****
****

HARMONIC	A	B	AMPLITUDE	H[W]	GAIN[DB]	PHASE
0	2576.15	0.00	2576.15			
1	6.25	1590.93	1590.94	0.97007	-0.264	0.004
2	-66.50	-18.67	69.07	0.08423	-21.490	-1.845
3	15.46	478.36	478.61	0.87549	-1.155	0.032
4	-29.16	-37.98	47.88	0.11679	-18.652	-2.487
5	34.98	264.29	266.59	0.81276	-1.801	0.132
6	-12.83	-44.11	45.94	0.16807	-15.490	-2.858
7	58.79	174.98	184.59	0.78788	-2.071	0.324

FREQUENCY = 50.00 Hz

****FOURIER ANALYSIS****
****

HARMONIC	A	B	AMPLITUDE	H[W]	GAIN[DB]	PHASE
0	3044.69	0.00	3044.69			
1	-90.08	1791.57	1793.84	0.92546	-0.673	-0.050
2	11.61	-14.42	18.52	0.01911	-34.377	2.464
3	-21.06	526.78	527.20	0.81537	-1.767	-0.040
4	24.39	-9.96	26.53	0.05474	-25.234	1.956
5	10.65	280.97	281.17	0.72530	-2.790	0.038
6	32.97	-6.29	33.56	0.10389	-19.669	1.759
7	22.16	184.79	186.12	0.67214	-3.451	0.119

APPENDIX C

COMPUTER PROGRAM

(ATEST)

```
 0 UAFORTRAN LINES 5000
 1       TRACE2
 2       MASTER ATEST
 3 C     ************************************************************************
 4 C     ************************************************************************
 5 C     ************************************************************************
 6 C     ***                                                                  ***
 7 C     ***                                                                  ***
 8 C     *** THEORITICAL RESPONSE FUNCTION AND PHASE LAG CALCULATIONS         ***
 9 C     ***                                                                  ***
10 C     ***                                                                  ***
11 C     ************************************************************************
12 C     ************************************************************************
13 C     ************************************************************************
14 C      1      INDICATES FAST IMAGINARY
15 C      2      INDICATES THERMAL IMAGINARY
16 C      3      INDICATES FAST REAL
17 C      4      INDICATES THERMAL REAL
18 C      SIGR1 REMOVAL CROSS SECTION OF FAST IMAGINARY
19 C      SIGR2 REMOVAL CROSS SECTION OF THERMAL IMAGINARY
20 C      SIG12 CROSS SECTION OF PRODUCTION OF NEUTRONS IN GROUP 2 BY DOWNSC
21 C     1ATTERING
22 C      SIG21 CROSS SECTION OF PRODUCTION OF NEUTRONS IN GROUP 1 FROM GROU
23 C     1P 2(FROM FISSION OR UPSCATTERING)
24 C      SIG13 ETC.HAVE SIMILAR MEANING TO SIG12
25 C      SIG31 ETC.HAVE SIMILAR MEANING TO SIG21
26 C      W      FREQUENCY IN RADIAN UNIT
27 C      V1     FAST NEUTRON VELOCITY
28 C      V2     THERMAL NEUTRON VELOCITY
29 C      D1     DIFIUSION COEFFICIENT OF FAST GROUP
30 C      D2     DIFIUSION COEFFICIENT OF THERMAL GROUP
31 C      ANSF2 NU*SIGF2 (NU NO.OF NEUTRONS PER FISSION,SIGF2 FISSION CROSS
32 C     1SECTION)
33 C      ALAND DELAYED NEUTRON DECAY CONSTANT
34 C      BETA  DELAYED NEUTRON FRACTION
```

```
C      RC     CORE RADIUS
C      H      CORE HEIGHT
C      Z      AXIAL POSITION FOR WHICH FLUXES ARE WANTED
C      A14    COEFFICIENT OF (B**2)**4 IN QUADRATIC EQUATION
C      B14    COEFFICIENT OF (B**2)**3 IN QUADRATIC EQUATION
C      C14    COEFFICIENT OF (B**2)**2 IN QUADRATIC EQUATION
C      D14    COEFFICIENT OF (B**2)**1 IN QUADRATIC EQUATION
C      E14    COEFFICIENT OF (B**2)**0 IN QUADRATIC EQUATION
C      A3     COEFFICIENT OF (Z**2) IN CUBIC EQUATION
C      B3     COEFFICIENT OF  Z    IN CUBIC EQUATION
C      C3     COEFFICIENT OF (Z**0) IN CUBIC EQUATION
C      P      COEFFICIENT OF  Y1    IN REDUCED FORM OF CUBIC EQUATION
C      Q      COEFFICIENT OF (Y1**0) IN REDUCED FORM OF CUBIC EQUATION
C      CT1    COSINE TETA ONE
C      ALF21  (ALFA1)**2 WHERE ALFA1 IS CORRECTED FOR RADIAL LEAKAGE
C      BET21  (BETA1)**2
C      ALF22  (ALFA2)**2 WHERE (ALFA2 IS CORRECTED FOR RADIAL LEAKAGE
C      BET22  (BETA2)**2
C      RS     REFLECTOR SAVINGS
C      SI     CROSS SECTIONS FOR ZERO FREQUENCIES
C      AL21U  (ALFA1)**2  WHERE ALFA1 IS UNCORRECTED FOR RADIAL LEAKAGE
C      AL22U  (ALFA2)**2  WHERE ALFA2 IS UNCORRECTED FOR RADIAL LEAKAGE
C      Q2     NET CURRENT OF THERMAL NEUTRON
C      A1F    FLUX COEFFICIENT
C      A2F    FLUX COEFFICIENT
C      FY4W   THERMAL REAL FLUX FOR FREQUENCY W
C      FY2W   THERMAL IMAGINARY FLUX FOR FREQUENCY W
C      FY40   THERMAL REAL FLUX FOR ZERO FREQUENCY
       INTEGER H,Z
       READ(1,10)SIGR1,SIGR2,ANSF2,SIG12,D1,D2,BETA,ALAND,V1,V2,RC,H,RS,Q
      12
    10 FORMAT(8(F6.4/),(F9.1/),(F8.1/),(F4.1/),(I2/),(F3.1/),(F8.1))
       FREQ1=0
       W1=2*3.1415927*FREQ1
       SI10=SIGR1
```

```
      SI20=SIGR2
      SI130=0
      SI210=ANSF2
      SI230=0
      SI240=0
      SI310=0
      SI340=SIG12
      SI410=0
      SI420=0
      SI430=SI210
      TEM1=(D1*SI20+D2*SI10)
      TEM2=(TEM1)**2-4*D1*D2*(SI10*SI20-SI210*SIG12)
      B120=(-TEM1+(TEM2)**0.5)/(2*D1*D2)
      B220=(-TEM1-(TEM2)**0.5)/(2*D1*D2)
      R=RC+RS
      TEM3=(2.405/R)**2
      B110=(TEM3-B120)**0.5
      B210=(TEM3-B220)**0.5
      R310=((SI20)+(D2*B120))/(SIG12)
      R320=((SI20)+(D2*B220))/(SIG12)
      TEM4=EXP(-B110*2*H)
      TEM5=EXP(-B210*2*H)
      TEM6=R310/R320
      A1F0=(-Q2/D2)/(-B110*(1+TEM4)-TEM6*((1-TEM4)/(1-TEM5))*(-B210)*(1+
     1TEM5))
      A2F0=-(TEM6)*(A1F0)*((1-TEM4)/(1-TEM5))
      Z=5
   25 FY40=A1F0*(EXP(-B110*Z)-EXP(-B110*(2*H-Z)))+A2F0*(EXP(-B210*Z)-EXP
     1(-B210*(2*H-Z)))
      FY20=0
      AMP0=((FY40)**2+(FY20)**2)**0.5
   50 READ(1,20)FREQ
   20 FORMAT(25F6.0)
      IF(FREQ)35,45,15
   15 W=2*3.1415927*FREQ
```

```
105       SIG1=SIGR1-(3*D1*(W**2))/(V1**2)
106       SIG2=SIGR2-(3*D2*(W**2))/(V2**2)
107       SIG13=W*(1+3*D1*SIGR1)/V1
108       SIG21=(1-(BETA*(W**2))/((W**2)+(ALAND**2)))*ANSF2
109       SIG23=((W*ALAND*BETA)/((W**2)+(ALAND**2)))*ANSF2
110       SIG24=(W*(1+3*D2*SIGR2))/V2
111       SIG31=-SIG13
112       SIG34=SIG12
113       SIG41=-SIG23
114       SIG42=-SIG24
115       SIG43=SIG21
116       A14=(D1**2)*(D2**2)
117       B14=2*D1*D2*(D1*SIG2+D2*SIG1)
118       C14=(4*D1*SIG1*D2*SIG2)-(2*D1*SIG12*D2*SIG21)+((D1**2)*(SIG2**2))+
119      1((D2**2)*(SIG1**2))+((D1**2)*(SIG24**2))+((D2**2)*(SIG13**2))
120       D14=(2*D1*SIG12*SIG23*SIG24)+(2*SIG12*SIG13*D2*SIG23)-(2*SIG1*SIG1
121      12*D2*SIG21)-(2*D1*SIG12*SIG2*SIG21)+(2*D1*SIG1*(SIG24**2))+(2*D2*S
122      1IG2*(SIG13**2))+(2*D1*SIG1*(SIG2**2))+(2*D2*SIG2*(SIG1**2))
123       E14=((SIG1**2)*(SIG2**2))+((SIG12**2)*(SIG21**2))+((SIG12**2)*(SIG
124      123**2))+((SIG1**2)*(SIG24**2))+((SIG13**2)*(SIG24**2))+((SIG2**2)*
125      1(SIG13**2))-(2*SIG1*SIG2*SIG21*SIG12)+(2*SIG12*SIG13*SIG21*SIG24)+
126      1(2*SIG12*SIG13*SIG2*SIG23)+(2*SIG1*SIG12*SIG23*SIG24)
127       A4=B14/A14
128       B4=C14/A14
129       C4=D14/A14
130       D4=E14/A14
131       P4=(B4-(3.0/8.0)*(A4**2))
132       Q4=((1.0/8.0)*(A4**3)-((1.0/2.0))*(A4*B4)+C4)
133       R4=(-(3.0/256.0)*(A4**4)+(1.0/16.0)*(A4**2)*B4-(1.0/4.0)*(A4*C4)+D
134      14)
135       A3=P4/2
136       B3=((P4**2)-4*R4)/16
137       C3=-((Q4)**2)/64
138       P=-(A3**2)/3+B3
139       Q=(2*(A3**3))/27-(A3*B3)/3+C3
```

```
      CT1=-Q/(2*((-P/3)**3)**0.5)
      TETA1=ATAN(((1-CT1**2)**0.5)/CT1)
      TETA2=(TETA1)/3.0
      U=2*((-P/3)**0.5)
      Z1=ABS(U*COS(TETA2)-A3/3)
      Z2=ABS(-U*COS((3.1415927/3)+TETA2)-A3/3)
      Z3=ABS(-U*COS((3.1415927/3)-TETA2)-A3/3)
      R=RC+RS
      ALF21=-(Z1**0.5)-A4/4-((2.405/R)**2)
      BET21=((Z2**0.5)+(Z3**0.5))
      ALF22=(Z1**0.5)-A4/4-((2.405/R)**2)
      BET22=((Z3**0.5)-(Z2**0.5))
      A1=ABS(((((ALF21**2+BET21**2)**0.5)+ALF21)/2)**0.5)
      A2=ABS(((((ALF22**2+BET22**2)**0.5)+ALF22)/2)**0.5)
      B1=ABS(((((ALF21**2+BET21**2)**0.5)-ALF21)/2)**0.5)
      B2=ABS(((((ALF22**2+BET22**2)**0.5)-ALF22)/2)**0.5)
      F10=1-(EXP(-B1*2*H))*COS(A1*2*H)
      F20=1-(EXP(-B2*2*H))*COS(A2*2*H)
      FD10=-B1-(EXP(-B1*2*H))*(B1*COS(A1*2*H)+A1*SIN(A1*2*H))
      FD20=-B2-(EXP(-B2*2*H))*(B2*COS(A2*2*H)+A2*SIN(A2*2*H))
      G10=-(EXP(-B1*2*H))*SIN(A1*2*H)
      G20=-(EXP(-B2*2*H))*SIN(A2*2*H)
      AL21U=-(Z1**0.5)-A4/4
      AL22U=(Z1**0.5)-A4/4
      AL2R1=D2*AL21U+SIG2
      AL2I1=D2*BET21
      AL3R1=D1*AL21U+SIG1
      AL3I1=D1*BET21
      AL4R1=D2*AL21U+SIG2
      AL4I1=D2*BET21
      AL2R2=D2*AL22U+SIG2
      AL2I2=D2*BET22
      AL3R2=D1*AL22U+SIG1
      AL3I2=D1*BET22
      AL4R2=D2*AL22U+SIG2
```

```
      AL4I2=D2*BET22
      E11=SIG13*AL4R1*AL2R1-SIG13*AL4I1*AL2I1+SIG23*SIG12*AL4R1+((SIG24)
     1**2)*SIG13+SIG24*SIG12*SIG21
      E21=SIG13*AL4R1*AL2I1+SIG13*AL4I1*AL2R1+SIG23*SIG12*AL4I1
      E31=SIG12*SIG13*AL2R1+((SIG12)**2)*SIG23+SIG12*SIG24*AL3R1
      E41=SIG12*SIG13*AL2I1+SIG12*SIG24*AL3I1
      E12=SIG13*AL4R2*AL2R2-SIG13*AL4I2*AL2I2+SIG23*SIG12*AL4R2+((SIG24)
     1**2)*SIG13+SIG24*SIG12*SIG21
      E22=SIG13*AL4R2*AL2I2+SIG13*AL4I2*AL2R2+SIG23*SIG12*AL4I2
      E32=SIG12*SIG13*AL2R2+((SIG12)**2)*SIG23+SIG12*SIG24*AL3R2
      E42=SIG12*SIG13*AL2I2+SIG12*SIG24*AL3I2
      R31=(E11+E41*(E21*E31-E11*E41)/((E31**2)+(E41**2)))/E31
      P31=(E21*E31-E11*E41)/((E31**2)+(E41**2))
      R32=(E12+E42*(E22*E32-E12*E42)/((E32**2)+(E42**2)))/E32
      P32=(E22*E32-E12*E42)/((E32**2)+(E42**2))
      F11=AL3R1*AL4R1-AL3I1*AL4I1-SIG13*SIG24-SIG12*SIG21
      F21=AL3I1*AL4R1+AL3R1*AL4I1
      F31=SIG13*AL2R1+SIG23*SIG12+SIG24*AL3R1
      F41=SIG13*AL2I1+SIG24*AL3I1
      F12=AL3R2*AL4R2-AL3I2*AL4I2-SIG13*SIG24-SIG12*SIG21
      F22=AL3I2*AL4R2+AL3R2*AL4I2
      F32=SIG13*AL2R2+SIG23*SIG12+SIG24*AL3R2
      F42=SIG13*AL2I2+SIG24*AL3I2
      R21=(F11+F41*(F21*F31-F11*F41)/((F31**2)+(F41**2)))/F31
      P21=(F21*F31-F11*F41)/((F31**2)+(F41**2))
      R22=(F12+F42*(F22*F32-F12*F42)/((F32**2)+(F42**2)))/F32
      P22=(F22*F32-F12*F42)/((F32**2)+(F42**2))
      A1F=-(Q2/D2)/(FD10-FD20+(R31*F10-P31*G10)/(R32*F20-P32*G20))
      A2F=-A1F*(R31*F10-P31*G10)/(R32*F20-P32*G20)
      FY4W=A1F*((EXP(-B1*Z))*COS(A1*Z)-(EXP(-B1*(2*H-Z)))*COS(A1*(2*H-Z)
     1))+A2F*((EXP(-B2*Z))*COS(A2*Z)-(EXP(-B2*(2*H-Z)))*COS(A2*(2*H-Z)))
      FY2W=A1F*(R21*((EXP(-B1*Z))*COS(A1*Z)-(EXP(-B1*(2*H-Z)))*COS(A1*(2
     1*H-Z)))-P21*((EXP(-B1*Z))*SIN(A1*Z)-(EXP(-B1*(2*H-Z)))*SIN(A1*(2*H
     1-Z))))+A2F*(R22*((EXP(-B2*Z))*COS(A2*Z)-(EXP(-B2*(2*H-Z)))*COS(A2*
     1(2*H-Z)))-P22*((EXP(-B2*Z))*SIN(A2*Z)-(EXP(-B2*(2*H-Z)))*SIN(A2*(2
```

```
      1*H-Z))))
       AMPW=(((FY2W)**2)+((FY4W)**2))**0.5
       PHASE=ATAN(FY2W/FY4W)
       RESFU=(AMPW)/(AMP0)
       WRITE(2,60)
   60  FORMAT(1H 20HFREQUENCY              ,20HAXIAL POSITION       ,20HRESPO
      1NSE FUNCTION    ,20HPHASE                    ,20HAMPLITUDE            )
       WRITE(2,200)
  200  FORMAT(1H )
       WRITE(2,40)FREQ,Z,RESFU,PHASE,AMPW
   40  FORMAT(F9.3,I20,F20.5,F16.4,F30.8)
       WRITE(2,300)
  300  FORMAT(1H )
       GO TO 50
   35  Z=Z+5
       IF(Z-H)25,45,45
   45  STOP
       END
       FINISH
```

APPENDIX D

COMPUTER PROGRAM

(GAMMARESFU)

```
 0 DAFORTRAN LIB NAGF
 1       MASTER GAMMARESFU
 2       INTEGER HH,DETCH,FREQ
 3       AMU1=0.33523
 4       AMU2=0.03390
 5       REXT=37.4
 6       A=15
 7       R=32
 8       DETCH=15
 9    36 READ(1,6)FREQ
10     6 FORMAT(I6)
11       IF(FREQ)16,16,76
12    76 HH=5
13     26 H=DETCH-HH
14     30 M1=1
15       R1=2
16       TETA1=0.0785398
17       FY1=ATAN(R1*SIN(TETA1)/(R+A-R1*COS(TETA1)))
18       ALFA1=3.1415927-TETA1-FY1
19       TLA=(R1**2+(R+A)**2-2*R1*(R+A)*COS(TETA1))**0.5
20       TLA1=R1*COS(ALFA1)+(R**2-(R1**2)*(SIN(ALFA1))**2)**0.5
21       TLA2=TLA-TLA1
22       TPLA=(TLA**2+H**2)**0.5
23       TPLA1=TLA1*TPLA/TLA
24       TPLA2=TPLA-TPLA1
25       DA=4*R1*0.1570796*S17AAF(2.405*R1/REXT)
26       DB=DA
27       AT141=(EXP(-(AMU1*TPLA1+AMU2*TPLA2))/(TPLA**2))*DA
28     10 M1=M1+1
29       IF(M1-20)15,15,25
30     15 TETA2=0.1570796*M1-0.0785398
31       FY2=ATAN(R1*SIN(TETA2)/(R+A-R1*COS(TETA2)))
32       ALFA2=3.1415927-TETA2-FY2
33       TLB=(R1**2+(R+A)**2-2*R1*(R+A)*COS(TETA2))**0.5
34       TLB1=R1*COS(ALFA2)+(R**2-(R1**2)*(SIN(ALFA2))**2)**0.5
```

```
      TLB2=TLB-TLB1
      TPLB=(TLB**2+H**2)**0.5
      TPLB1=TLB1*TPLB/TLB
      TPLB2=TPLB-TPLB1
      AT241=(EXP(-(AMU1*TPLB1+AMU2*TPLB2))/(TPLB**2))*DB
      AT141=AT241+AT141
      GO TO 10
   25 R1=R1+4
      IF(R1-32)55,55,65
   55 M2=1
      TETA3=0.0785398
      FY3=ATAN(R1*SIN(TETA3)/(R+A-R1*COS(TETA3)))
      ALFA3=3.1415927-TETA3-FY3
      TLC=(R1**2+(R+A)**2-2*R1*(R+A)*COS(TETA3))**0.5
      TLC1=R1*COS(ALFA3)+(R**2-(R1**2)*(SIN(ALFA3))**2)**0.5
      TLC2=TLC-TLC1
      TPLC=(TLC**2+H**2)**0.5
      TPLC1=TLC1*TPLC/TLC
      TPLC2=TPLC-TPLC1
      DC=4*R1*0.1570796*S17AAF(2.405*R1/REXT)
      DD=DC
      AT181=(EXP(-(AMU1*TPLC1+AMU2*TPLC2))/(TPLC**2))*DC
   20 M2=M2+1
      IF(M2-20)35,35,45
   35 TETA4=0.1570796*M2-0.0785398
      FY4=ATAN(R1*SIN(TETA4)/(R+A-R1*COS(TETA4)))
      ALFA4=3.1415927-TETA4-FY4
      TLD=(R1**2+(R+A)**2-2*R1*(R+A)*COS(TETA4))**0.5
      TLD1=R1*COS(ALFA4)+(R**2-(R1**2)*(SIN(ALFA4))**2)**0.5
      TLD2=TLD-TLD1
      TPLD=(TLD**2+H**2)**0.5
      TPLD1=TLD1*TPLD/TLD
      TPLD2=TPLD-TPLD1
      AT281=(EXP(-(AMU1*TPLD1+AMU2*TPLD2))/(TPLD**2))*DD
      AT181=AT281+AT181
```

```
      GO TO 20
   45 AT141=AT141+AT181
      GO TO 25
   65 TATH5=AT141
      READ(1,300) AMPU5,ALAM5,AMP05
  300 FORMAT(F9.2,F9.4,F10.2)
      IF(ALAM5)620,621,621
  621 ALAM5=ALAM5-3.1415927
  620 AT=TATH5*AMPU5
      ALAM1=ALAM5
      AT0=TATH5*AMP05
  210 HH=HH+5
      IF(HH-80)130,205,200
  130 N5=1
      R2=2
      H=DETCH-HH
      TETA5=0.0785398
      FY5=ATAN(R2*SIN(TETA5)/(R+A-R2*COS(TETA5)))
      ALFA5=3.1415927-TETA5-FY5
      TLE=(R2**2+(R+A)**2-2*R2*(R+A)*COS(TETA5))**0.5
      TLE1=R2*COS(ALFA5)+(R**2-(R2**2)*(SIN(ALFA5))**2)**0.5
      TLE2=TLE-TLE1
      TPLE=(TLE**2+H**2)**0.5
      TPLE1=TLE1*TPLE/TLE
      TPLE2=TPLE-TPLE1
      DE=4*R2*0.1570796*SIN(2.405*R2/REXT)
      DF=DE
      AT142=(EXP(-(AMU1*TPLE1+AMU2*TPLE2))/(TPLE**2))*DE
  110 N5=N5+1
      IF(N5-20)115,115,125
  115 TETA5=0.1570796*N5-0.0785398
      FY6=ATAN(R2*SIN(TETA6)/(R+A-R2*COS(TETA6)))
      ALFA6=3.1415927-TETA6-FY6
      TLE=(R2**2+(R+A)**2-2*R2*(R+A)*COS(TETA1))**0.5
      TLE1=R2*COS(ALFA6)+(R**2-(R2**2)*(SIN(ALFA6))**2)**0.5
```

```
      TLF2=TLF-TLF1
      TPLF=(TLF**2+H**2)**0,5
      TPLF1=TLF1*TPLF/TLF
      TPLF2=TPLF-TPLF1
      AT242=(EXP(-(AMU1*TPLF1+AMU2*TPLF2))/(TPIF**2))*DF
      AT142=AT242+AT142
      GO TO 110
  125 R2=R2+4
      IF(R2-32)155,155,165
  155 M4=1
      TETA7=0.0785398
      FY7=ATAN(R2*SIN(TETA7)/(R+A-R2*COS(TETA7)))
      ALFA7=3.1415927-TETA7-FY7
      TLG=(R2**2+(R+A)**2-2*R2*(R+A)*COS(TETA7))**0.5
      TLG1=R2*COS(ALFA7)+(R**2-(R2**2)*(SIN(ALFA7))**2)**0.5
      TLG2=TLG-TLG1
      TPLG=(TLG**2+H**2)**0,5
      TPLG1=TLG1*TPLG/TLG
      TPLG2=TPLG-TPLG1
      DG=4*R2*0.1570796*S17AAF(2.405*R2/REXT)
      DH=DG
      AT182=(EXP(-(AMU1*TPLG1+AMU2*TPLG2))/(TPIG**2))*DG
  120 M4=M4+1
      IF(M4-20)135,135,145
  135 TETA8=0.1570796*M4-0.0785398
      FY8=ATAN(R2*SIN(TETA8)/(R+A-R2*COS(TETA8)))
      ALFA8=3.1415927-TETA8-FY8
      TLH=(R2**2+(R+A)**2-2*R2*(R+A)*COS(TETA8))**0.5
      TLH1=R2*COS(ALFA8)+(R**2-(R2**2)*(SIN(ALFA8))**2)**0.5
      TLH2=TLH-TLH1
      TPLH=(TLH**2+H**2)**0,5
      TPLH1=TLH1*TPLH/TLH
      TPLH2=TPLH-TPLH1
      AT282=(EXP(-(AMU1*TPLH1+AMU2*TPLH2))/(TPIH**2))*DH
      AT182=AT282+AT182
```

```
      GO TO 120
  145 AT142=AT182+AT142
      GO TO 125
  165 ATH10=AT142
      READ(1,400)AMH10,ALA10,AMG10
  400 FORMAT(F9.2,F9.4,F10.2)
      IF(ALA10)610,611,611
  611 ALA10=ALA10-3.1415927
  610 ALAM2=ALA10
      A2=ATH10*AMH10
      A3=(A1**2+A2**2+2*A1*A2*COS(ALAM1-ALAM2))**0.5
      ALAM1=ATAN((A1*SIN(ALAM1)+A2*SIN(ALAM2))/(A1*COS(ALAM1)+A2*COS(ALA
     1M2)))
      A1=A3
      IF(ALAM1)600,601,601
  601 ALAM1=ALAM1-3.1415927
  600 A20=ATH10*AMG10
      A10=A20+A10
      GO TO 210
  205 RESFU=A1/A10
      WRITE(2,46)
   46 FORMAT(1H ,20HDETECTOR HEIGHT      ,20HFREQUENCY              ,20HPHAS
     1E                ,20HRESPONSE FUNCTION    )
      WRITE(2,56)
   56 FORMAT(1H )
      WRITE(2,500)DETCH,FREQ,ALAM1,RESFU
  500 FORMAT(F7,F19,F21.4,F24.5)
      WRITE(2,56)
   60 FORMAT(1H )
      GO TO 56
   16 DETCH=DETCH+20
      IF(DETCH-60)30,56,200
  200 STOP
      END
      FINISH
```

REFERE N CES

(1) J.H. MANLEY, L.J. HAWORTH, E.A. LUEBKE
The mean life time of neutron in water and hydrogen capture cross-section.

Physical Review
vol. 61, 152 (1942)

(2) K.H. BECKURTS
Reactor physics research with pulsed neutron sources.

Nuclear Instrument and Methods
vol. 11, 144-168 (1961)

(3) W.M. LOPEZ and J.R. BEYSTER
Measurement of neutron diffusion parameters in water by pulsed neutron method.

Nuclear Science and Engineering
vol. 12, 190-202 (1962)

(4) E. GARLIS
Survey of pulsed neutron source methods for multiplying media.

General Electric Company
vallecitos atomic laboratory

(5) EDWARD GARELIS and JOHN L. RUSSEL
Theory of pulsed neutron source measurements.

Nuclear Science and Engineering
vol. 16, 263-270 (1963)

(6) BROWN, J.R., YOUNG, J.C., BEYSTER, J.R. HOUSTON, et al.
Measurements of subcritical reactivity using a pulsed neutron source.

General Atomic RPT4338 (1964)

(7) V. RAIEVSKI and J. HOROWITZ
Measurement of the mean free transport path of thermal neutrons in heavy water by source modulation.

Compt. rend. 238, (1954)

(8) Determination of the mean transfer free path of thermal neutrons by measurement of complex diffusion length.

PIGG5, 42, (1955)

(9) R.B. PEREZ and R.E. UHRIG
Propagation of neutron waves in moderating media.

Nuclear Science and Engineering
vol. 17, 90-100 (1963)

(10) GLEN A. MORTENSEN and HAROLD P. SMITH, Jr.
Neutron-wave propagation using P1 approximation.

Nuclear Science and Engineering
vol. 22, 321-327 (1965)

(11) R. WANGER
Neutron wave experiments in a heavy water-natural uranium subcritical assembly.

Journal of Nuclear Energy
vol. 24, 71-84 (1970)

(12) S. SOBHANA, J.C. GOYAL, OM PAL SINGH and A.K. GHATAK
Study of neutron wave propagation through a subcritical assembly.

Journal of Nuclear Energy
vol. 27, 441-447 (1973)

(13) GERHARD JACOB
On the diffusion of neutrons in moderating and multiplying media with a periodical neutron source.

Second U.N. International Conference on peaceful uses of atomic energy
A/CONF. 15/P/2272 (1958)

(14) M.N. MOORE
The dispersion law of moderator.

Nuclear Science and Engineering
vol. 26, 354-381 (1966)

(15) M.M.R. WILLIAMS
The dispersion law of a neutron wave in a finite system.

Journal of Nuclear Energy
vol. 22, 153 (1968)

(16) J. WOOD
An interpretation of the neutron wave experiment.

Journal of Nuclear Energy
vol. 23, 17 (1969)

(17) R.L. BREHM
Analysis of neutron-wave type experiments, proc. symp. Neutron Noise and Pulse Propagation.

A.E.C. Symposium series 9, U.S.AEC, 69 (1967)

(18) H.H. Kunaish
Consistent P3 theory of neutron wave propagation, proc. Symp. Neutron noise, wave and pulse propagation.

A.E.C. Symposium series 9, U.S.AEC, 87 (1967)

(19) L.Doukas
Reactivity investigation using a periodic neutron source in a subcritical assembly.

Ph.D. Dissertation, Dept. of Physics, U. of Aston in Birmingham, Nov. (1971)

(20) CHARLES E. COHN and ROBERT J. JOHNSON and R.N.MACDONALD.
Calculating space-dependent reactor transfer function using statics techniques.

Nuclear Science and Engineering.
vol. 26, 198-206 (1966)

(21) CHANG-HWASHEN
Noise analysis of Pennsylvania State University reactor.

Pennsylvania State University
Master thesis (1964)

(22) R.J. GELIANS and R.K. OSBORN
Reactor noise analysis by photon observation.

Nuclear Science and Engineering
vol. (24), 184-192 (1966)

(23) WAYNE K. LEHTO and JOHN M. CARPENTER
Reactor noise measurements using gamma rays.

Nuclear Science and Engineering
vol. 32, 142-145 (1968)

(24) WAYNE K. LEHTO and JOHN M. CARPENTER
Determination of reactor kinetic parameters by photon observation.

Nuclear Science and Engineering
vol. 33, 237-255 (1968)

(25) BRUNO BARS and ESKO MARKKANEN
Reactor parameters from neutron and gamma-ray noise

Nuclear Science and Engineering
vol. 48, 202-210 (1972)

(26) A. GILRAMOS
The spatial response of a multiplying system to a periodic neutron source.

Ph.D. Dissertation thesis, submitted to University of Aston in Birmingham, July (1974)

(27) Reactor physics constants, ANL-5800, second etc.

P.360. ANL(1963)

(28) Gamma rays associated with fission, second U.N. International Conference on peaceful uses of atomic energy.

A/CONF. 15/P/670
June (1958)

(29) Pulse height spectra of gamma rays emitted by the stainless steel clad bulk shielding reactor.

II(BSR-KK)
ORNL-3609 (1964)

(30) Neutron sources. Industrial target for neutron generators (62)

(31) L. TWUM-DANSO
Investigation of neutron diffusion parameters in liquid moderators and liquid moderated multiplying assemblies.

Ph.D. Dissertation thesis submitted to the U. of Aston in Birmingham, Sept.(1969)

(32) G. GRUNBERG, J. Phys. Radium Phys. Appl. 22 (1961)

(33) N.N. HANNA and M.J. HARRIS
Decay of a thermalised neutron pulse in graphite.

Journal of Nuclear Energy
vol. 22, 587 (1968)

(34) B. MILLAR
A Remote control and telemetering system for a Van-der-Graaf generator part (I) and part (II).

Electronic Engineering
446, 506, NOV (1953)

(35) Z. SZARBQ
Pulsed neutron source for reactor physics

Nuclear Instrument and Methods
vol. 78, 199-205 (1970)

(36) P.N. COOPER and L. DOUKAS
External pulsing of an accelerator

Nuclear Instrument and Methods
vol. 92, 581-584 (1971)

(37) P.N. COOPER and GILRAMOS
Improvements to a method of externally pulsing an accelerator.

Nuclear Instrument and Methods
vol. 109, 617-618 (1973)

(38) W.E. BURCHAM
Nuclear physics (An introduction). Pages 130 and 138

(39) R.M. SINGER
Introduction to experimental nuclear physics, page 54.

(40) ADOLF F. VOIGT, DUANCE E, BECKNELL et al.
Comparison of solid state and scintillation gamma-ray spectrometry in analysis.

Institute for Atomic Research and Chemistry Dept. IOWA State University, Ames, IOWA

(41) Neutron cross-sections, B.N.L. 325, (1958)

(42) AITKEN, J.H. and DIXON, W.R.
Nuclear Physics, pages 67, 395 (1965)

(43) BIRKS, J.B.
The theory and practice of scintillation counting
Pergamon Press
New York (1964)

(44) C.E. CROUTHAMEL, F. ADAMS and R. ADAMS
Applied gamma-ray spectrometry, page 37.

(45) WILLIAM J. PRICE
Nuclear radiation detection, page 175.

(46) Neutron cross-sections
B.N.L. supplement No. 2.
325 (1964)

(47) DAY, R.B.
Physical Review
vol. 102, 767 (1956)

(48) D.I. GARBER and R.P. KINSEY
Neutron cross-sections
National Neutron Cross-section Centre.
Brookhaven National Laboratory, 267, June 1976.

(49) R.M. TENNENT
Science data book

(50) New cross-section for boron.
Neutron cross-section evaluation group.
Nucleonic, vol. 19, June 1961

(51) F.D. BROOK,
A scintillation counter with neutron to gamma ray discrimination.
Nuclear Instrument and Methods
vol. 4, 151 (1959)

(52) P.N. COOPER and R.M. MEGAHID
Calibration and neutron spectrum unfolding for a proton recoil neutron spectrometer using pulse shape discrimination.

(53) D. ALIAGA-KELLY and D.R. NICOLL
Recent developments in scintillation detectors.
Nuclear Enterprises(G.B.)Ltd
Nuclear Instrument and Methods
vol.43, 110-115 (1966)

(54) BOAS, MARY.L.,
Mathematical methods in the physical sciences
John Wiley and Sons Inc., 287 (1966)

(55) STEPHENSON, G.
Mathematical methods for science students,
Longmans, 240 (1966)

(56) A.J.M. SPENCER, D.F. PARKER, et al.
Engineering Mathematics vol. 1, 53 (1977)

(57) R.W. HAMMING
Numerical methods for scientist and engineers.
McGraw-Hill, 67 (1962)

(58) SCHEID, F.
Theory and problems of numerical analysis
McGraw-Hill, 293 (1968)

(59) MIFSUD, C.J.
Collected algorithms from CACM
CACM Library Algorithm 157

(60) MURRAY, R.L.
Nuclear Reactor Physics
London, MacMillan & Co. Ltd. page 110 (1959)

(61) RAM, K.S.
Basic Nuclear Engineering.
Wiley Eastern Ltd. pp. 88-101 (1977)

(62) PAUL F. ZWEIFEL
Reactor Physics
McGraw-Hill Koga Kusha Ltd. 127-188 (1973)

(63) BONNET, D.J.
The elements of nuclear power
Longman Group Ltd. pp. 100-116 (1972)

(64) LAMARSH, J.R.
Introduction to nuclear engineering.
Addison-Wesley Publishing Co.
pp. 223-240 (1975)

(65) McCALLIEN, C.W.J.
'SNAP', a two dimensional neutron diffusion code, TRG Report 1990 (R), UKAEA (Reactor Group).
Warrington, Lancs.

(66) McCALLIEN, C.W.J.
Squified and Snap: Some programming details, Risley
Computer Section, UKAEA, RCN7/70, Sept.(1971)

(67) MUNDAY, P.J.
'SNAP', TNPG/MTS. Int. 1779, The nuclear power group Ltd. Radbroke Hall, Knutsford, Cheshire, Feb. (1971)

(68) MUNDAY, P.J.
'SNAP$_2$', TNPG/MTS. Int. 1779, The Nuclear Power Group Ltd. Radbroke Hall, Knutsford, Cheshire, May (1971)

(69) KORN and KORN
Mathematical handbook for scientist and engineers
(22-25)

(70) EVANS, R.D.
The Atomic Nucleus, McGraw-Hill
703 (1955)

(71) JELLEY, J.V.
Cerenkov radiation and its application

(72) TOPPING, J.
Errors of the observation and their treatment, Fourth Ed.
Pergamon Press
38-43 (1972)